DANMARKS OG GRØNLANDS GEOLOGISKE UNDERSØGELSE RAPPORT 2008/23

Effects of future climate change on water resources in Denmark

Lieke v. Roosmalen, Torben O. Sonnenborg,
Karsten H. Jensen & Gyrite Brandt

GEOLOGICAL SURVEY OF DENMARK AND GREENLAND
MINISTRY OF CLIMATE AND ENERGY

GEUS

DANMARKS OG GRØNLANDS GEOLOGISKE UNDERSØGELSE RAPPORT 2008/23

Effects of future climate change on water resources in Denmark

Lieke v. Roosmalen, Torben O. Sonnenborg,
Karsten H. Jensen & Gyrite Brandt

GEOLOGICAL SURVEY OF DENMARK AND GREENLAND
MINISTRY OF CLIMATE AND ENERGY

GEUS

Table of contents

1. Project description 2
- **1.1 Introduction** 2
- **1.2 Study area** 2
- **1.3 Climate-forcing data sets** 4

2. Model Improvements 6
- **2.1 Inclusion of the unsaturated zone** 6
- **2.2 Horizontal discretization** 8
- **2.3 Topography** 8
- **2.4 Land use map** 9
- **2.5 Irrigation** 11
- **2.6 Division of groundwater withdrawals between water supply and irrigation** 12
- **2.7 Comparison of recharge and the water balance** 13
- **2.8 Comparison of river discharges** 15
- **2.9 Comparison of simulated and observed groundwater heads** 18

3. Effects of Climate Change on Water Resources 22
- **3.1 Change in water balance and groundwater recharge** 22
- **3.2 Change in mean groundwater heads** 24
- **3.3 Change in river discharges** 28
- **3.4 Effect of sea-level rise** 33

4. Indirect effects of climate change on water resources 37
- **4.1 Changes in irrigation volume** 37
- **4.2 Effects of changes in land use** 42
- **4.3 Change in infiltration zones to wells** 43

5. Summary and conclusions 52

Acknowledgments 54
References 55
Annex 1 58

1. Project description

1.1 Introduction

The most recent Intergovernmental Panel on Climate Change (IPCC) report states that global atmospheric concentrations of green house gases have increased markedly since 1750 as a result of human activities (IPCC, 2007). The increase in carbon dioxide concentrations is mainly caused by the burning of fossil fuels, but the contribution of land use changes (primarily deforestation) is also significant. Agriculture mainly contributes to the increases in atmospheric concentrations of methane and nitrous oxide. The increasing green house gas concentrations affect the radiation balance and hence the world's climate. Changes in meteorological variables are expected to impact hydrological systems in Europe significantly (e.g. Andréasson et al., 2004; Arnell, 1999; Caballero et al., 2007; Graham et al., 2007; Kleinn et al., 2005; Thodsen, 2007). At the same time these systems are also largely influenced by the demands of the different users of the water resources of the system.

It is therefore of great interest to study the combined effects of climate changes and anthropogenic changes on the terrestrial, hydrological cycle. This calls for a catchment scale approach to be able to account for the total amount of incoming and outgoing water fluxes to the system. Regional-scale studies on the effects of global climate change are of great interest because often the most significant impacts are manifested at the regional scale. Moreover, water resources management measures take place at a regional level in a framework of basin level policies. In this study a regional-scale, hydrological model is used to study the effects of climate change and land use changes on the hydrological components within the catchment.

The objective of this study is to quantify the effects of climate and land use changes on the water resources in a catchment in the western part of Denmark. A deterministic, distributed, physically-based model called the DK-model (Henriksen et al., 2003; Henriksen and Sonnenborg, 2003; Sonnenborg et al., 2003) is used to study changes in the groundwater system and its discharge to rivers and drains. We present the results of the model simulations using the climate-forcing data sets for the current climate and the IPCC A2 and B2 scenarios (IPCC, 2000). The effects on groundwater recharge, groundwater heads and stream discharges are examined. Also the effect of sea level rise on groundwater levels is investigated. The results of these simulations can be defined as the direct effects of climate change. Additionally, "indirect" anthropogenic effects, such as abstractions for water supply and industry and for irrigation, are simulated. This shows the effect of human activities on the hydrological system, but also the effects of climate change on irrigation are investigated. Finally, the effects of land use changes are compared to the effects of climate change on the groundwater recharge.

1.2 Study area

The study area is located in the western part of Jutland, Denmark, between the Jutland Ridge and the west coast (Fig. 1.1) with an area of 5459 km^2. The topography slopes gently from east to west with land surface elevations from 125 meters above sea level (masl) in the eastern part to sea level at the coast. The area is bounded by the North Sea to the west, while the regional water divide at the Jutland Ridge serves as the boundary to

the east. The northern and southern boundaries are delineated on the basis of local water divides.

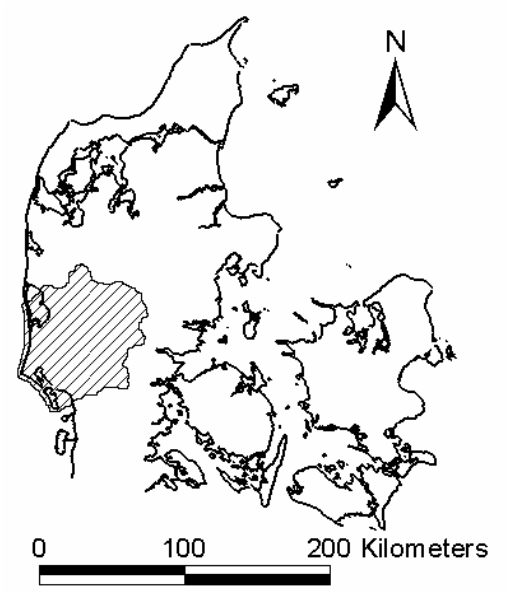

Figure 1.1 Location of the study catchment in Denmark

The climate in western Jutland is typical of the maritime regime, dominated by westerly winds and frequent passages of extratropical cyclones. Maximum precipitation is in autumn and minimum in spring. The Danish Meteorological Institute has developed a climate grid for Denmark (Scharling, 1999) providing daily values for temperature, precipitation and reference evapotranspiration (potential evapotranspiration for a well-watered grass of uniform height) at a 40-km resolution. For each grid cell representative time series based on data from available climate stations is estimated. For this study we have retrieved data for the period 1990–2004. The precipitation is corrected for wetting and aerodynamic effects using the standard correction methods of Allerup et al. (1998). The average precipitation in the area equals 1073 mm/year. The reference evapotranspiration is calculated using the Makkink (1957) formula, and has an average value of 570 mm/year. The average annual temperature is 8.2 ºC with a maximum of 16.5 ºC in August and a minimum of 1.4 ºC in January.

The shallow geology in Western Jutland is dominated by glacial outwash sand and gravel originating from the glaciers' meltdown. Isolated islands of Saalian sandy till are found between the outwash plains (Fig. 1.2). The thickness of the Quaternary deposits is generally less than 50 m in the central and northeastern part of the area, while the thickness increases in the southern and western part and in some places reaches depths of approximately 250 m. Miocene sediments are found below the Quaternary deposits. The Miocene sediments are formed by alternating layers of clayey and sandy marine deposits with a total thickness of generally 200–300 m. The Miocene layers dip slightly to the west. Beneath the Miocene sequence, Paleogene clay sediments of regional extent are found. The Paleogene unit is conceptualized as an aquitard that acts as a lower boundary to groundwater flow. The Quaternary and Miocene sand formations often form large interconnected aquifers. In general, groundwater flows from east to west.

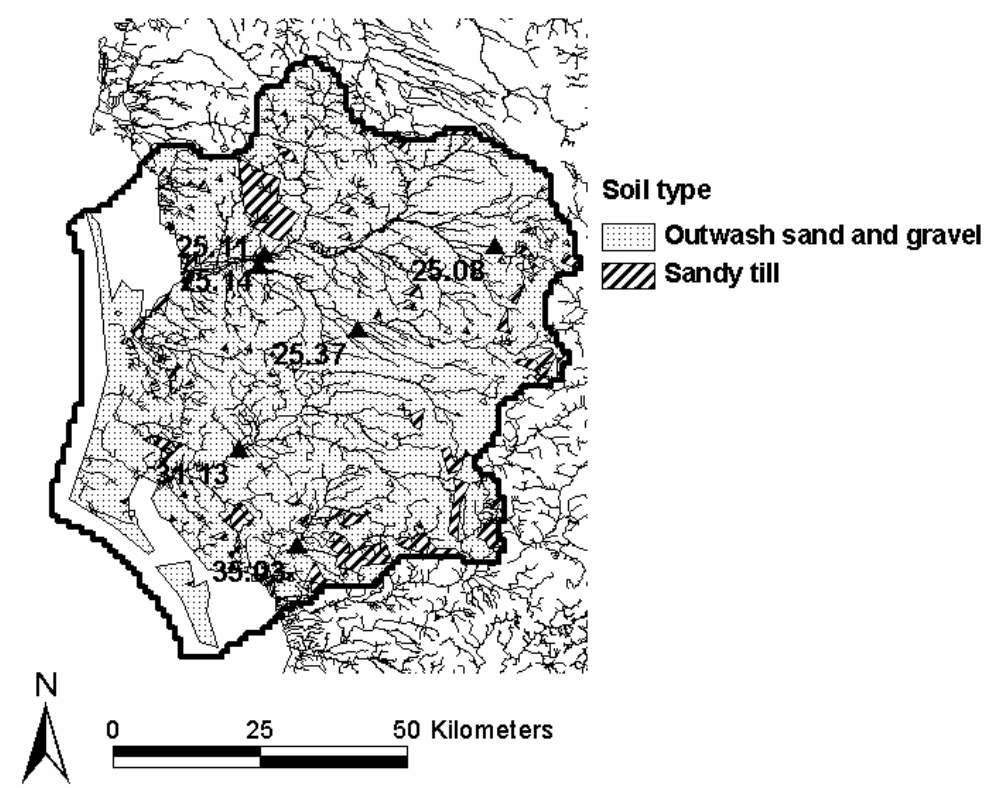

Figure 1.2 Soil type map of the catchment area. Six discharge stations (▲) are indicated, which are used for the analysis of the results.

1.3 Climate-forcing data sets

In this study, a physically-based, regional climate model (RCM) is used to dynamically downscale the climate change signals projected by the AOGCM. Due to the anomalies between the simulation of the historic climate (1961–1990) of the RCM and the observed climate, a transfer method is necessary to construct the climate scenario data sets for the hydrological model simulations. The meteorological input for the hydrological simulations of the current climate are the daily precipitation, temperature and reference evapotranspiration data of the climate grid for Denmark. This data set is also used as a baseline for the climate-forcing data sets for the scenario simulations. The scenario data sets are constructed using the delta change method (Hay et al., 2000), where the baseline precipitation and reference evapotranspiration is multiplied by monthly change factors, while for temperature an absolute value is added, which also varies for every month of the year. The monthly change factors are calculated from the anomalies in atmospheric outputs from a RCM for the current climate (1961–1990) and the scenario period (2071–2100). A more detailed description of the construction of the data sets can be found in Roosmalen et al. (2007).

Output was extracted for the IPCC A2 and B2 scenarios (IPCC, 2000) from the regional climate model HIRHAM, developed by the Danish Meteorological Institute (Christensen et al., 1996, 1998). For both scenarios HIRHAM was forced by the general circulation model HadAM3H developed by the Hadley Centre. HIRHAM output for the A2 scenario is available at a horizontal grid resolution of 12 km and the B2 scenario at a 50 km

resolution. The B2 scenario is a more moderate scenario than the A2 scenario, resulting in lower temperature increases. The mean annual temperature in the catchment increases 2.2 °C for the B2 scenario and 3.2 °C for the A2 scenario. The increases in mean annual precipitation are 116 mm (12%) and 160 mm (16%) for the A2 and B2 scenarios, respectively. The absolute increase in annual reference evapotranspiration is around 110 mm for the A2 scenario and 80 mm for the B2 scenario. Figure 1.3 shows the mean monthly input for the current climate and both climate scenarios.

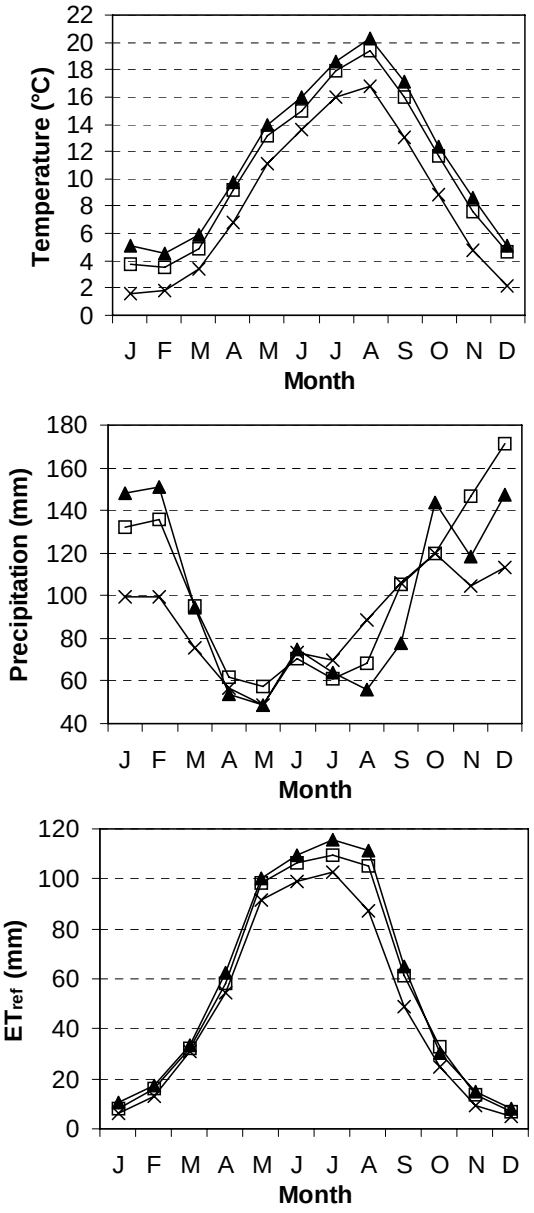

Figure 1.3 Mean monthly temperature (°C), precipitation (mm), and reference evapotranspiration (mm) for the current climate (x) and the A2 (▲) and B2 (□) scenarios.

2. Model Improvements

The hydrological model used in this study is based on the National Water Resources Model for entire Denmark (the DK model), described in Henriksen et al. (2003) and Sonnenborg et al. (2003). The DK model is a distributed groundwater-surface water model based on the MIKE SHE code (Refsgaard and Storm, 1995; Graham and Butts, 2006). A number of changes have been made to the original model to be able to study the effects of land use changes and sea level rise, but also changes to improve simulations in general, such as the inclusion of the unsaturated zone and the higher resolution for topography and calculation grid. The changes to the model are described in this section.

2.1 Inclusion of the unsaturated zone

In the original (2001) version of the model the net precipitation was calculated in an external root zone module using the meteorological input and information on root zone capacity, land use and location of the groundwater table. The net precipitation output was then used as input to the MIKE-SHE model. In the new version of the model, the unsaturated zone (UZ) has been included, so that the external root zone module is not necessary anymore and capillary rise from the groundwater to the unsaturated zone is possible. All meteorological data (climate grid Denmark) is now included directly in MIKE-SHE.

Two-layer unsaturated zone model

Unsaturated zone processes are computed by a two-layer water balance method (Yan and Smith, 1994) available in the MIKE SHE system (DHI, 2007). The main purpose of the module is to calculate actual evapotranspiration and the amount of water that recharges the saturated zone. The controlling parameter is the root zone capacity, defined as the difference between water content at field capacity and wilting point, multiplied by the depth of the root zone. The higher the root zone capacity, the higher the fraction of infiltrating water that can be removed by evapotranspiration will be. The model only considers average conditions and does not account for the relation between unsaturated hydraulic conductivity and soil moisture content. The module is particularly useful for areas with a shallow groundwater table, where the actual evapotranspiration rate is close to the potential rate.

In the two-layer water balance method the soil column has an upper limit, Z_{surf}, equal to the land surface elevation minus the thickness of the capillary fringe, and a lower limit, Z_{ext}, defined as the root depth plus the thickness of the capillary fringe, $Z_{ext} = d_r + H_c$. If the water table rises above Z_{surf}, potential evapotranspiration is assumed to take place and soil water is replaced by capillary rise. Z_{ext} is defined as the maximum depth from where water can be removed by transpiration. It is If the water table is below Z_{ext}, then the water removed from the root zone by evapotranspiration cannot be replaced by capillary rise, and the water content of the root zone will decrease when evapotranspiration takes place. The upper layer of the unsaturated zone is defined to extend from the ground surface to the higher of the water table and Z_{ext}. The second layer extends from the bottom of the first layer to the water table. Thus, if the water table is above Z_{ext}, the thickness of the lower layer is zero. Evapotranspiration is only allowed from the upper of the two layers.

Average water content

The actual average water content (Θ_{act}) of the two-layer model varies, depending on the location of the groundwater table:

1. If the water table is at the ground surface, then Θ_{act} equals the saturated moisture content (Θ_{sat}), and all ET is taken from the saturated zone.
2. If the water table is below the ground surface, but above the ET_{surf}, then Θ_{act} is a linear function of the depth of the water table. Θ_{act} is not dependent on ET and any water lost to ET will be replaced from the groundwater table through capillary action.
3. If the water table is below the ET_{surf}, but above the ET_{ext}, then Θ_{act} will vary between a minimum, Θ_{min}, and a maximum value, Θ_{max}. The minimum and maximum values of the water content vary linearly with the depth to the water table. Vertical infiltration to the saturated zone only occurs when Θ_{act} equals Θ_{max}.
4. If the water table is below ET_{ext}, then Θ_{act} of the lower ET layer is equal to the field capacity, Θ_{FC}. Θ_{act} of the upper ET layer can range between Θ_{FC} and the moisture content at wilting point, Θ_{WP}.

Evapotranspiration

Potential evapotranspiration, ET_p, is described as the reference evapotranspiration multiplied by a crop factor, K_c. Actual evapotranspiration is calculated as the sum of evaporation from canopy interception, E_{can}, evaporation from water ponded on the ground surface, E_{pon}, transpiration from the unsaturated zone, E_{uz}, and transpiration from the saturated zone, E_{sz}. Evaporation from the canopy is found as:

$$E_{can} = \min\left\{I^*_{act}, ET_p \cdot \Delta t\right\} \tag{1}$$

where Δt is the time step and I^*_{act} is the actual interception storage calculated as

$$I^*_{act} = \min\left\{C_{\text{int}} \cdot LAI, P \cdot \Delta t\right\} \tag{2}$$

where C_{int} is the interception coefficient (mm), LAI is the leaf area index, and P is the precipitation. C_{int} defines the interception storage capacity of the vegetation and has a typical value of about 0.05 mm. The volume of water in interception storage is subsequently updated as $I_{act} = I^*_{act} - E_{can}$.

If the interception storage cannot satisfy the potential evapotranspiration, additional water may be removed from the ponded water storage, d_{oc}:

$$E_{pon} = \min\left\{d^*_{oc}, ET_p \cdot \Delta t - E_{can}\right\} \tag{3}$$

where d^*_{oc} is the water ponded at ground surface at the beginning of a time step. The ponded water storage is subsequently updated as $d_{oc} = d^*_{oc} - E_{pon}$.
If the potential ET is not satisfied, water is extracted from the unsaturated zone

$$E_{uz} = \min\left\{V_{uz}, ET_p \cdot \Delta t - E_{can} - E_{pon}\right\} \tag{4}$$

where V_{uz} is the available water in the unsaturated zone, given as

$$V_{uz} = (\theta_{act} - \overline{\theta}_{\min}) \cdot z_{wt} \tag{5}$$

where z_{wt} is the depth to the water table, θ_{act} is the actual moisture content, and $\overline{\theta}_{\min}$ is the minimum water content of the unsaturated zone. $\overline{\theta}_{\min}$ is defined as the average minimum water capacity over a soil moisture profile which can vary between the water content at wilting point and the saturated water content at the water table.

If potential evapotranspiration has not been reached, water may be extracted from the saturated zone. The amount extracted depends on the depth to the water table, z_{wt}

$$E_{sz} = \begin{cases} ET_p \cdot \Delta t - E_{can} - E_{pon} - E_{uz}, & z_{wt} < Z_{surf} \\ \max\left\{ ET_p \cdot \Delta t - E_{can} - E_{pon} - E_{uz},\ ET_p \cdot \Delta t \dfrac{Z_{ext} - z_{wt}}{Z_{ext} - Z_{surf}} \right\}, & Z_{surf} \le z_{wt} \le Z_{ext} \\ 0, & z_{wt} > Z_{ext} \end{cases} \tag{6}$$

If the average water content Θ_{act} exceeds Θ_{max}, groundwater recharge is produced:
$Q_R = \max((\Theta_{act}-\Theta_{max}(z_d))*z_d),0)$

Where Q_R is the groundwater recharge [m] and z_d is the depth of the water table [m].

The parameters of the unsaturated zone have been calibrated using the water balance output and groundwater heads from the version of the model before inclusion of the unsaturated zone. Table 2.1 shows the parameters used in the UZ. By far the largest part of the model area has soil type sand and gravel and the rest is clay (Fig. 1.2).

Table 2.1 Parameters used in the 2-layer unsaturated zone module. θ = average moisture content, sat = at saturated conditions, fc = at field capacity, wp = at wilting point.

	Θ_{sat}	Θ_{fc}	Θ_{wp}	z_{surf} (m below ground surface)	Infiltration capacity (m/s)
Sand and gravel	0.3	0.15	0.03	0.35	$5.0\ e^{-4}$
Clay	0.4	0.25	0.06	0.5	$1.0\ e^{-6}$

2.2 Horizontal discretization

The discretization of the horizontal calculation grid is reduced from 1000 m to 500 m. This increases the number of cells on the surface within the model area from 5990 to 23960 cells. The main reason for using a finer discretization, in combination with the topography at a 500 m resolution, is to improve the representation of the stream valleys in the area.

2.3 Topography

The topography in the original model had a 1000m grid size, but in this version of the model a new topography file at a 500 m resolution is included (Figure 2.1). The new topography file results in a number of new files because they are derived from the topography file:

1) The lower-level files, which give the bottom elevation of a layer, for the upper 4 computational layers of the saturated zone model because they are related to the surface topography. From layer 5 and downwards the bottom level is a fixed value being -10 m for layer 5 and decreasing with 10 m for each layer.
2) The drain level file because the drains are located 0.5 m below surface level throughout the whole model area.
3) The horizontal extent of the sea because the sea is defined as the area where the topography is equal to zero.

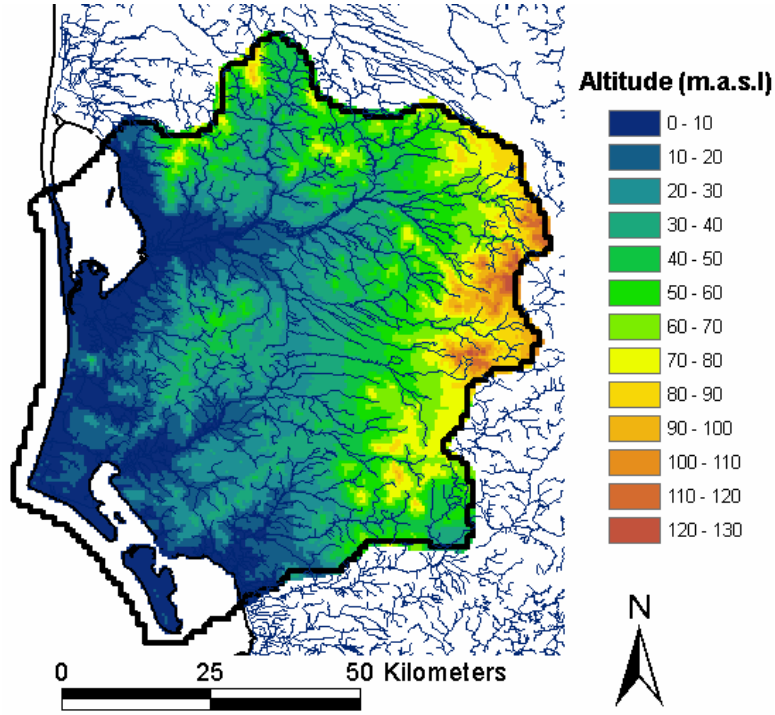

Figure 2.1 The topography of the catchment.

2.4 Land use map

In the old version of the model the following land use groups were defined: forest, grassland and wetland. The grasslands were divided into 8 groups depending on the combination of the soil type (sand or clay), the altitude (high or low), and whether irrigation was applied. The net precipitation (recharge) was calculated for these 10 land use groups (8 grassland, 1 forest, 1 wetland) within every meteorological climate grid. Within MIKE SHE a land use code map then distributed these various recharge amounts within the model area.

A new land use map is included in the model (Figure 2.2). Based on satellite data from 9th May 2001, the land use is defined as grain and corn (56%), grass (29%), forest (7%), heather (5%) and urban (2%). As this is still early in the growing season, some of the agricultural land had no vegetation. The bare areas are defined as grain areas, whereas the other agricultural land is defined as grass. Since 1990 the agricultural area covered by corn has increased from less than 1% to approximately 10% (Statistics Denmark). However, in this study grain and corn are pooled together and represented by grain. Most of the forest consists of conifer trees.

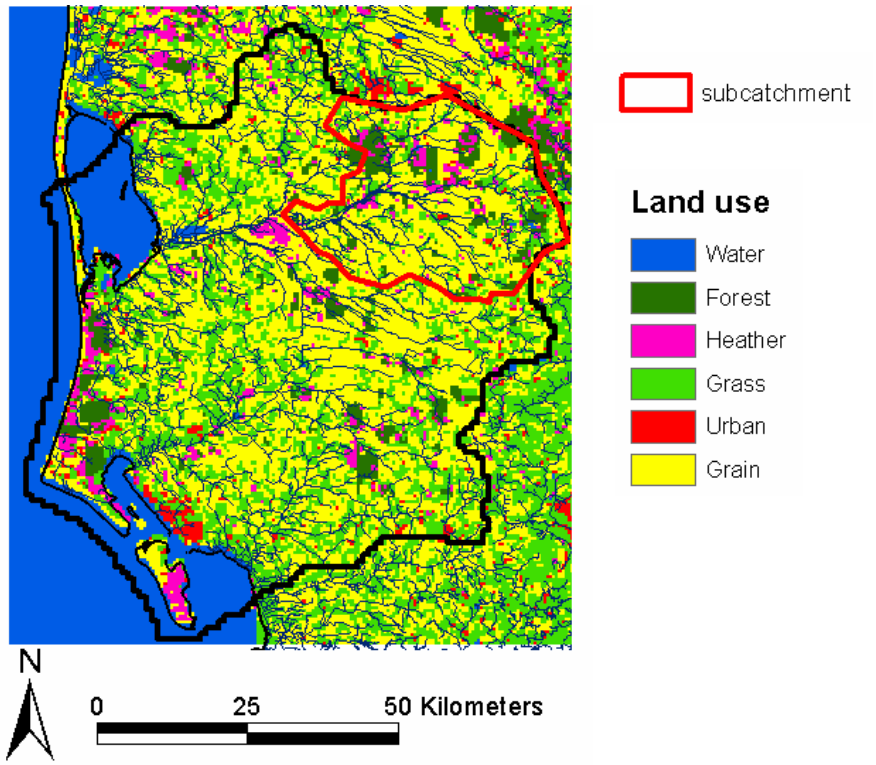

Figure 2.2 Land use classification map of the catchment area and the location of the subcatchment used for the land use change simulations.

The land use types are parameterized according to Table 2.2. The parameters for grain vary throughout the growing season of 120 days starting on May 1 every year. The growing season is divided into seven stages, with maximum values of LAI, d_r and K_c from day 60 to day 120. After the growing season the grain area is assumed to be represented by bare soil for the winter season. The other land use types have constant parameters throughout the year. The K_c-value used for forest is relatively high. However, based on investigations by Mossin and Ladekarl (2004) and van der Salm et al. (2006) especially evaporation from the intercepted water is responsible for a relatively high potential evapotranspiration from conifer trees in this area.

Table 2.2 Values used for the leaf area index, LAI, root depth, and crop factor, K_c, for the various land use types.

	LAI (-)	d_r (m)	K_c (-)
Grain	1.5 – 5	0.2 – 1	1 – 1.2
Bare soil	1	0.2	1
Grass	3	0.54	1
Forest	6	1.5	1.3
Heather	2	0.4	1
Bare soil	1	0.2	1

2.5 Irrigation

To specify irrigation with the 2-layer water balance method, the "shallow well source" type is selected, which places one well in each cell of the command area. As this model is a regional scale hydrological model, each cell can in reality contain many shallow groundwater wells. The shallow well source can be used to simply extract water for irrigation from a cell without having to know the exact locations of these wells.

Irrigation water withdrawal
A maximum depth to the water table is specified, and pumping will stop, if the water level drops below that depth. The maximum depth should be large (in this case 100 m below ground surface), if water is allowed to be pumped from deep reservoirs. The maximum extraction rate for the wells is 0.25 m^3/s. The irrigation water is applied as sprinkler irrigation, which is the typical irrigation method in Western Jutland, and using this method the irrigation water is simply added to the precipitation component.

The depth of the top and bottom of the screen is used to determine from which numerical layers water can be extracted. The top and bottom of the screen are equal to 10 m and 240 m below ground surface. Throughout the model area water for irrigation can be extracted from computational layer 5 and downwards because the bottom level of layer 5 is at -10 masl. Whether water for irrigation is extracted from computational layers 1 to 4 depends on the topography because the higher the surface elevation, the greater the thickness of the computational layers 1 to 4.

Irrigation water demand
Irrigation demand is described by the maximum allowed deficit method. Here, the available water for crop transpiration (AW) is the difference between the actual water content, θ_{act}, and the water content at wilting point, θ_{wp}. The maximum available water for crop transpiration (MAW) is the difference between the water content at field capacity, θ_{fc}, and wilting point, respectively. The soil water deficit (SWD) is defined as the fraction of MAW that is missing:

$$SWD = \frac{MAW - AW}{MAW} = \frac{\theta_{fc} - \theta_{act}}{\theta_{fc} - \theta_{wp}} \tag{7}$$

Irrigation is specified to start when SWD is higher than the threshold value SWD_{ir}. Irrigation is applied until the actual water content equals the water content at field capacity.

Irrigation area
The irrigation command and demand areas are the same in the model and correspond to the areas with land use "grass" (Fig. 2.2). In reality, irrigation also occurs in areas covered by grain and corn, but due to the uncertainties related to changes in cropping patterns and the growing season for these crops, it was decided to only study the changes in irrigation for grass. The grass-covered area equals 30% of the total area, which is equal to the irrigated area in the old version of the model.

2.6 Division of groundwater withdrawals between water supply and irrigation

In the old version of the model groundwater withdrawals for water supply, industry, irrigation and other uses were all included in one single abstraction file. They were defined as abstractions with a fixed volume for a certain year for each borehole location and filter depth. The irrigation volume was estimated based on the extraction licenses and the reported withdrawal for the years where data was available. This annual volume was then divided equally over the months May up to and including August, the irrigation season.

In the new version of the model the abstractions for water supply, industry and other users are separated from the abstractions for irrigation. The abstractions for water supply, industry, and other users are still included as a fixed volume for each borehole location and filter depth, but now irrigation withdrawals are coupled to the water content in the root zone. Figure 2.3 shows the volume of water used for irrigation for the old and new version of the model, and the volumes of the withdrawals for water supply, industry, and other users. The volumes for irrigation are not directly comparable because the values for the old version of the model equal the volume of water added to the root zone module to simulate irrigation. In the old version the root zone module and the groundwater model were not coupled, so an indirect method was necessary to transfer the information on the volume of water added for irrigation in the root zone to the volume of water withdrawn from the groundwater model. The volumes in Figure 2.3 for the new version of the model are the volumes of the total withdrawal of groundwater from the model for irrigation.

Figure 2.3 shows that the irrigation volumes for the new version of the model are considerably lower than for the old version, but due to the uncertainty of the values in the old version of the model, it was decided to keep the selected values for irrigation in the new version of the model as they are.

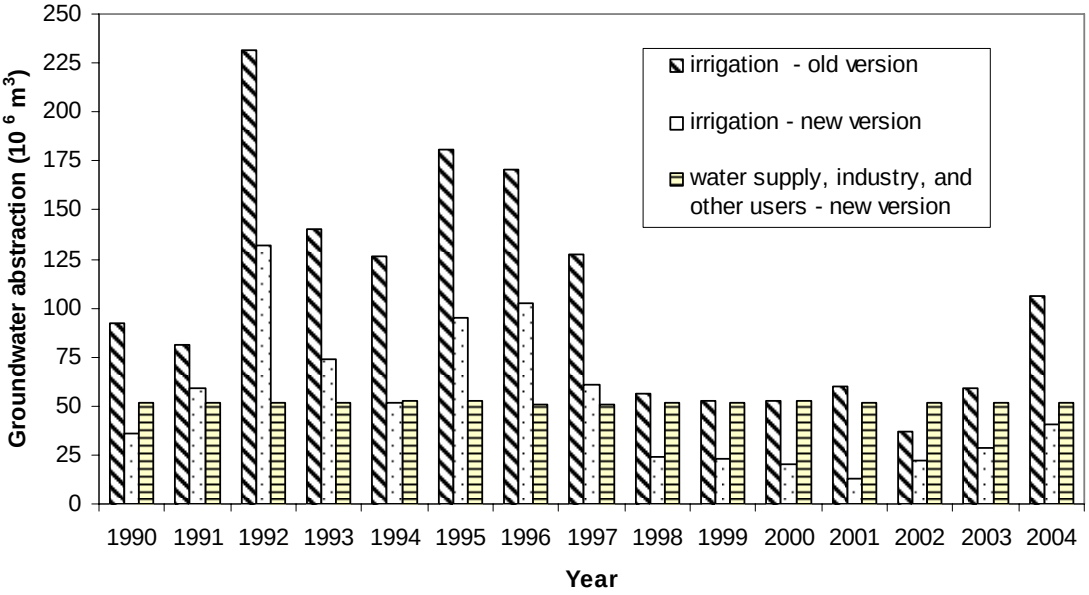

Figure 2.3 Volume of annual groundwater abstraction for irrigation water (Mm^3) in the old and new version of the model, and for water supply, industry, and other users in the new version.

2.7 Comparison of recharge and the water balance

Recharge to the saturated zone

The main objective for the calibration of the unsaturated zone is the net recharge to the upper groundwater reservoir, to simulate the same amount of water infiltrating to the saturated zone as in the original version of the model. By far the largest contribution to the net recharge is infiltration from the unsaturated zone to the saturated zone. Other contributions are the inflow and outflow from the saturated zone to the overland component, which result in a net flux to the saturated zone of around 2% of the net recharge. Evapotranspiration from the saturated zone reduces the net recharge by up to 5%.

Figure 2.4 and 2.5 show the mean annual and monthly recharge to the saturated zone for the old version of the model, not including a root zone, and the final version of the model including all changes to the model setup. The recharge is averaged for the whole land area of the catchment. Each simulation is run from 01/01/1971–31/12/2004, but only the period from 01/01/1990 is used for the water balance extraction to ensure comparable initial values for all simulations. The mean annual recharge for the old version of the model is 519 mm with a standard deviation (SD) of 171 mm and for the new model it is 542 mm with an SD of 177 mm. The annual recharge in the new version of the model is 4% larger than in the old version, but due to the uncertainties related to the recharge in the old version, it was decided not to tune the parameters of the unsaturated zone module to less realistic values.

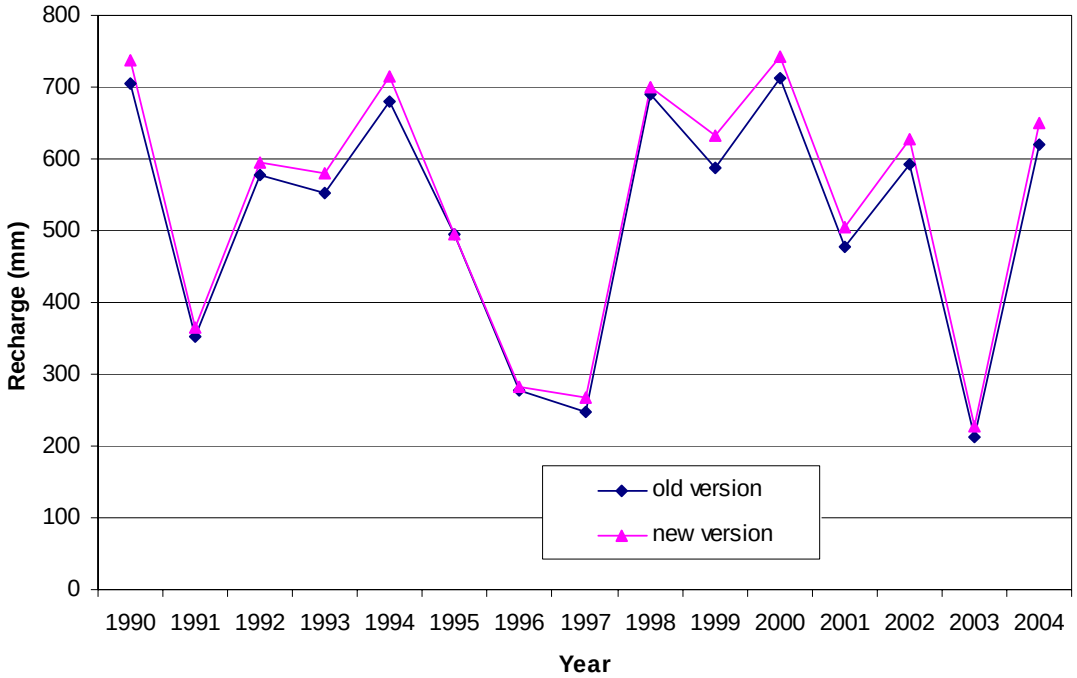

Figure 2.4 Net annual recharge (mm) for the period 1990–2004 for the old version not including the root zone and the new version of the model. Abstractions are not included.

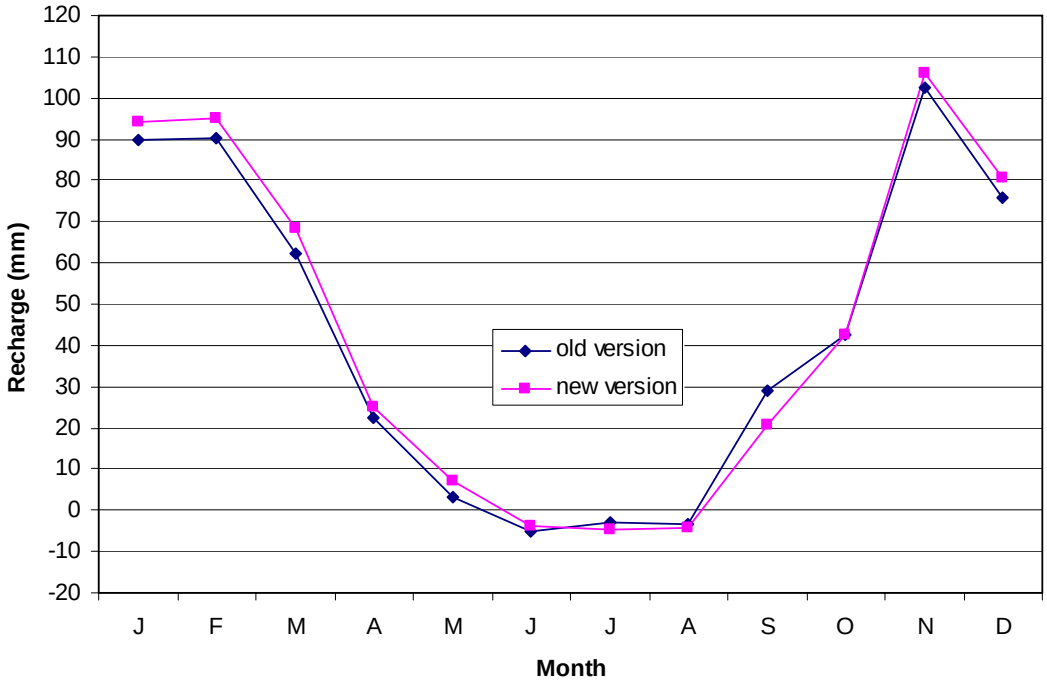

Figure 2.5. Net monthly recharge (mm) for the period 1990–2004 for the original version and the new version of the model. Abstractions are not included.

Model versions

To study the effects of the changes in the model setup, a number of simulations are run, where the changes are introduced step-wise. The following simulations are run, not including abstractions and irrigation:

1) The original 2001 version of the model with a 1000 m horizontal grid and the unsaturated zone not coupled to the groundwater model.
2) A new version of the model using all the same original 1000m input files, but then with the unsaturated zone included.
3) The model including the unsaturated zone and all the original 1000m input files, except for the topography file and related input files. The new topography has a 500m resolution.
4) The model including the unsaturated zone and all the original 1000m input files, except for the horizontal calculation grid file. The new calculation grid has a 500m resolution.
5) The model including the unsaturated zone and both the calculation grid and topography at 500m resolution.
6) The final version of the model including the unsaturated zone, the calculation grid and topography at 500m resolution, and the new landuse file.

Total water balance

The water balance provides a general insight into the hydrological cycle of the catchment (Table 2.3 and Table 2.4 for the model simulations not including and including abstractions, respectively). The results are the spatially-averaged, mean annual values for a 15 year period for the six simulations described above. The net recharge is defined as the flow out of the root zone minus the sum of evapotranspiration from the water table and net potential flow from the groundwater zone to the overland compartment, which occurs when the soil profile becomes completely saturated and the unsaturated zone is no

longer active. The net horizontal boundary outflow is the net flow across the catchment boundary out of the catchment and accounts primarily for groundwater flow to the sea. Drain flow includes drainage from groundwater to rivers in the catchment and drainage to the sea in coastal regions. Base flow is the net flow resulting from groundwater flow to rivers.

Table 2.3 Average total water balance (mm/year) for the period 1990–2004 for the various model versions. No abstractions for water supply, industry, or irrigation are included in these model versions.

		Net recharge	Hor. Bou. Outflow	SZ Stor. Change	Drain Flow	Base Flow
1	1000m grid-no UZ	519	39	6	180	307
2	1000m grid-with UZ	531	36	3	177	322
3	1000m grid- 500m topography	537	29	3	211	301
4	500m grid- 1000m topography	506	23	3	210	278
5	500m grid-500m topography	529	22	3	272	239
6	500m grid-500m topography-new landuse	542	23	3	280	242

Table 2.4 Average total water balance (mm/year) for the period 1990–2004 for the old (UZ not included) and new model version including abstractions for water supply, industry, and irrigation.

Model version	Net recharge	Hor. Bou. Outflow	SZ Stor. Change	Water Supply/ Industry	Irrigation	Drain Flow	Base Flow
Old	-521	39	-10	10	15	171	297
New	-544	22	-3	10	10	270	236

Distribution drain flow and base flow

A pronounced change occurs with respect to the contribution of base flow and drain flow to the rivers when both the 500 m computational grid and the topography at 500 m are included. Drain flow increases and base flow decreases considerably. This can be explained by the more detailed representation of the river valleys. Now that the groundwater table in the valleys changes between two adjacent cells of 500 m instead of having an averaged value for the groundwater table for a 1000 m cell covering this distance, more cells have a “higher” groundwater table. As a result more cells have groundwater tables above the drains giving a larger contribution of drain flow to the total river discharge. The total discharge to rivers increases by 7% when comparing the final version of the model to the old version without the root zone included.

2.8 Comparison of river discharges

The simulated discharges for the various model versions are compared to the observed discharge at six discharge stations in the catchment (Table 2.5). Figure 1.2 shows the

location of these stations in the model area. Four stations with a relatively large catchment area (25.14, 25.11, 31.13, 35.03) are selected and two with a relatively small catchment (25.08, 25.37).

Table 2.5 The discharge station numbers, on which river they are located and the area of the subcatchment drained.

Station	**River**	**Catchment area (km^2)**
25.14	Skjern Aa	1558
25.11	Omme Aa	612
31.13	Varde Aa	814
35.03	Sneum Aa	223
25.08	Skjern Aa	82
25.37	Hoven Aa	50

Total river discharge

Annex 1 shows the daily flow records at 6 locations (Fig. 1.2) in the Jutland study area for the period 1990–2004. For each location the simulated discharges for the two versions of the model and observations are shown. The new model version with the root zone included shows more drying during summer than the old version without the root zone. This can be seen as an improvement of the model because when comparing the simulated flows to the observed flows, the simulated flows are often higher than the observed flows during the low flow periods. During wetter years the model including the root zone often simulates higher peaks than the version without the root zone, though the observed peaks are still higher than the simulated peaks for most wet years.

The mean error (ME) describes the average difference between the simulated and observed discharge for each time step:

$$ME = \frac{1}{n}\sum_{i=1}^{n}(Q_{obs,i} - Q_{sim,i}) \quad (8)$$

Where n = number of days in the period 1990–2004. If the observed discharges are only available for a shorter period, then the observation period is used. Table 2.6 shows the ME for various model versions.

Table 2.6 Mean error when comparing the simulated discharges (m^3/s) to the observed discharges for the period 1990–2004 for the various model versions.

Discharge stations	Original version-1000m-no UZ	1000m grid-with UZ	1000m grid-500m topo	500m grid-1000m topo	500m grid-500m topo	500m grid-500m topo-new landuse
OmmeAa_25.11	-0.17	-0.16	-0.10	-0.25	-0.30	-0.44
VardeAa_31.13	-2.02	-1.56	-1.52	-1.28	-1.17	-1.47
SneumAa_35.03	0.09	0.17	0.21	-0.12	-0.12	-0.19
SkjernAa_dnst_25.14	-1.21	-0.42	-0.57	-0.31	-0.46	-0.84
HovenAa_25.37	-0.32	-0.15	-0.12	-0.15	-0.20	-0.24
SkjernAa_upst_25.08	-0.63	0.09	0.07	0.12	0.14	0.11

Both the old version and the final version of the model simulate larger discharges than the observed values. At some stations the absolute value of the ME is reduced, but at others it increases. This makes it difficult to conclude whether the new version performs better or worse than the old version of the model.

Another performance statistic is the Nash-Sutcliffe efficiency coefficient (E) of which the values are presented in Table 2.7. E is described as follows:

$$E = 1 - \frac{\sum_{t=1}^{T} (Q_{obs}^{t} - Q_{sim}^{t})^2}{\sum_{t=1}^{T} (Q_{obs}^{t} - \overline{Q_{sim}})^2} \quad (9)$$

Table 2.7 Nash-Sutcliffe model efficiency (E) when comparing the simulated discharges (m^3/s) to the observed discharges for the period 1990–2004 for the various model versions.

Discharge stations	Original version-1000m-no UZ	1000m grid-with UZ	1000m grid-500m topo	500m grid-1000m topo	500m grid-500m topo	500m grid-500m topo-new landuse
OmmeAa_25.11	0.84	0.83	0.74	0.85	0.76	0.81
VardeAa_31.13	0.70	0.63	0.41	0.73	0.65	0.67
SneumAa_35.03	0.81	0.77	0.65	0.78	0.71	0.75
SkjernAa_dnst_25.14	0.88	0.84	0.75	0.85	0.77	0.82
HovenAa_25.37	-0.08	-0.43	-1.37	-0.57	-1.70	-1.54
SkjernAa_upst_25.08	-1.19	0.67	0.67	0.62	0.59	0.64

Table 2.7 shows that the model efficiency (E) for the new version of the model is very close to, but slightly smaller than the E for the old version. In Table 2.8 the values for F_{bal} are presented. F_{bal} is described as follows:

$$F_{bal} = 100 \frac{\overline{Q_{obs}} - \overline{Q_{sim}}}{\overline{Q_{obs}}}, \quad (\%) \quad (10)$$

Table 2.8 F_{bal} (%) when comparing the simulated discharges (m^3/s) to the observed discharges for the period 1990–2004 for the various model versions.

Discharge stations	Original version-1000m-no UZ	1000m grid-with UZ	1000m grid-500m topo	500m grid-1000m topo	500m grid-500m topo	500m grid-500m topo-new landuse
OmmeAa_25.11	-2	-2	-1	-3	-4	-5
VardeAa_31.13	-17	-13	-13	-11	-10	-12
SneumAa_35.03	3	5	6	-4	-4	-6
SkjernAa_dnst_25.14	-5	-2	-3	-1	-2	-4
HovenAa_25.37	-60	-28	-22	-29	-37	-44
SkjernAa_upst_25.08	-40	6	4	8	9	7

Especially the F_{bal} value for the upstream Skjern Aa station (25.08) is improved, when comparing the final model version to the old version of the model, but also some of the other stations show improvements.

Based on the statistics above, the performance of the new model with respect to discharge is comparable to the old model. As can be seen in the figures in Annex 1, the new version shows an improved drying during the low-flow periods, approaching the low-flows better. During the high-flow periods, the new version sometimes gives too high peaks as compared to observations.

2.9 Comparison of simulated and observed groundwater heads

Comparison of simulated heads for various model versions

Important output for the study of the effects of climate change on water resources are the mean groundwater heads in various computational layers. In this study computational layers 1 and 5 are used because layer 1 is the upper groundwater reservoir and layer 5 is the main aquifer in the region. The mean is calculated for the period 1990–2004. Table 2.9 shows the mean groundwater heads for both layers for the same models versions as in Table 2.3.

Table 2.9 Mean groundwater heads (m) for computational layers 1 and 5 for various model versions. In brackets the standard deviation.

		Computational layer 1	Computational layer 5
1	1000m grid-no UZ	34.0 (±23.1)	32.0 (±21.8)
2	1000m grid-with UZ	33.9 (±23.0)	31.9 (±21.6)
3	1000m grid- 500m topography	33.8 (±23.2)	31.8 (±21.7)
4	500m grid- 1000m topography	33.8 (±23.3)	31.9 (±22.0)
5	500m grid-500m topography	33.5 (±23.4)	31.5 (±22.1)
6	500m grid-500m topography-new landuse	33.6 (±23.5)	31.6 (±22.1)

Comparison of simulated heads to observed heads

A tool is available that compares observed head values to simulated heads at the same location, depth, and time. The first simulated head value stored after the observation date is used for the comparison and a bilinearly interpolated value for the simulated head in the cell where the observation is located and the three closest cells is used, to account for the fact that an observation often is not located in the centre of the cell. This tool does not work for the original 2001 version. Therefore only three new versions of the model are compared to observed head data. One version of the model, called 1000m version-no abstractions, has all the same input files as the old version of the model, but with the 2-layer UZ-zone included. The other two are the final versions of the model with and without abstractions and irrigation and are called 500m version-no abstractions and 500m-with abstractions, respectively.

Observed head data from the national database JUPITER is used for this comparison. In total 4920 observations are used, located throughout the study area and the computational layers. The data set includes 13 longer time series (1990–2000) of monthly observations,

located mostly in computational layers 1, 2, and 3 and one series in layer 4 of the model. 1734 of the observations are a part of these time series.

Table 2.10 shows the distribution of the observations throughout the calculation layers. There is a slight difference in the distribution for the top 5 layers of the 1000m and 500m model versions because the lower-level boundaries for these layers are derived from different topography files. In total the number of observations is the same for the top 5 layers of both model versions.

ME and RMSE values were calculated as follows:

$$ME = \frac{1}{n}\sum_{i=1}^{n}(H_{obs,i} - H_{sim,i}) \tag{11}$$

$$RMS = \sqrt{\frac{1}{n}\sum_{t=1}^{T}(H_{obs} - H_{sim})^2} \tag{12}$$

Where n is the number of observations, and H_{obs} and H_{sim} are the observed and simulated heads, respectively.

Table 2.11 and 2.12 show the ME and RMS values for each calculation layer, respectively. The mean ME and RMS values, averaged for all layers, show a slight improvement for the 500m model versions.

Table 2.10 The number of groundwater head observations used per calculation layer for the 1000m and 500m model versions.

Computational layer	No. of observations – 1000m version	No. of observations – 500m version
1	814	789
2	1480	1352
3	1291	1452
4	463	450
5	233	238
6	176	176
7	96	96
8	73	73
9	49	49
10	57	57
11	75	75
12	64	64
13	25	25
14	14	14
15	9	9
16	1	1
Total	4920	4920

Table 2.11 ME (m) per calculation layer for the simulated groundwater head values compared to the observations for three model versions.

Computational layer	1000m version – no abs.	500m version – no abs.	500m version – with abs.
1	-0.21	0.14	0.23
2	1.04	0.98	1.25
3	0.54	0.20	0.44
4	0.14	0.58	0.83
5	-1.91	-1.62	-1.45
6	-1.43	-1.12	-0.94
7	-1.04	-0.69	-0.53
8	-2.45	-2.30	-2.10
9	-1.69	-1.65	-1.39
10	-2.27	-2.06	-1.72
11	-1.44	-1.23	-0.96
12	-1.51	-1.14	-0.75
13	-0.51	-0.44	0.12
14	-2.81	-2.66	-2.21
15	-0.82	-0.79	-0.44
16	7.37	6.42	6.87
Average all layers	-0.56	-0.46	-0.17
Average top 5 layers	-0.08	0.06	0.26

Table 2.12 RMS (m) per calculation layer for the simulated groundwater head values compared to the observations for three model versions.

Computational layer	1000m version – no abs.	500m version – no abs.	500m version – with abs.
1	2.81	2.75	2.77
2	3.44	3.58	3.82
3	3.19	2.78	2.90
4	5.26	5.44	5.44
5	5.70	5.37	5.33
6	4.32	4.22	4.18
7	3.21	3.06	3.04
8	4.08	4.04	3.92
9	3.34	3.43	3.37
10	3.66	3.63	3.63
11	2.82	2.75	2.75
12	3.09	2.97	2.94
13	3.83	3.60	3.86
14	4.05	4.00	4.09
15	4.64	4.45	4.59
16	7.37	6.42	6.87
Average all layers	4.05	3.91	3.97
Average top 5 layers	4.08	3.99	4.05

An average RMS value below 4 m is considered excellent for a large scale model such as the present covering Western Jutland.

3. Effects of Climate Change on Water Resources

Here the results are presented for the model simulations for South-West Jutland either including or not including abstractions for water supply, industry, and irrigation. The model is used in transient mode for the period 1971–2004. 1971 to 1989 is a warm up period, where the model is allowed to adjust itself to the prevailing hydrological conditions. The period from 1990 to 2004 is used as the prediction period.

3.1 Change in water balance and groundwater recharge

The water balance provides a general insight into the changes in the hydrological cycle of the catchment as a result of climate change. Table 3.1 and 3.2 show the spatially-averaged, mean annual values of the water balance for the groundwater system, for the simulations not including and including abstractions and irrigation, respectively. Both the absolute values and the relative changes in the water balance fluxes, when comparing the scenario runs to the current climate, are listed. The net recharge is defined as the flow out of the root zone minus the sum of evapotranspiration from the water table and net potential flow from the groundwater zone to the overland compartment, which occurs when the soil profile becomes completely saturated and the unsaturated zone is no longer active. The net horizontal boundary outflow is the net flow across the catchment boundary out of the catchment and accounts primarily for groundwater flow to the sea. Drain flow includes drainage from groundwater to rivers in the catchment and drainage to the sea in coastal regions. Base flow is the net flow resulting from groundwater flow to rivers.

Table 3.1 Average total water balance (mm/year) for the period 1990–2004 for the current climate, and the A2 and B2 scenarios (no abstractions included).

	Net Recharge	Horizontal Boundary Outflow	Storage Change	Drain Flow	Base Flow
Current climate	542	23	3	280	242
A2 scenario	605 (12%)	24 (4%)	7 (133%)	334 (19%)	255 (5%)
B2 scenario	652 (20%)	24 (4%)	6 (100%)	371 (33%)	263 (9%)

Table 3.2 Average total water balance (mm/year) for the period 1990–2004 for the current climate, and the A2 and B2 scenarios (abstractions included).

Scenario	Net Recharge	Horizontal Boundary Outflow	Storage Change	Drain Flow	Base Flow	Water Supply	Irrigation
Current climate	544	22	3	270	236	10	10
A2 scenario	610 (12%)	23 (5%)	7 (133%)	318 (18%)	247 (5%)	10	19 (90%)
B2 scenario	656 (21%)	24 (9%)	6 (100%)	357 (32%)	257 (9%)	10	15 (50%)

Net recharge from the unsaturated zone increases for both climate scenarios as a result of increases in precipitation during the winter months. The changes in recharge are of great interest because these changes drive the changes in the groundwater system and the stream discharges. Of the two scenarios B2 shows the largest increase (Table 3.1 and 3.2) because of less increase in evapotranspiration during summer and higher precipitation in the last two months of the year in comparison with the A2 scenario. Drain flow is the variable of the water balance that shows the largest absolute increases for the A2 and B2 climate scenarios. The increase in drain flow is the result of the groundwater levels reaching above the drain levels more often and in larger areas.

Figure 3.1 shows the spatially-averaged, mean monthly recharge from the unsaturated zone to the upper groundwater reservoir for the simulations that do not take abstractions and irrigation into account. However, as shown in Table 3.2 abstractions and irrigation only have little impact on the water balance components. Figure 3.1 clearly illustrates that the seasonal dynamics in recharge increase for both climate scenarios, with significant increase in recharge in the period from December to March and decreasing recharge during the late summer period from July to September.

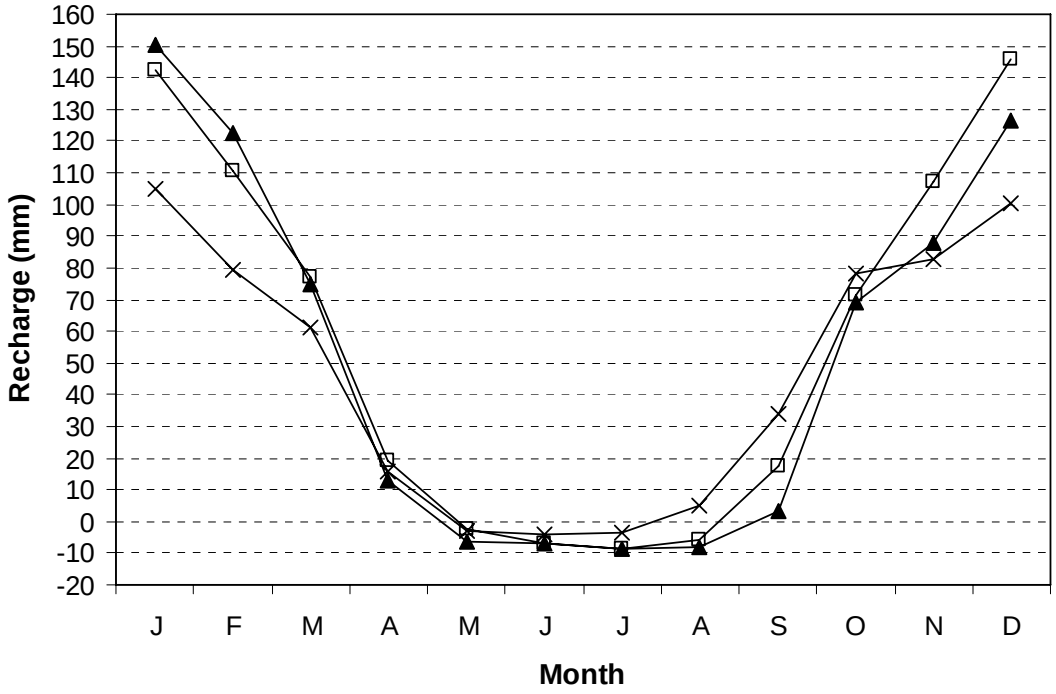

Figure 3.1 The area-averaged, mean monthly recharge from the unsaturated zone for the current climate (x) and A2 (▲) and B2 (□) scenarios for the simulations not including abstractions and irrigation.

The recharge to the main aquifer (layer 5) for the current climate and two scenarios is given in Table 3.3. As for recharge from the unsaturated zone to the upper layer of the groundwater system, the recharge to layer 5 shows a larger increase for the B2 scenario than for the A2 scenario. Figure 3.2 shows the mean monthly recharge to layer 5 for the simulations without abstractions and including abstractions, and for the current climate and two scenarios. During the winter months the recharge to the aquifer is the same for

the simulations with and without abstractions because irrigation does not occur (irrigation starts in May). The largest increases occur from January to April when comparing the climate scenarios to the current climate. During summer and autumn the scenario runs only show a slight increase or even a slight decrease in recharge, when abstractions are not included. The effect of irrigation on the recharge to layer 5 is obvious during the summer months, when the increase in recharge is much larger for the simulations including abstractions and irrigation.

Table 3.3 Mean recharge (mm/year) to the main aquifer (layer 5) for the current climate, and the A2 and B2 scenarios.

	Current	A2	B2
No abstractions	199	214	222
Incl. abstractions	204	221	228

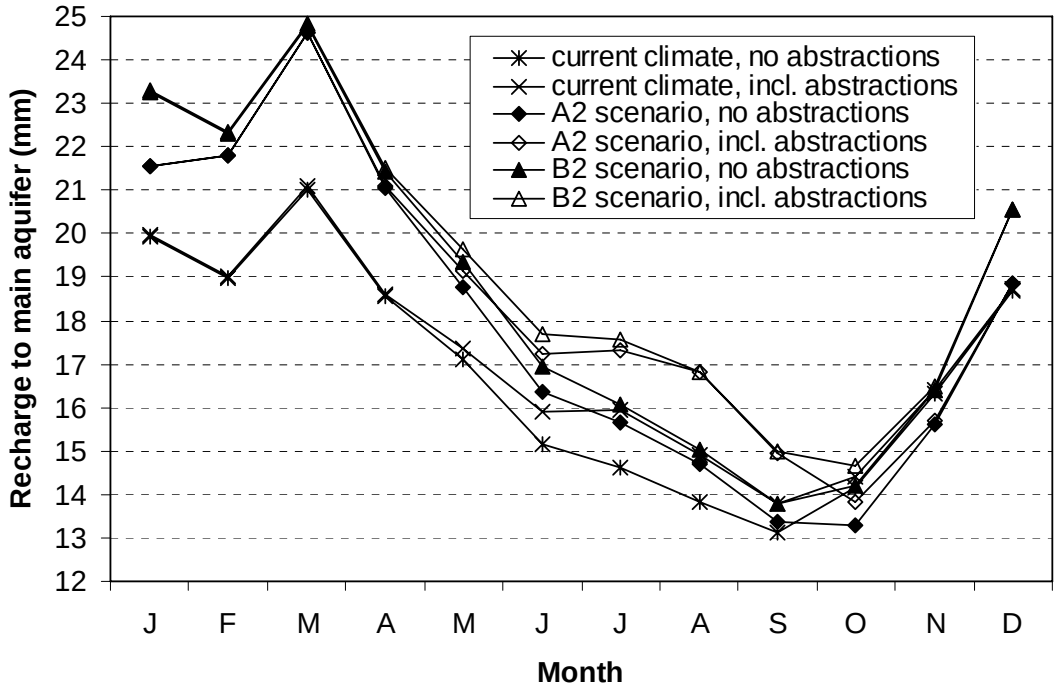

Figure 3.2 Mean monthly recharge (mm) to the main aquifer (layer 5) for the simulations not including and including abstractions, and for the current climate and both scenarios.

3.2 Change in mean groundwater heads

Table 3.4 shows the absolute change in mean groundwater head for model layer 1 and 5 when comparing the A2 and B2 scenario runs to the current climate simulation. For the current climate the spatially-averaged, mean annual groundwater heads in layer 1 are 33.6 and 33.5 m for the simulations not including and including abstractions, respectively. In layer 5 the mean annual groundwater heads equal 31.6 and 31.4 for the current climate, for the simulations not including and including abstractions, respectively. Corresponding to the larger increase in recharge, the B2 scenario also shows larger increases in mean annual groundwater heads. The groundwater heads in layer 5 increase more than in layer

1 because in layer 1 the rise in groundwater level is restricted by the drains, which have been defined in the entire catchment at a depth of 0.5 m below ground surface.

Table 3.4 Change in mean groundwater head (m) for model layer 1 and 5, when comparing the A2 and B2 scenario runs to the current climate simulation for the model versions with and without abstractions (abs).

	A2 scenario		B2 scenario	
	No abs	With abs	No abs	With abs
Upper unconfined aquifer (computational layer 1)	0.19	0.17	0.32	0.31
Main aquifer (computational layer 5)	0.28	0.22	0.45	0.44

Table 3.5 shows the percentage of the model area with an increase in head between 0.25–1.00 m and greater than 1.0 m. Figures 3.3 and 3.4 show the spatial distribution of the absolute changes in mean groundwater head for layer 1 and 5 for the simulation without abstractions and including abstractions, respectively. A considerable variation in the changes in groundwater heads can be seen, controlled mainly by the distance from streams, the geology of the subsurface, and the depth to the groundwater table.

Table 3.5 Percentage of the model area with an increase in head between 0.25–1.0 m and greater than 1.0 m.

		Percentage of the model area (%)			
		A2 scenario		B2 scenario	
		No abs.	With abs.	No abs.	With abs.
Upper unconfined aquifer (computational layer 1)	0.25 – 1.0	23	21	31	31
	≥ 1.0	3	3	7	7
Main aquifer (computational layer 5)	0.25 – 1.0	38	30	51	50
	≥ 1.0	4	3	9	8

The spatially-averaged, mean groundwater heads in layer 1 are compared for the end of the winter (January to March) and after summer (August to October) for the A2 and B2 scenarios and the current climate. The results show that the seasonal amplitude increases 40–50% (e.g. from 0.7 m to 1 m for the A2 scenario including abstractions). This is mainly due to the increase in groundwater heads during the winter months, whereas the mean summer values show no change for the A2 scenario and slight increases for the B2 scenario when compared to the current climate. The spatial distribution does show a decrease in groundwater heads of up to 0.5 m in large parts of the catchment area for the summer period.

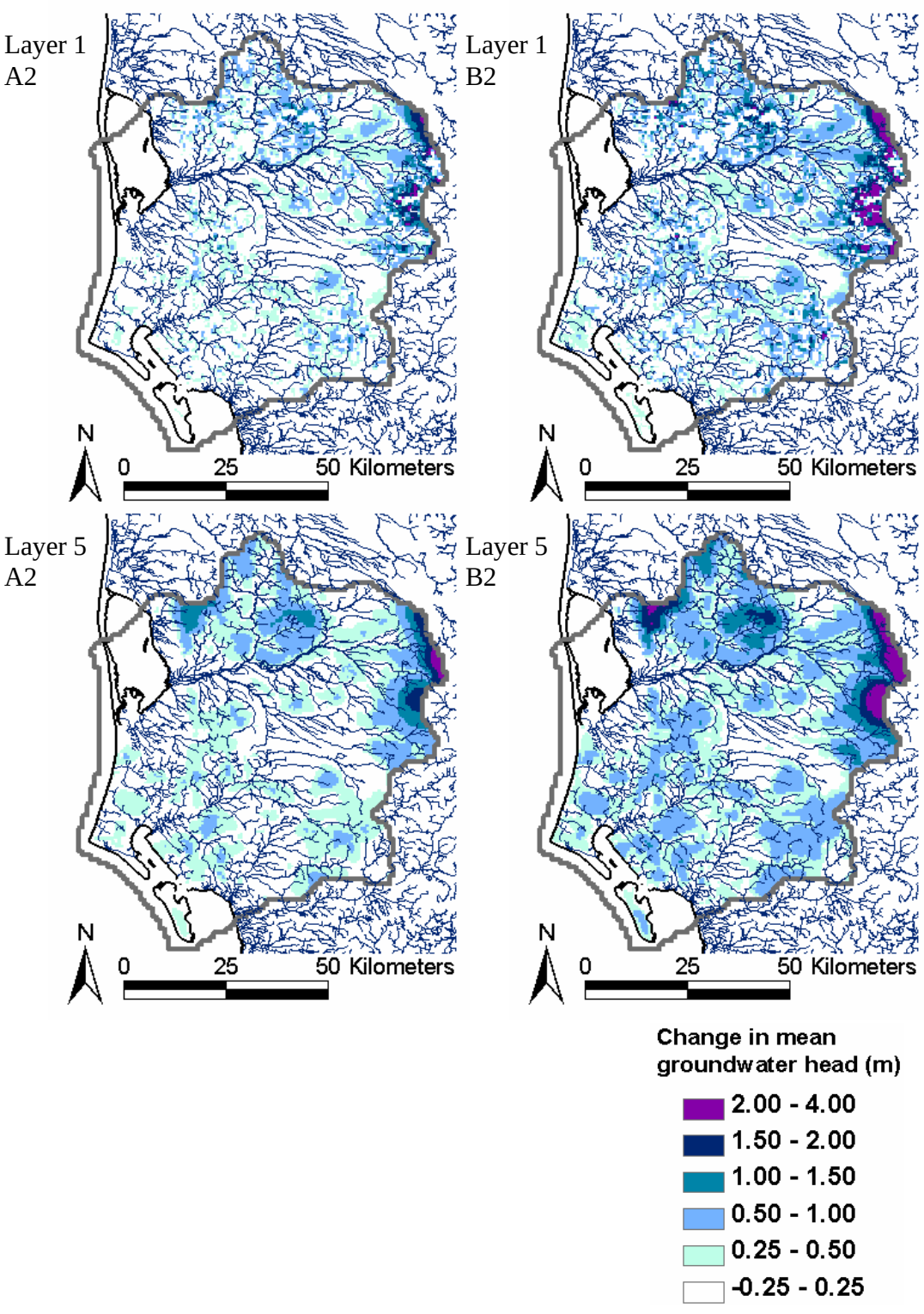

Figure 3.3 Change in mean groundwater head when comparing the A2 and B2 scenario results to the current climate results for model layer 1 and 5 (no abstractions or irrigation).

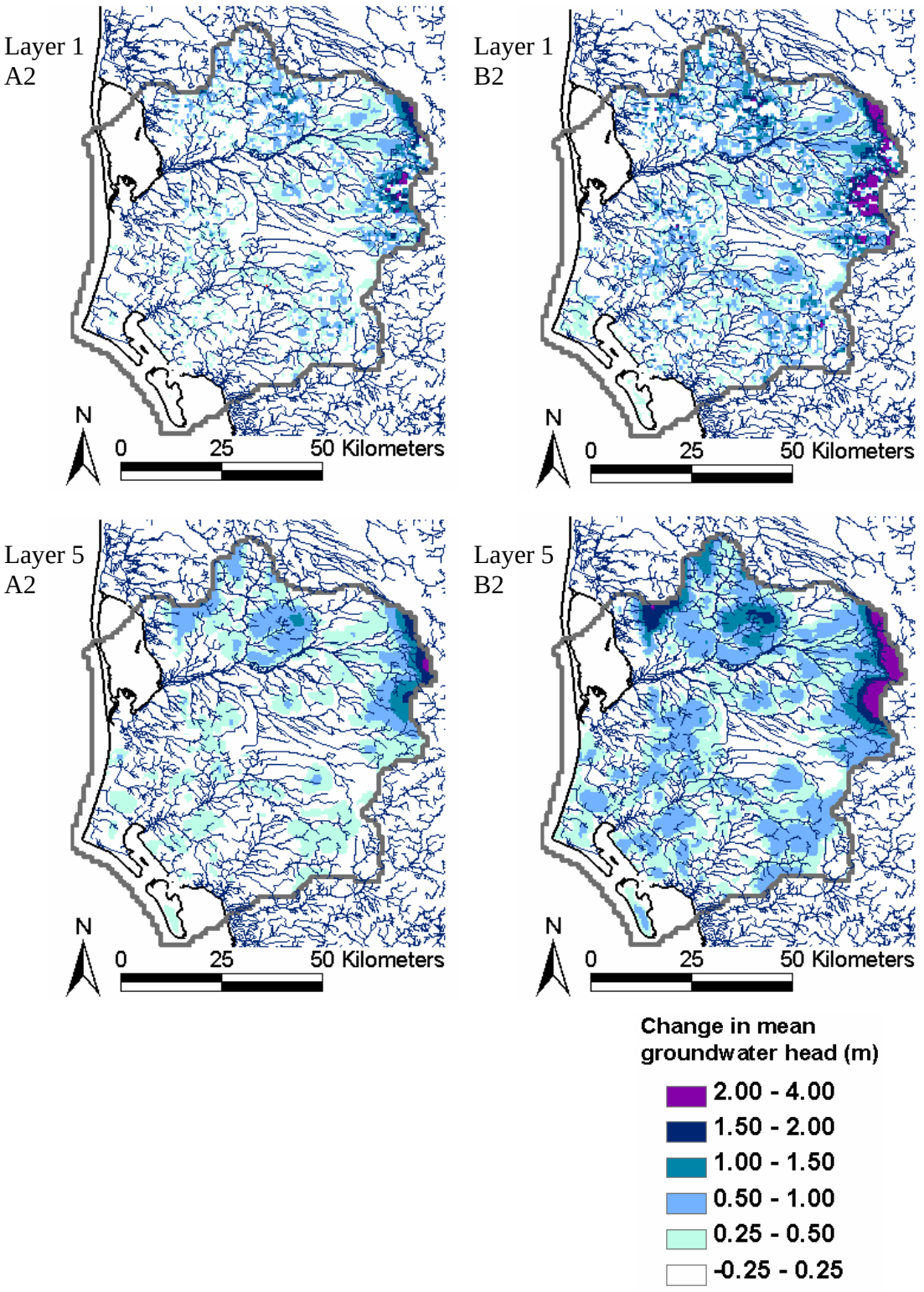

Figure 3.4 Change in mean groundwater head when comparing the A2 and B2 scenario results to the current climate results for model layer 1 and 5 (with abstractions and irrigation).

3.3 Change in river discharges

The changes in river discharge for the two scenario runs compared to the current climate run are retrieved for the six stations listed in Table 2.5. The rising groundwater levels result in increases in mean annual stream discharges partly due to increasing base flow and partly because of increasing drain flow, where the latter is due to the longer time and larger area where groundwater levels rise above the drain levels. The mean daily discharges for the current climate and scenarios A2 and B2 are presented in Table 3.6 for the simulations with and without abstractions. The mean daily discharges for the current climate for the simulations including abstractions are around 3% smaller than for the simulation without abstractions for most stations. For the three stations with the largest catchment area (25.14, 25.11, and 31.13) the A2 scenario results in a relative increase around 13%, whereas the B2 scenario results in an increase around 21%. The inclusion of abstractions results in slightly smaller relative increases when compared to the situation without abstractions, but the difference is generally below 1%.

As a result of the increased dynamics in recharge (Fig. 3.1) it can be expected that seasonal changes in stream discharge occur as well. The absolute and relative changes in monthly mean discharges for the simulations without abstractions are shown in Figures 3.5 and 3.6, respectively. The changes in monthly discharges for the situation with abstractions are shown in Figures 3.7 and 3.8. Large increases occur during the winter months, but also significant decreases during the late summer months are seen. Generally the relative changes in monthly mean discharges are very similar when comparing the changes for the simulations with and without abstractions. A slightly larger decrease in discharge can be seen for the A2 scenario during October/November at some of the stations for the simulation including abstractions.

Table 3.6 Simulated mean daily discharges (m^3/s) at the discharge stations for the current climate and scenarios A2 and B2 for the simulations with and without abstractions. N.a. means no abstractions. W.a. means with abstractions.

Scenario	Discharge stations											
	25.11		31.13		35.03		25.14		25.37		25.08	
	n.a.	w.a.	n.a.	w.a.	n.a.	w.a.	n.a.	w.a.	n.a.	w.a.	n.a.	w.a.
Current	8.9	8.6	13.5	13.0	3.5	3.4	23.8	23.1	0.9	0.8	1.5	1.3
A2	10.1	9.7	15.2	14.5	3.8	3.7	26.8	25.9	1.1	1.0	1.7	1.4
B2	10.9	10.5	16.3	15.6	4.1	4.0	28.5	27.7	1.2	1.1	1.8	1.6

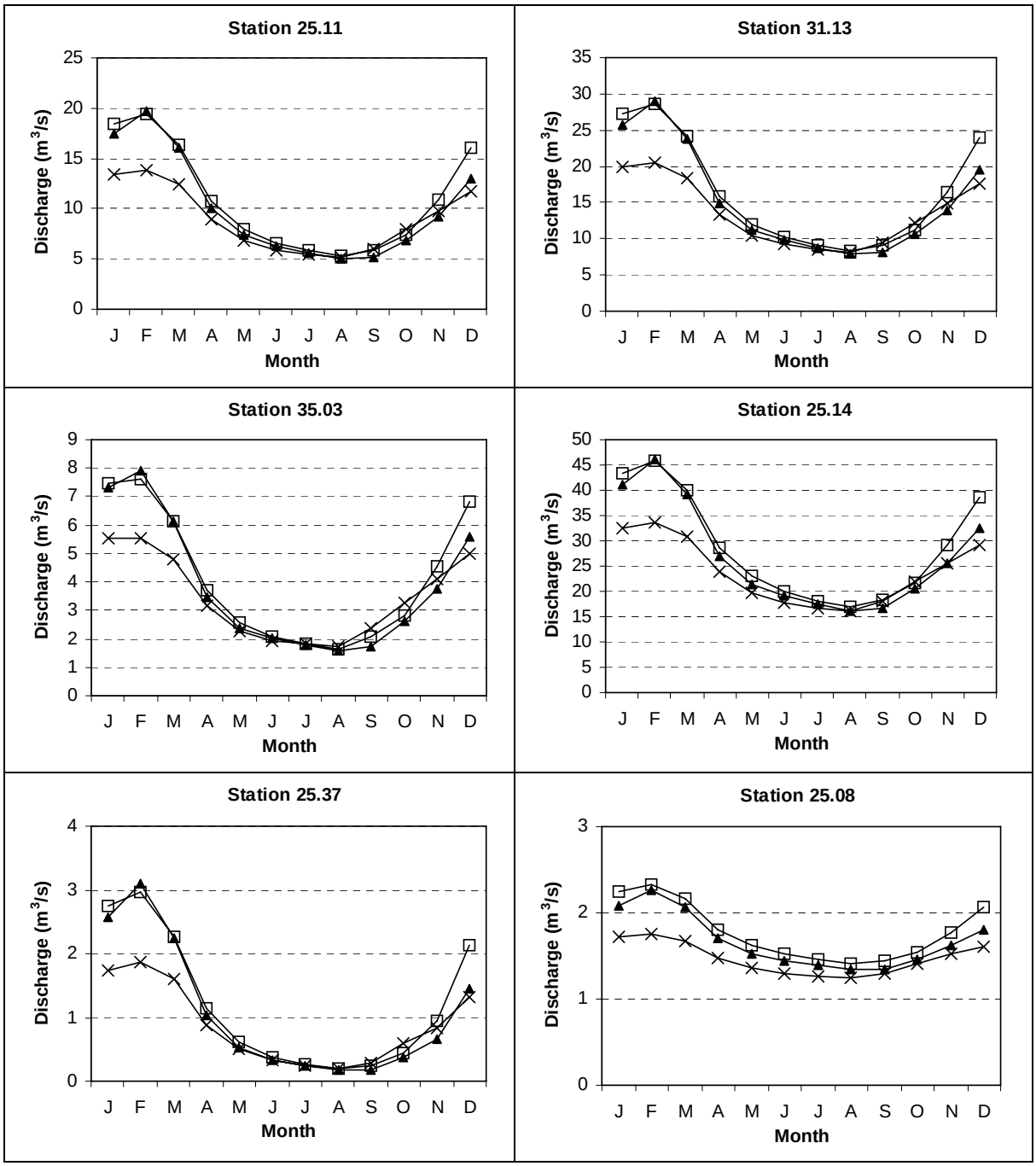

Figure 3.5 Monthly mean discharge for the current climate (x), the A2 scenario (▲), and the B2 scenario (□) for the situation without abstractions or irrigation.

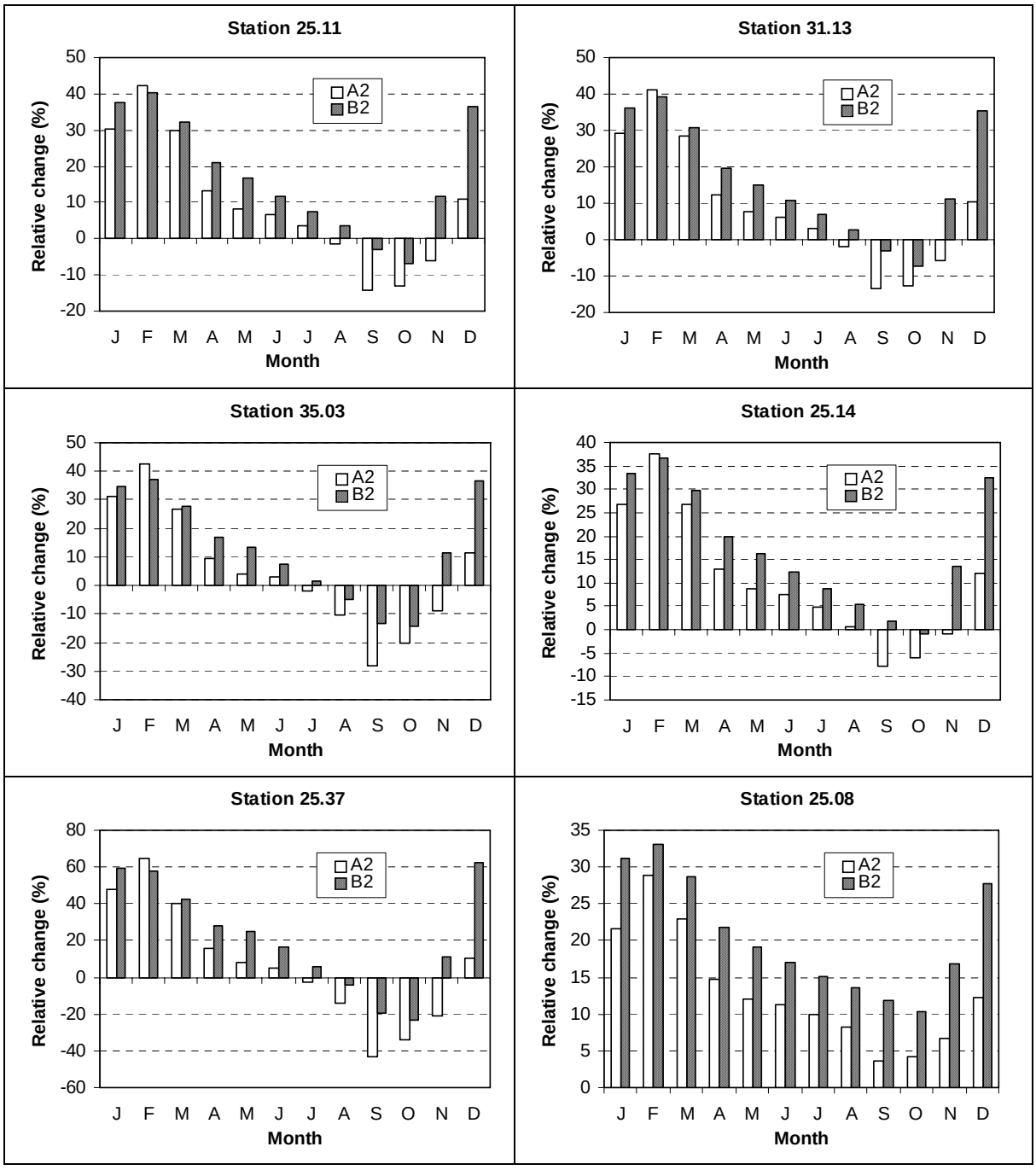

Figure 3.6 Relative change in monthly mean discharge when comparing the A2 and B2 scenario to the current climate for the situation without abstractions or irrigation.

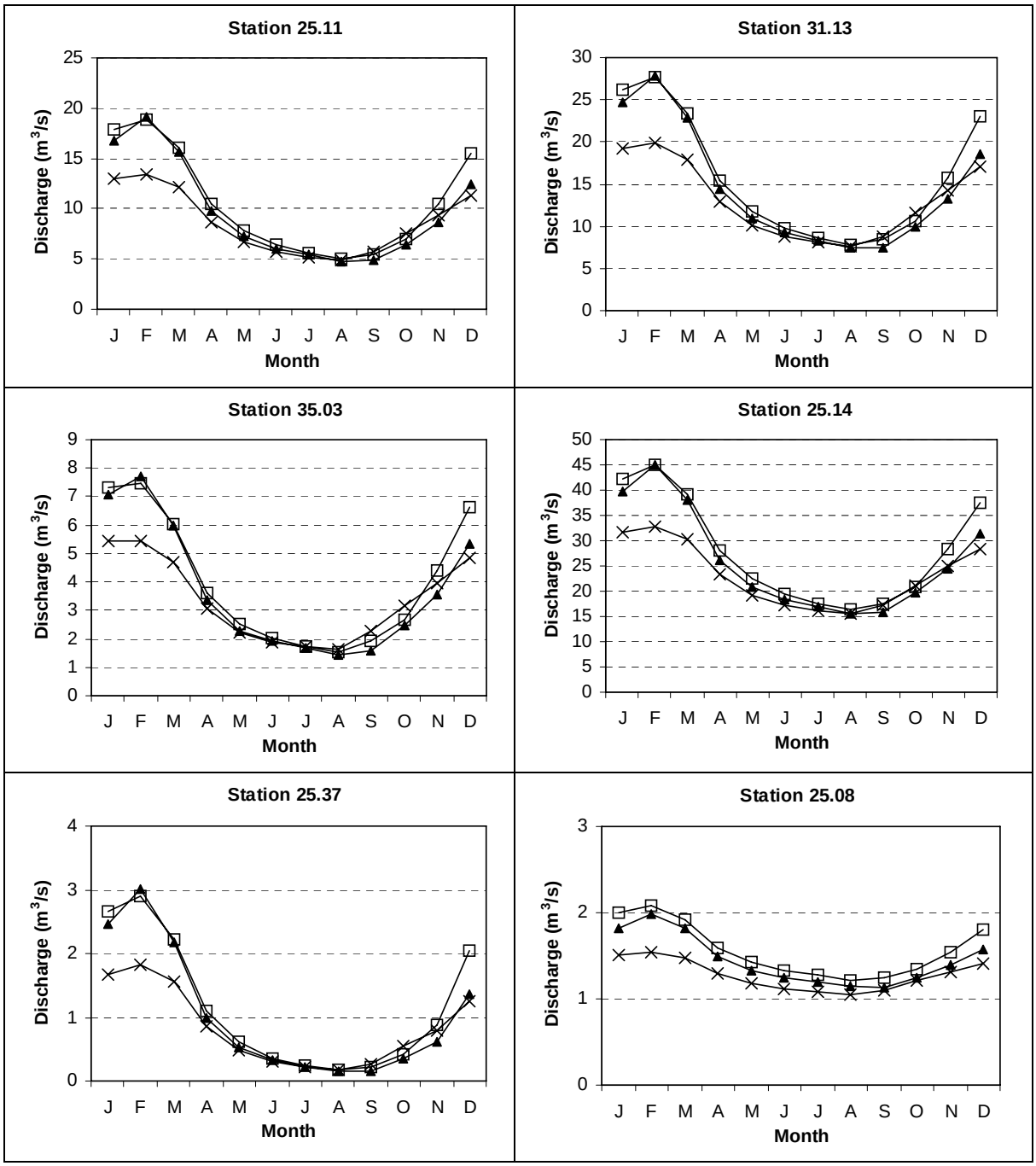

Figure 3.7 Monthly mean discharge for the current climate (x), the A2 scenario (▲), and the B2 scenario (□) for the situation including abstractions and irrigation.

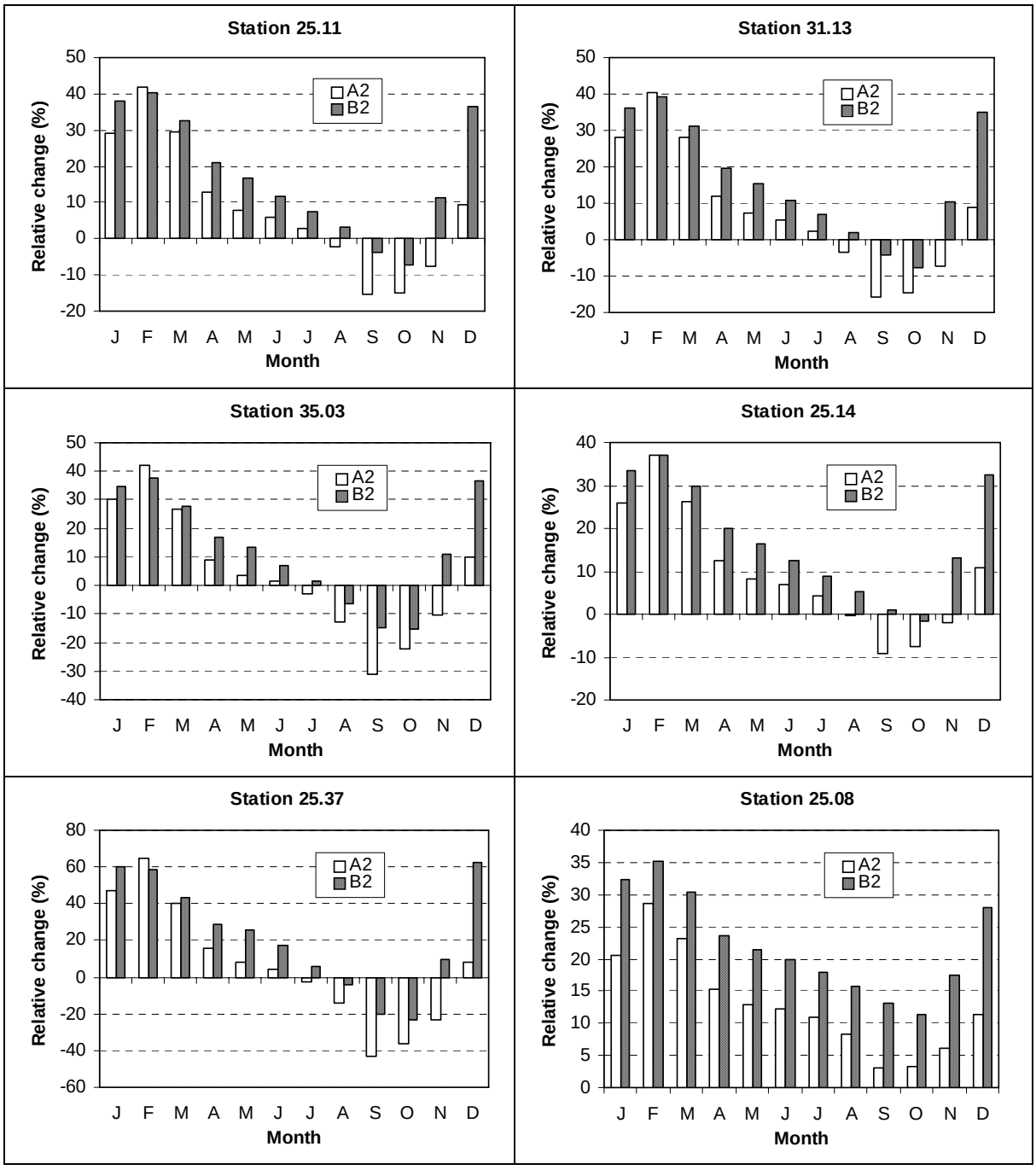

Figure 3.8 Relative change in monthly mean discharge when comparing the A2 and B2 scenario to the current climate for the situation including abstractions and irrigation.

Table 3.7 shows the percentile values for the current climate for the simulation without abstractions. Figure 3.9 shows the percentage change in these percentile values when comparing the A2 and B2 scenario values to the current climate values. Especially the higher percentile values increase when comparing the scenarios to the current climate.

Table 3.7 Percentile values for discharge (m^3/s) for the current climate (no abstractions or irrigation)

Station	Percentile value			
	5%	25%	75%	95%
25.11	4.43	5.52	10.48	19.65
31.13	7.03	8.66	15.65	29.11
35.03	1.46	1.88	4.14	8.48
25.14	14.49	17.02	27.29	44.18
25.37	0.13	0.237	1.06	3.05
25.08	1.15	1.27	1.58	2.05

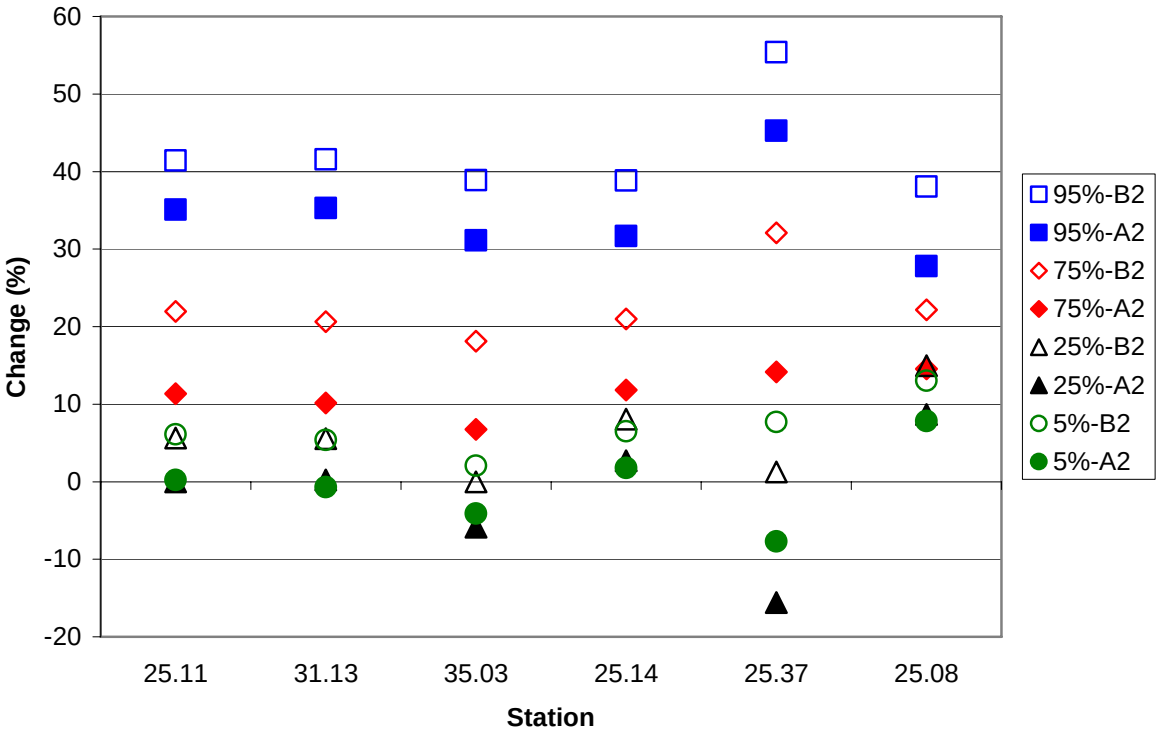

Figure 3.9 Relative change (%) in the percentile values for the A2 and B2 scenario compared to the current climate

3.4 Effect of sea-level rise

One of the scenarios investigated in this study is a 1 m sea level rise. Figure 3.10 shows the area which would be flooded if the sea level were to rise 1.0 m above the current mean average sea level (masl). The 1 m sea level rise is considerably higher than the projections of 0.23 to 0.51 m for the A2 scenario (Meehl et al., 2007), but 1 m is used as

a high-end estimate because of the considerable regional variability in sea level change (± 0.15 m for a typical AOGCM model projection) and the great uncertainty related to the increase in discharge from ice sheets. The set up for this simulation includes the transformation of all land areas below 1 m in the study catchment to sea, the removal of the drains in these areas, and the head boundary condition at the downstream end of the streams was raised from 0 to 1 m.

The eustatic sea level rise could be counter balanced by the isostatic uplift, which has been occurring in Denmark since the melting of the ice caps. In Mertz (1924) a map shows that the largest uplift occurs in the northernmost part of Denmark, whereas negligible uplift occurs in the middle of Jutland. For our study area no significant influence of isostatic uplifting on the relative sea level is expected as it is located just south of the 0 m uplift line.

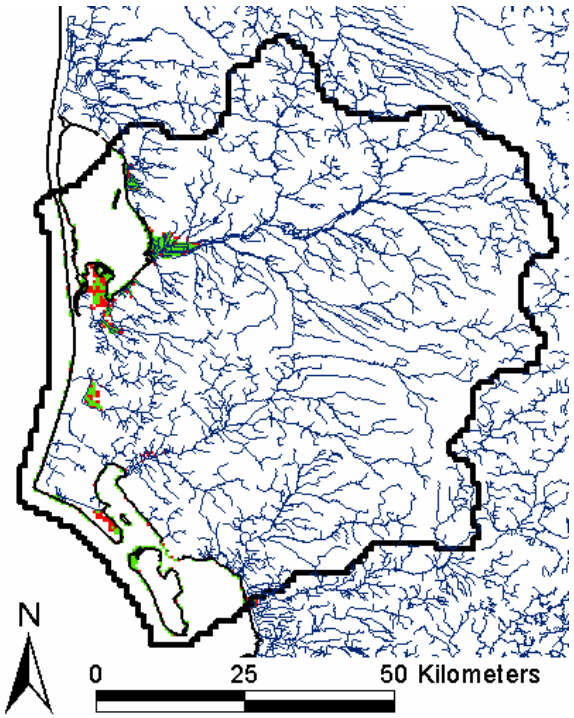

Figure 3.10 In green and red the flooded area, if the sea-level rise equals 0.5 m and 1.0 m above current mean average sea level, respectively.

The water balance is extracted, but only for the area which is not flooded (Table 3.8). Recharge increases slightly (3%) and drain flow increases considerably (10%) due to the higher groundwater levels in the upper layers when the sea level rises to 1 m.

Table 3.8 Average total water balance in mm/year for the period 1990-2004 for the current climate and the 1m sea-level rise scenario (no abstractions or irrigation)

	Net Recharge	Hor. Bou. Outflow	SZ Stor. Change	Drain Flow	Base Flow
Current climate	545	48	3	248	252
Current climate +1masl	560	33	3	276	254

Figure 3.11 shows the increases in mean groundwater levels, when comparing the 1 m sea level rise simulation to the current masl simulation for the current climate and the B2 scenario without abstractions. The sea level rise influences the groundwater heads up to 10 km inland along the coast. The effect of sea level rise is significant for low-lying areas, where the simulated increase in groundwater levels for the B2 scenario is up to 0.5 m. The values presented in Figure 3.11 only show the effect of the rise in sea level and should thus be added to the increase in groundwater levels due to the changes in meteorological input. No large differences in the increases in head occur, when comparing the effects of sea level rise for the current climate and for the B2 scenario.

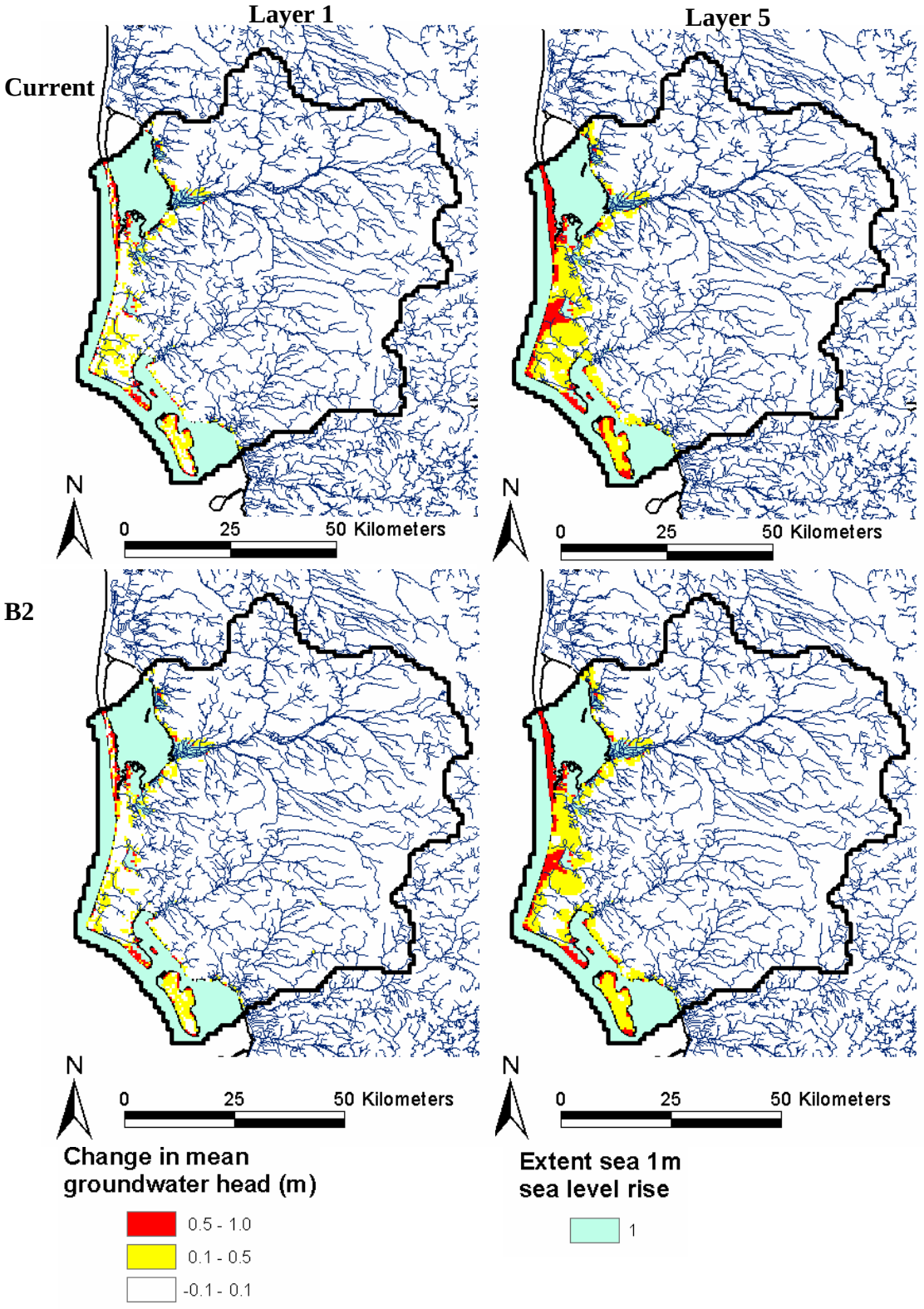

Figure 3.11 The difference in mean groundwater head (m) for computational layer 1 and 5, when substracting the mean groundwater head for the current climate and the B2 scenario, from the mean heads for the 1m sea level rise situation. The extent of the sea for the 1 m sea level rise scenario is indicated in blue.

4. Indirect effects of climate change on water resources

4.1 Changes in irrigation volume

As a result of climate change drier soil conditions are expected to occur during the summer months because of the decrease in precipitation and the increase in reference evapotranspiration. Figure 4.1 shows the soil moisture storage for each month, spatially-averaged for the whole catchment. From March to September soil moisture decreases for both climate scenarios compared to the current climate, whereas it increases from October to February. Especially in August a significant change occurs, where soil moisture continues to decrease for both climate scenarios, whereas it remains constant in the current climate. This indicates that significantly more drying occurs towards the end of the summer as a result of climate change than in the current climate. Most of the soils in the catchment area are sandy and the drying effect on such soils will be most pronounced. Irrigation demand is therefore expected to increase considerably in the catchment due to climate change.

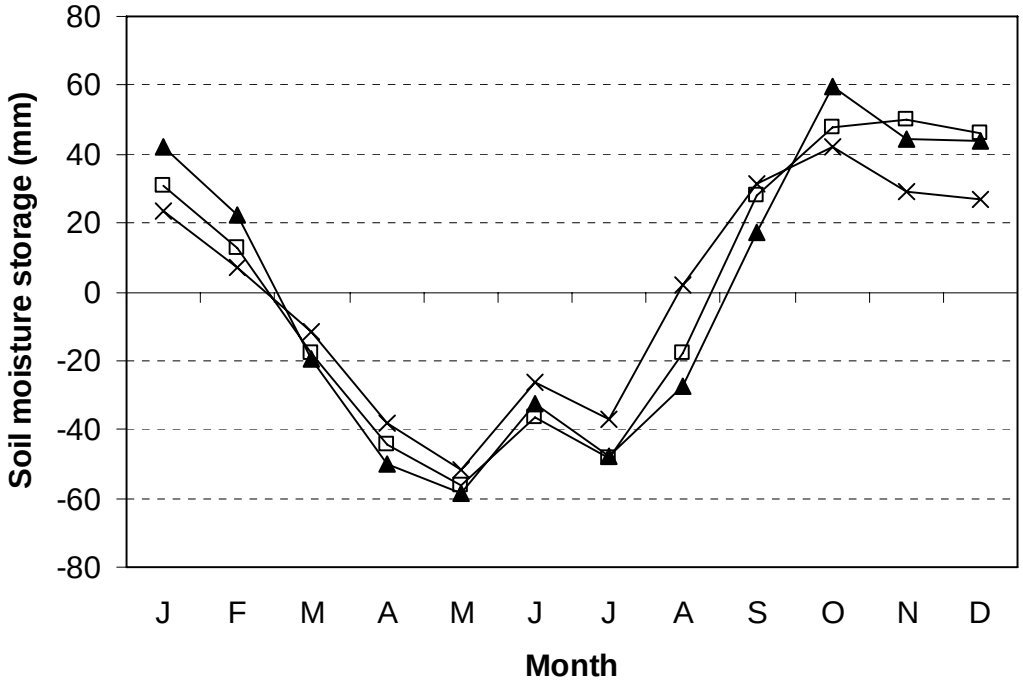

Figure 4.1 Soil moisture storage (mm) in the unsaturated zone for the current climate (x), the A2 scenario (▲), and the B2 scenario (□) for the simulations not including abstractions and irrigation.

When only the area covered by grass is considered, the mean annual irrigation volume for the current climate equals 52 * 10^6 m^3. Mean annual irrigation increases to 100 * 10^6 m^3 and 79 * 10^6 m^3 for the A2 and B2 scenario, respectively, corresponding to relative increases of 91% and 50%. Figure 4.2 shows the annual irrigation volume for the period 1990–2004 for the current climate, and the A2 and B2 scenarios. As expected, the A2 scenario results in the largest increases in irrigation. The increase in irrigation is especially large for the years, where less irrigation is needed in the current climate (e.g., up to 320% for the A2 scenario in 2001).

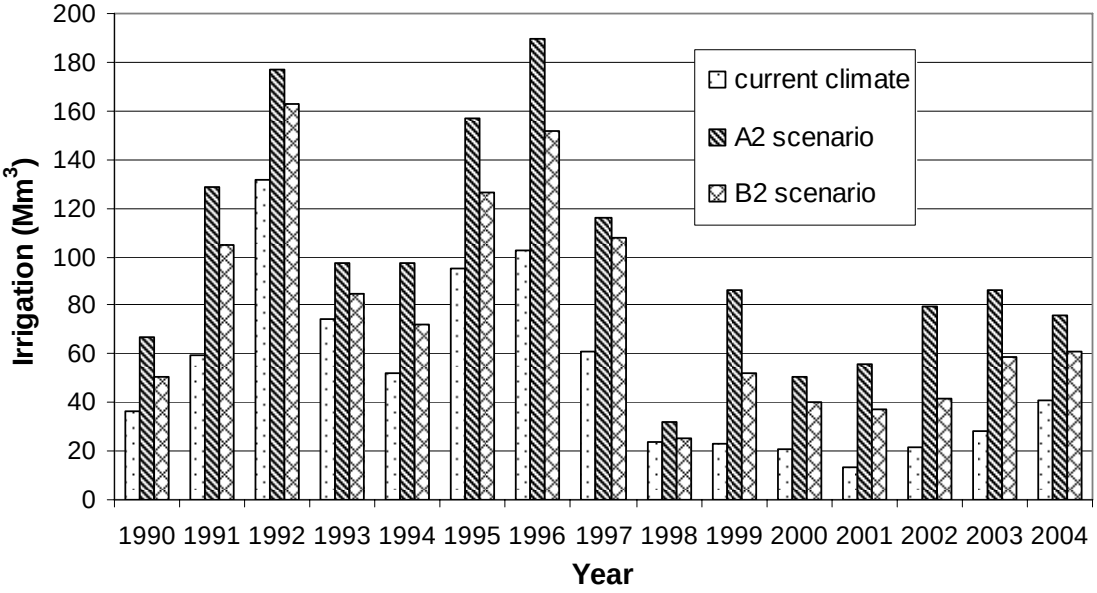

Figure 4.2 Mean annual irrigation for the current climate and the A2 and B2 scenarios.

Figure 4.3 shows the mean monthly irrigation volume for the current climate and both scenarios. The largest increases in irrigation occur in August and September. The peak irrigation month shifts from July to August for both scenarios. Table 3.2 shows that the abstractions for households, industry, and irrigation as a whole, only constitute a small part of the annual mean water balance. The absolute differences in mean groundwater levels and discharges are therefore not very large, when comparing the simulations including and not including abstractions and irrigation. However, since the irrigation water is primarily abstracted in the period June to September, where the net recharge is low or even negative (Fig. 3.1), it results in a pronounced impact on base flow to streams.

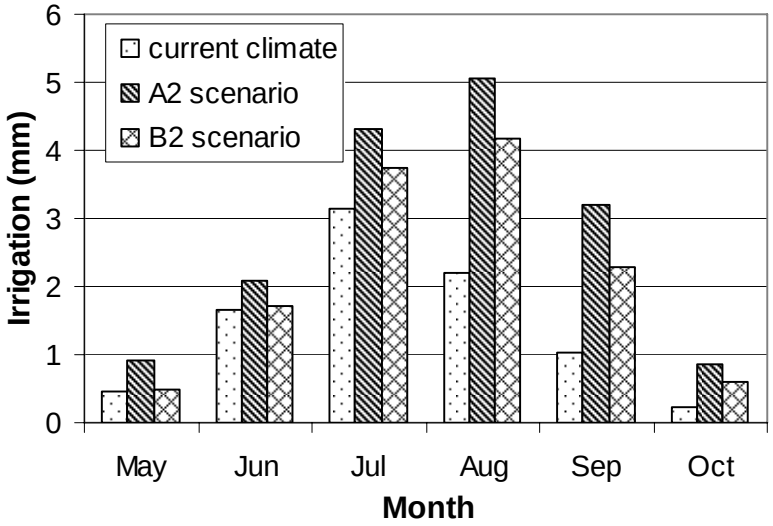

Figure 4.3 Mean monthly irrigation (mm) for the current climate and the A2 and B2 scenarios.

In Figure 4.4 the relative changes in mean monthly discharge are shown, when including abstractions and irrigation in the simulations. The mean monthly discharges during the summer months are a few percent lower when abstractions and irrigation are considered and the impact is further exacerbated in the scenario runs. For example, the October discharge for station 25.37 is changed by -10% for the A2 scenario while the relative change equals -7% for the present climate. It should be emphasized that irrigation demands have only been accounted for on areas covered by grass, whereas increasing demands for irrigation on other crops have not been included. Therefore, the effect of climate change on irrigation and hence on stream discharge during the low flow season, is most probably underestimated.

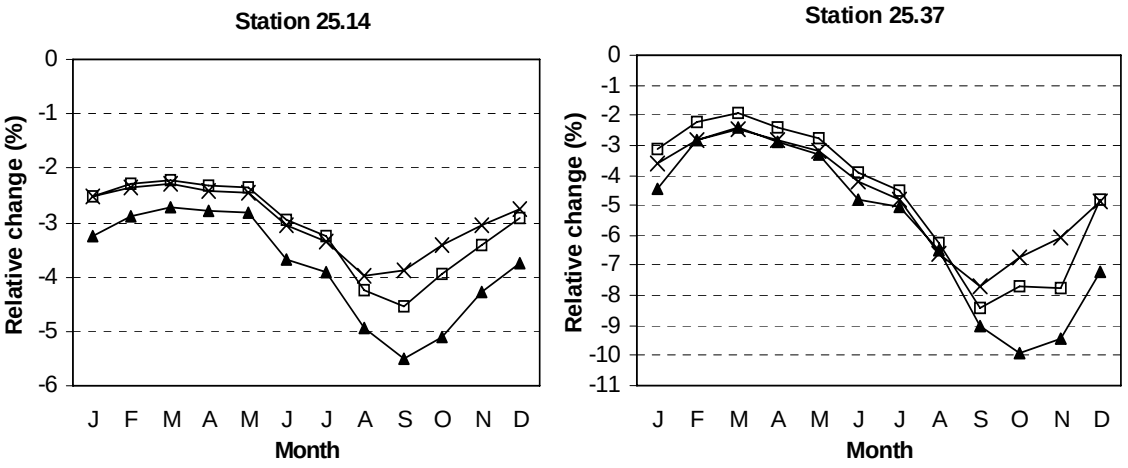

Figure 4.4 Relative difference (%) in mean monthly discharge, when comparing the simulation including abstractions and irrigation to the simulation not including abstractions and irrigation, for the current climate (x), the A2 scenario (▲), and the B2 scenario (□).

Figure 4.5 shows for every month the monthly irrigation volume for all years. In May and October irrigation only occurs in a few of the years in the current climate, and this remains the same for the scenarios, though irrigation occurs one or two years more often. August and September show three and two more years when irrigation occurs for the A2 and B2 scenarios, respectively, when comparing to the current climate.

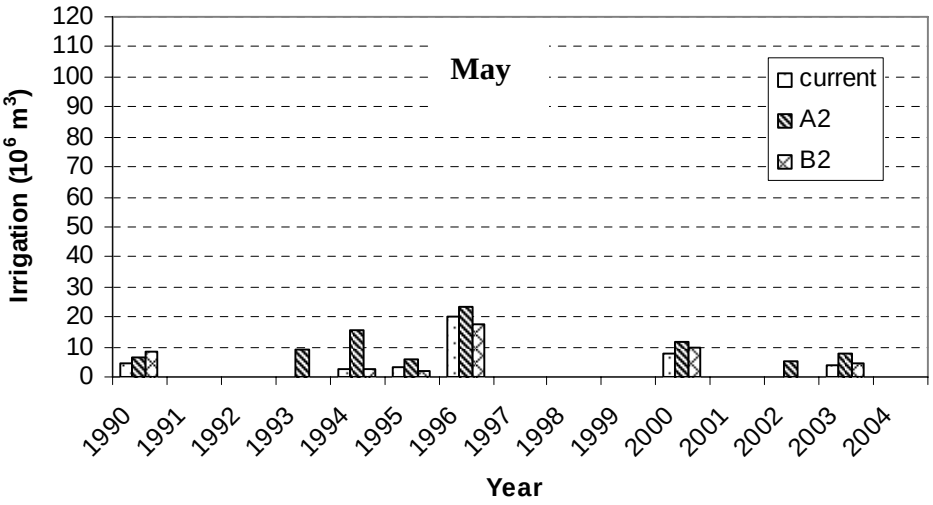
May
current
A2
B2
Irrigation (10^6 m^3)
Year

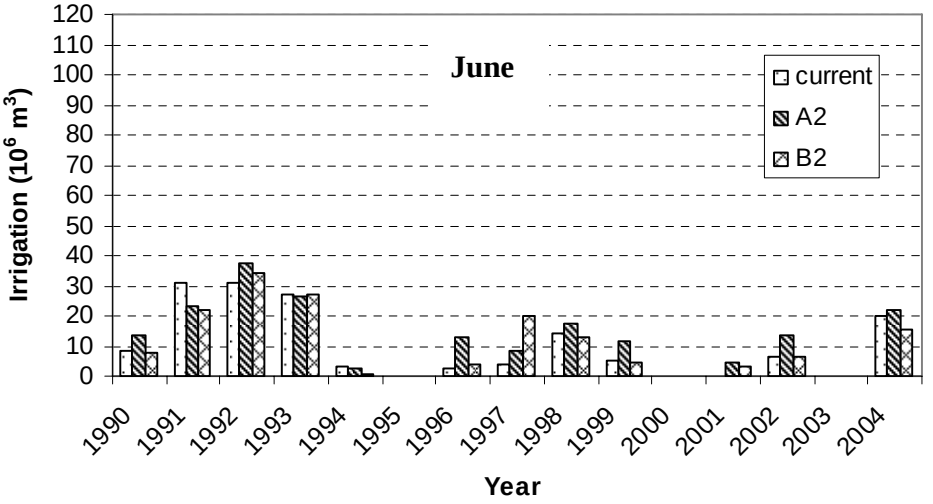
June
current
A2
B2
Irrigation (10^6 m^3)
Year

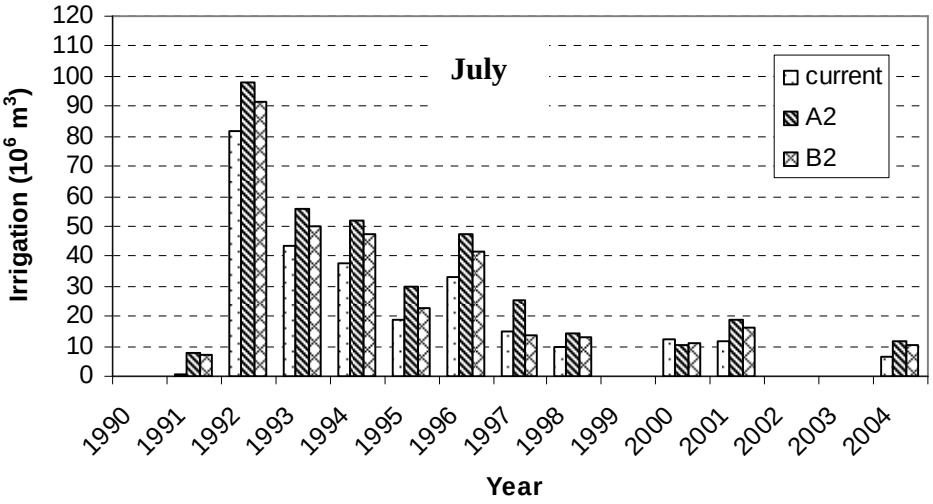
July
current
A2
B2
Irrigation (10^6 m^3)
Year

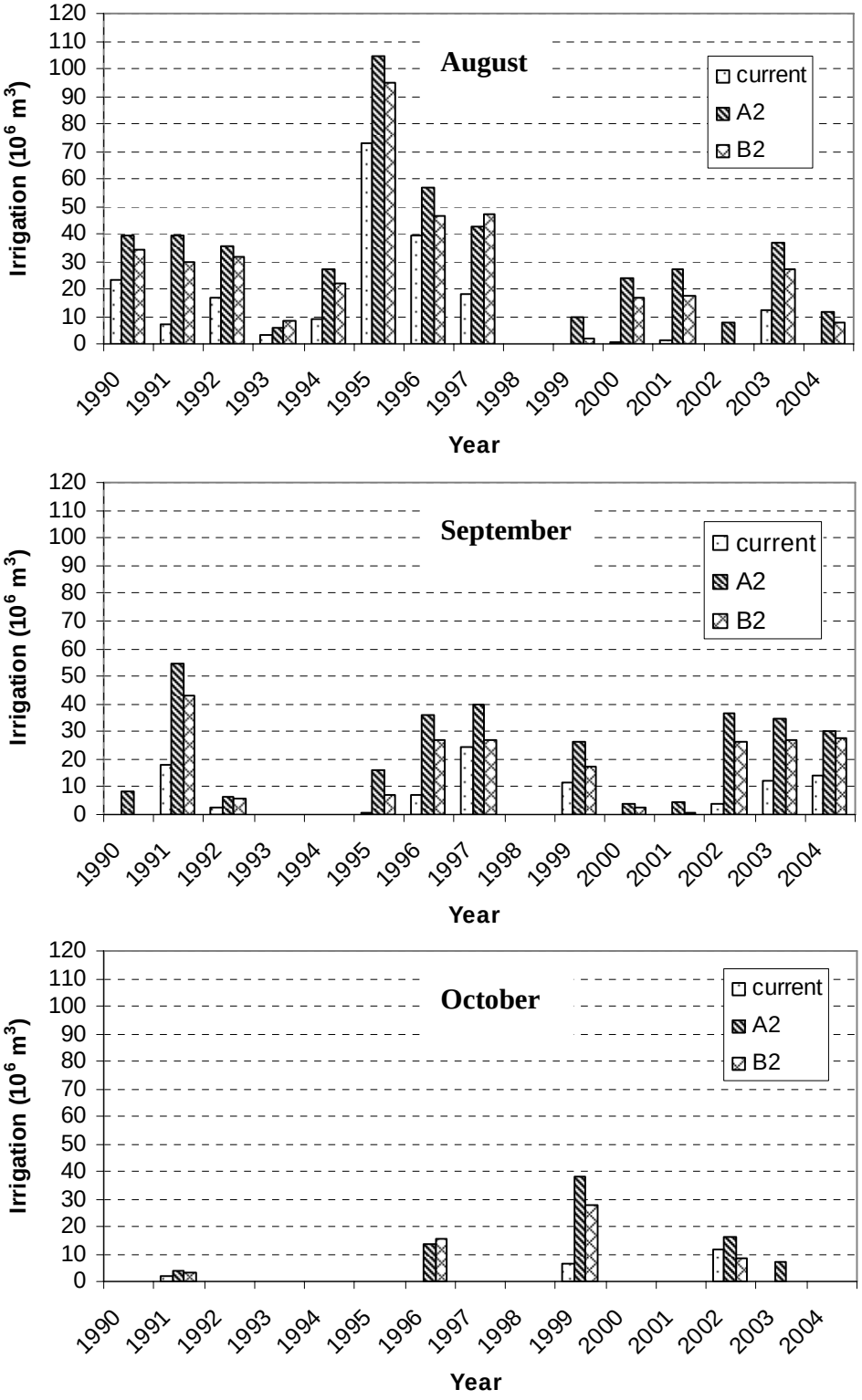

Figure 4.5 Monthly irrigation volume for all years for the current climate and the A2 and B2 scenarios.

4.2 Effects of changes in land use

To study the effects of land-use changes, a subcatchment is selected encompassing the upstream part of the Skjern River catchment (Fig. 2.2). The size of the subcatchment is 1038 km^2. The land use distribution is 61% grain, 2% urban, 18% grass, 6% heather, and 13% forest. A policy of the Danish government is to double the forested area in Denmark within the next 80 to 100 years. Because of the higher potential evapotranspiration for forests compared to agricultural areas, it is expected that this policy will impact the recharge in a catchment. To quantify these effects, simulations are run with the forested area twice as large as for the baseline scenario. This is done by changing all 724 grid cells with land use class grass in the subcatchment to forest, increasing the forested area to 230% of the original area. As a comparison another simulation is carried out, where 724 cells with land-use class grain are changed to forest. Figure 4.6 shows the mean monthly actual evapotranspiration for the grass-to-forest and no-land-use-change scenarios, for the current climate and the A2 scenario. It can be seen that changing the land use from grass to forest increases the actual evapotranspiration considerably from May to July, while the absolute increase is only very small in the winter.

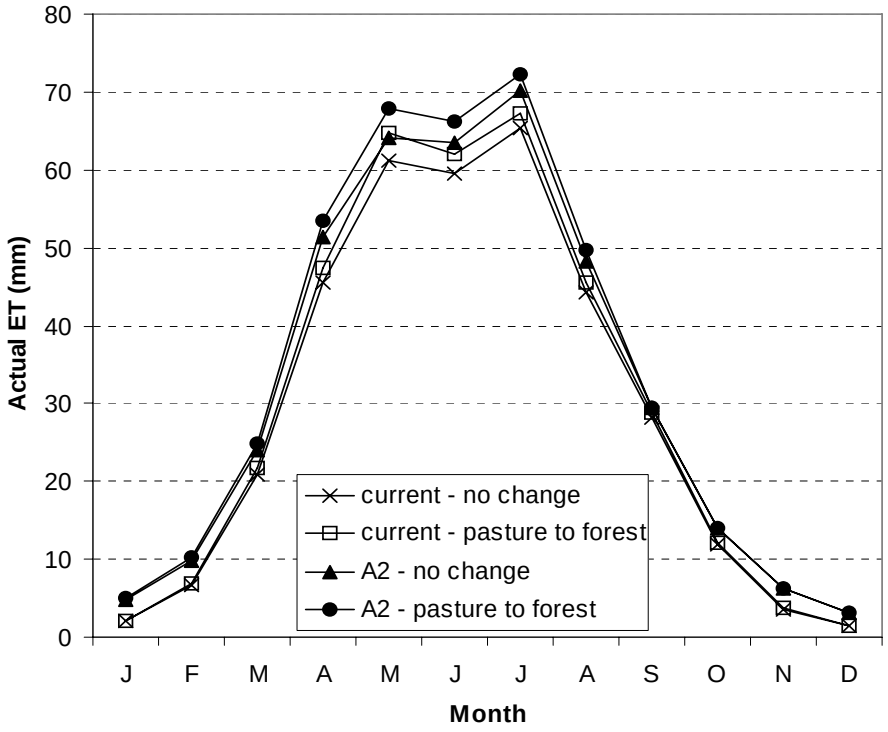

Figure 4.6 Mean monthly actual evapotranspiration for the grass-to-forest and the no-land-use-change scenarios, for the current climate and the A2 scenario.

When grass is changed to forest, the average recharge in the current climate is reduced from 551 mm/year to 526 mm/year, corresponding to a relative decrease of 5%. When grain is changed to forest, the recharge decreases with 4% to 531 mm/year. These simulation results suggest that forest transpires more than both grain and grass, and further that grain transpires more than grass. The relative change in recharge due to the doubling of forest area remains the same for the climate scenarios, reducing for example the recharge in the A2 scenario from 625 mm/year to 596 mm/year and 602 mm/year for the grass-to-forest and grain-to-forest scenarios, respectively. The mean monthly

recharge for the grass-to-forest and the grain-to-forest scenario are very similar for most months, though the recharge is slightly larger in September and October for the grain-to-forest scenario. The main effect of the land-use changes is the reduction in recharge during the late summer to autumn period.

Table 4.1 shows the changes in the mean total water balance for the subcatchment, when changing the land use for the current climate and the A2 scenario. When the land use is changed to forest, the recharge decreases, due to the increase in actual evapotranspiration. The decrease in recharge, due to land use change is the same for the current climate as for the A2 scenario.

Table 4.1 Mean total water balance (mm/year) for the subcatchment averaged over the period 1990–2004 for the current climate and the A2 scenario when changing the land use from grass or grain to forest (no abstractions or irrigation). In brackets the relative change compared to the current climate without land use changes.

	Recharge	Drain Flow	Base Flow
Current climate	551	200	355
Current climate Grass to Forest	526 (-5%)	186 (-7%)	347 (-2%)
Current climate Grain to Forest	531 (-4%)	182 (-9%)	344 (-3%)
A2 scenario	625 (13%)	251 (25%)	381 (7%)
A2 scenario Grass to Forest	596 (8%)	225 (13%)	369 (4%)
A2 scenario Grain to Forest	602 (9%)	229 (15%)	370 (4%)

4.3 Change in infiltration zones to wells

The study on the effects of climate change on infiltration zones to wells is not performed on the South-West Jutland catchment, but on the island of Zealand (Fig. 4.7). Zealand was chosen because of the higher pressure on water resources in this area than in SW-Jutland. The old version of the DK model is used, because an updated version for this area is not available. Particle tracking simulations are used to determine the changes in well infiltration zones and the changes in particle travel time to the well. Stationary MIKE SHE simulations for the period 1990–2004 for the current climate and the B2 scenario are run. The B2 scenario is used because it shows the largest increases in mean annual recharge. The particle tracking simulations are run for a 1000 year period from the 31/12/2004 where 500 particles per computational cell are released at the land surface. Though many of the particles released at the surface are removed by drains before even reaching the subsurface.

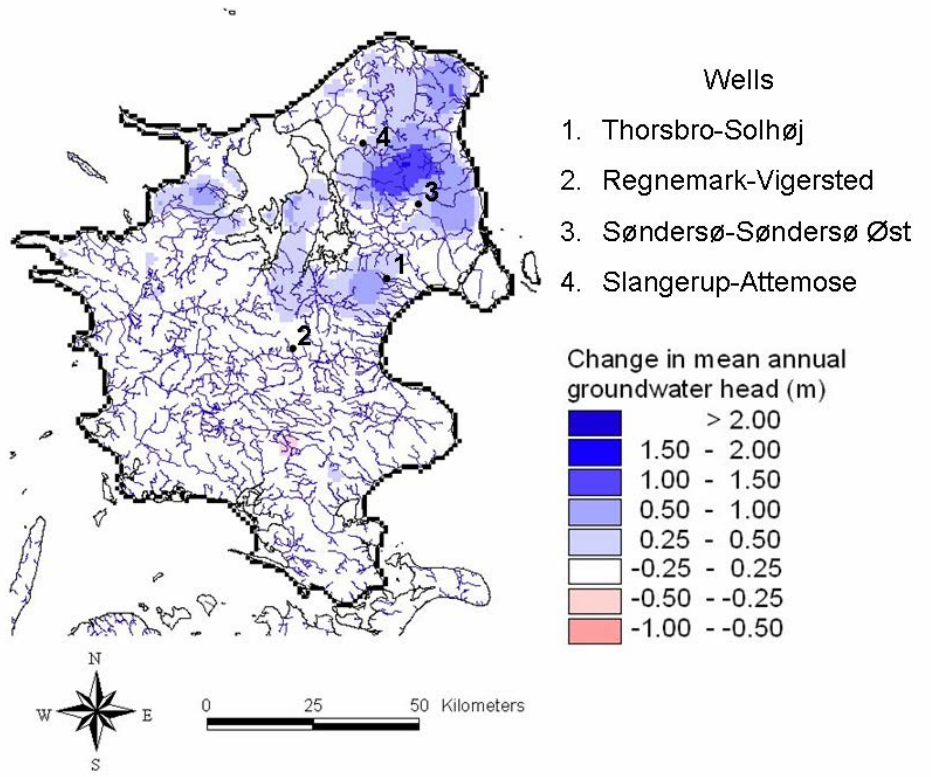

Figure 4.7 The change in mean annual groundwater head in the chalk aquifer (model layer 9) when comparing the B2 scenario to the current climate. The locations of the four wells on the island of Zealand, Denmark are indicated.

From the largest abstractions included in the model, four wells are selected which represent various geological settings. Also, the wells are selected based on whether a change in groundwater head is expected or not as a result of climate change. Figure 4.7 shows the change in mean annual groundwater head in the chalk aquifer (model layer 9) when comparing the B2 scenario to the current climate and the location of the four wells on Zealand. The following wells were selected:

1. Thorsbro-Solhøj well: the largest abstraction on Zealand; the thickness of the overlaying till layer is thin; located in an area where moderate changes in groundwater head occur for the B2 scenario.
2. Regnemark-Vigersted well: the second-largest abstraction on Zealand; thick layer of till above the aquifer; located in an area where the groundwater head is not expected to increase as a result of climate change.
3. Søndersø-Søndersø Øst well: the third-largest abstraction; hardly any overlying till layer; relatively large changes in groundwater head are expected in this area.
4. Slangerup-Attemose well: fifth-largest abstraction on Zealand; relatively thick till layer; very little change to groundwater head expected for the B2 scenario.

Table 4.2 Mean annual abstraction volumes and the model layer from which water is pumped for the four selected wells and for other wells in the well field.

Well	Volume (Mm^3)	Layer	Well	Volume (Mm^3)	Layer
Regnemark well field			**Søndersø well field**		
Vigersted	5135	9	Søndersø Øst	3854	9
Ravneshave	2719	9	Tipperup	3026	9
Slimminge	1680	9	Bogøgård	1999	7
Kimmerslev	1342	9	Egholm	1267	9
Valsømagle	640	9	Søndersø Vest	1132	9
Bøstofte	574	9	Bjellekær	886	7
Svenstrup	541	9	Kildedal	338	9
Alsgård	541	9	**Thorsbro well field**		
Ejby	532	9	Solhøj	5923	9
Gummersmarke	531	9	Thorsbro	1106	9
Nr. Dalby	460	9	St. Vejleå	777	9
Spanager	411	9	Tåstrup-Valby	503	9
Slangerup well field			Vardegård	467	9
Attemose	3422	9	Ishøj	295	9
Strø	2437	9	Karlslunde	249	9
Hørup	2217	9	Vallensbæk	231	9
Æbelholt	1494	7			
Havelse	1414	9			

Table 4.2 shows the mean annual abstraction volumes at the four wells and from which model layer the water is pumped and also the other wells at the same location are shown. Model layer 9 is the main chalk aquifer on Zealand and layer 7 is a regional sand aquifer above the chalk. Figure 4.8 shows the relative age distribution for the particles reaching the well from the land surface when 500 particles are released per cell for the current climate and the B2 scenario. For all wells except Søndersø Øst well, the mean travel time becomes shorter, which is in agreement with the higher recharge to the groundwater system. Figure 4.9 shows the location where infiltration to the four wells took place. Where possible, interpolation of the mean travel time between the various points was performed. The locations of the infiltration zones to Solhøj well and Søndersø well do not change much, but the zones do become slightly smaller. Slangerup well shows changes in infiltration locations in Dyrehaven close to Hillerød and close to Allerød. Also, a new infiltration zone just north of Lynge might occur for the B2 scenario. Vigersted well shows no change in infiltration zone.

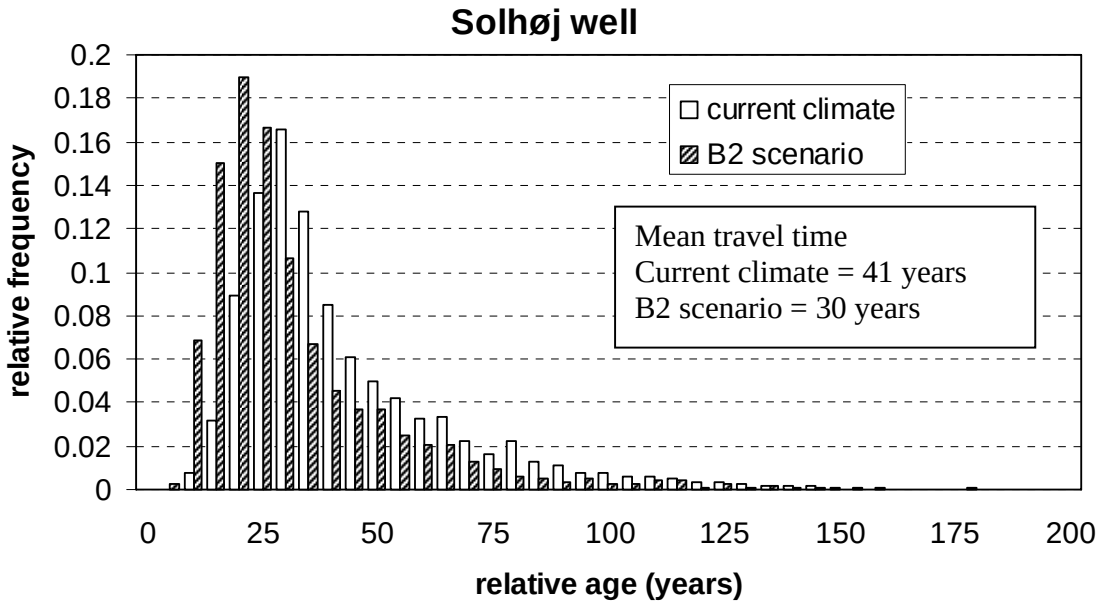

Figure 4.8A The relative age distribution for the particles reaching the Solhøj well from the land surface for the current climate and the B2 scenario.

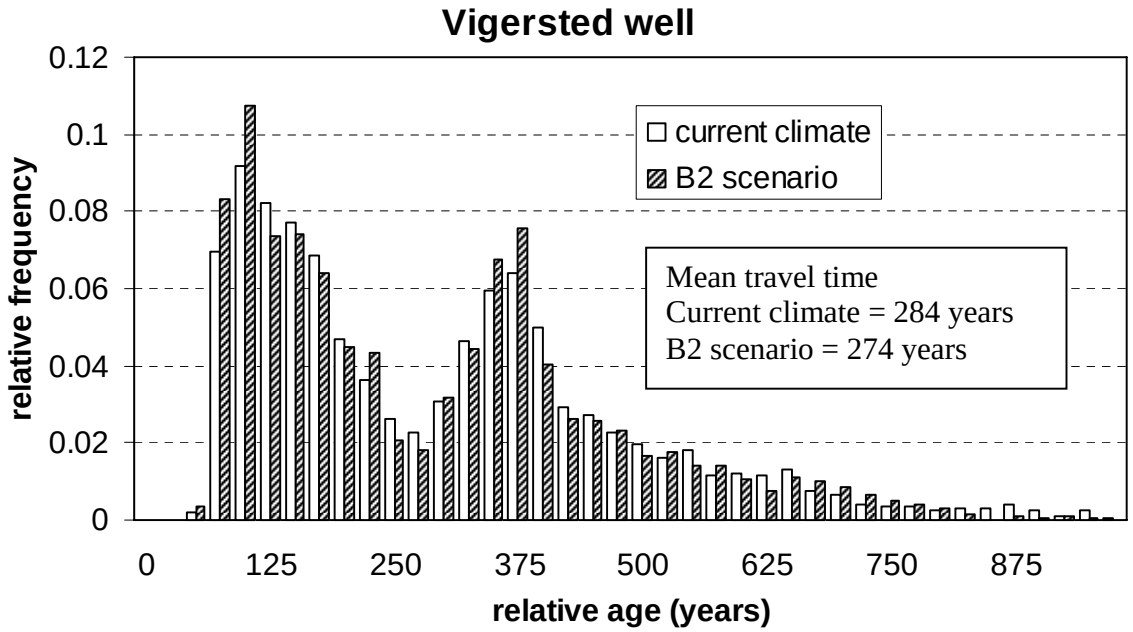

Figure 4.8B The relative age distribution for the particles reaching the Vigersted well from the land surface for the current climate and the B2 scenario.

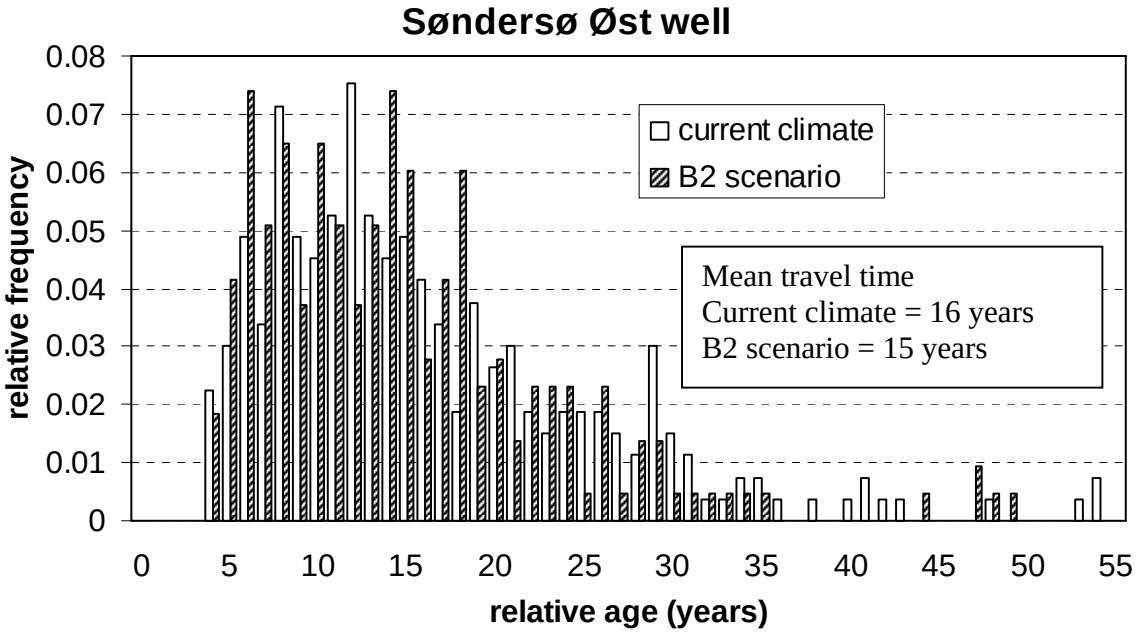

Figure 4.8C The relative age distribution for the particles reaching the Søndersø Øst well from the land surface for the current climate and the B2 scenario.

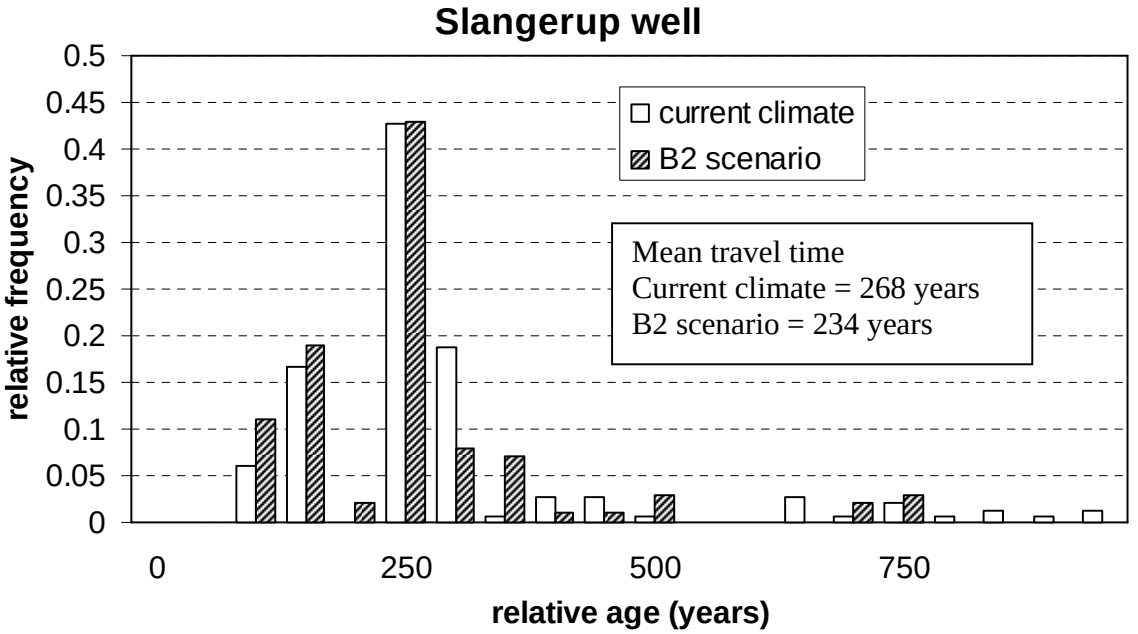

Figure 4.8D The relative age distribution for the particles reaching the Slangerup well from the land surface for the current climate and the B2 scenario.

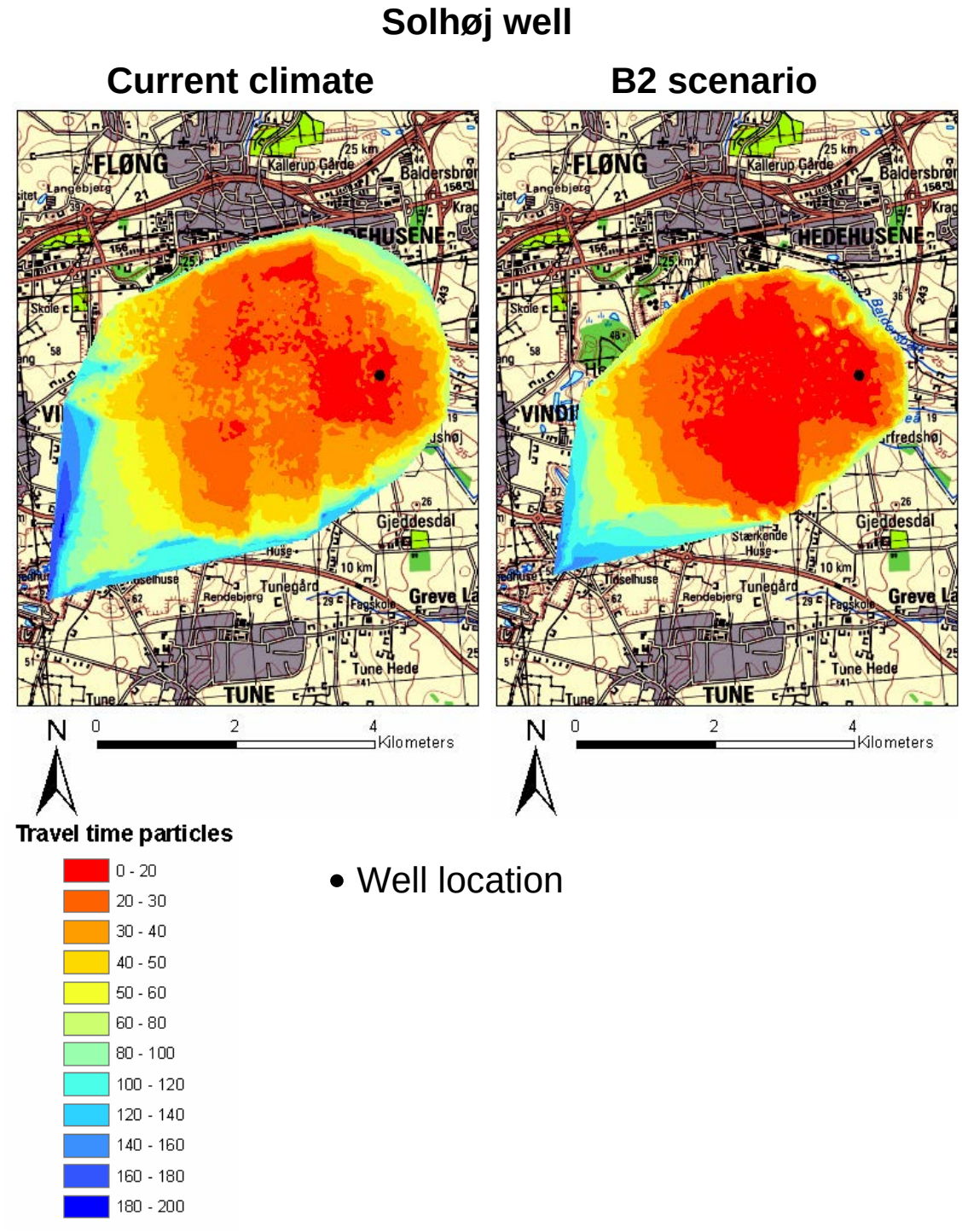

Figure 4.9A Infiltration zone to the Solhøj well and the mean travel time (years) of the particles to the well.

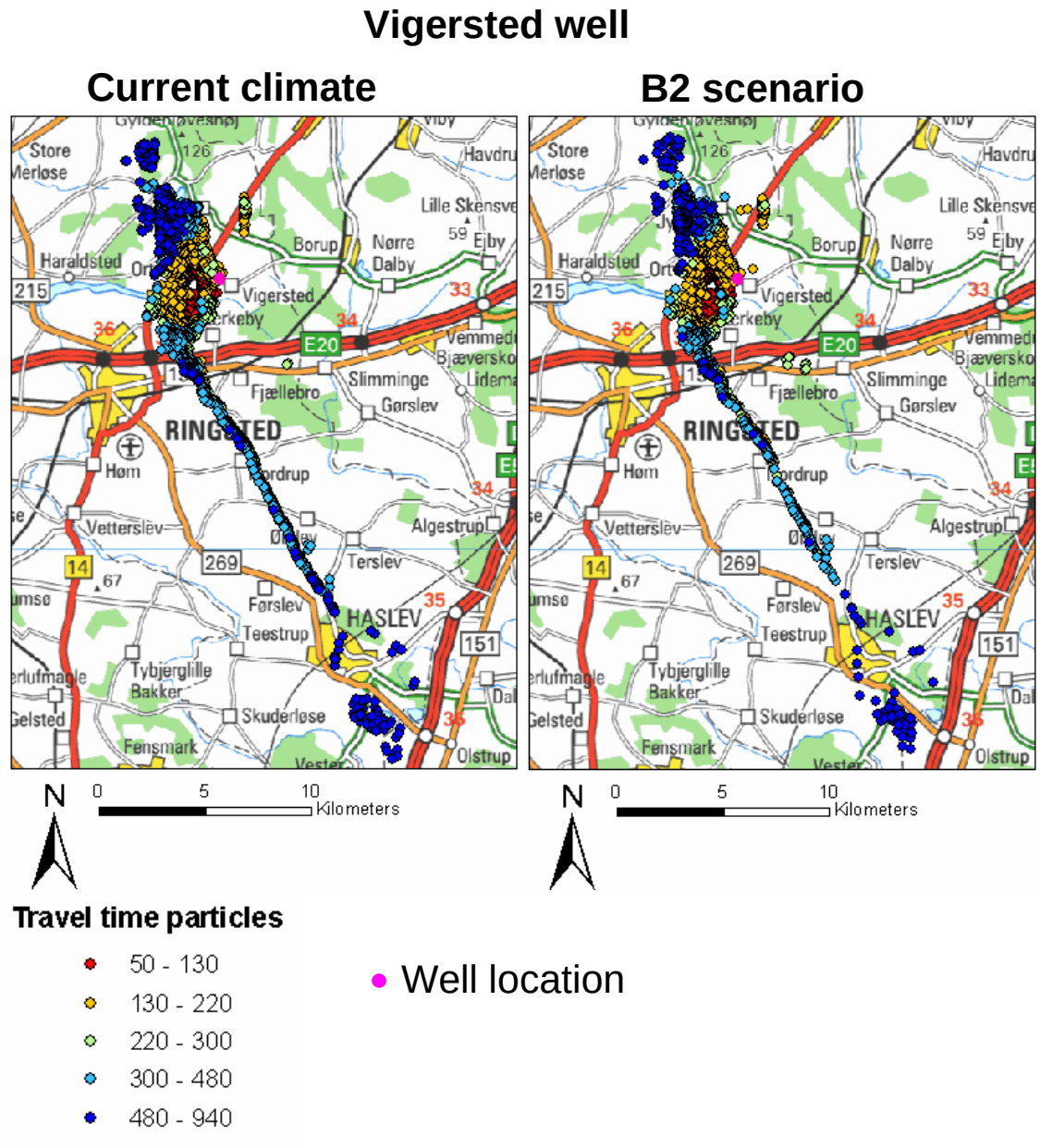

Figure 4.9B Infiltration zone to the Vigersted well and the mean travel time (years) of the particles to the well.

Slangerup well

Current climate

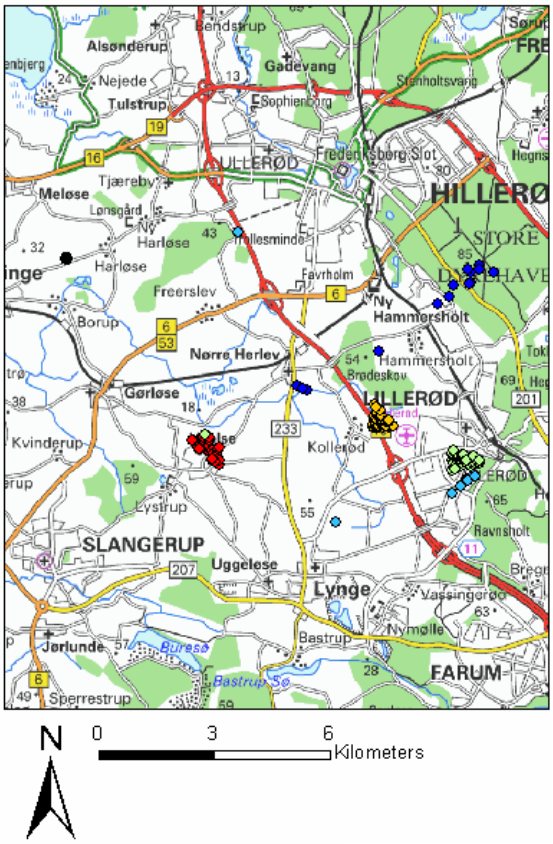

B2 scenario

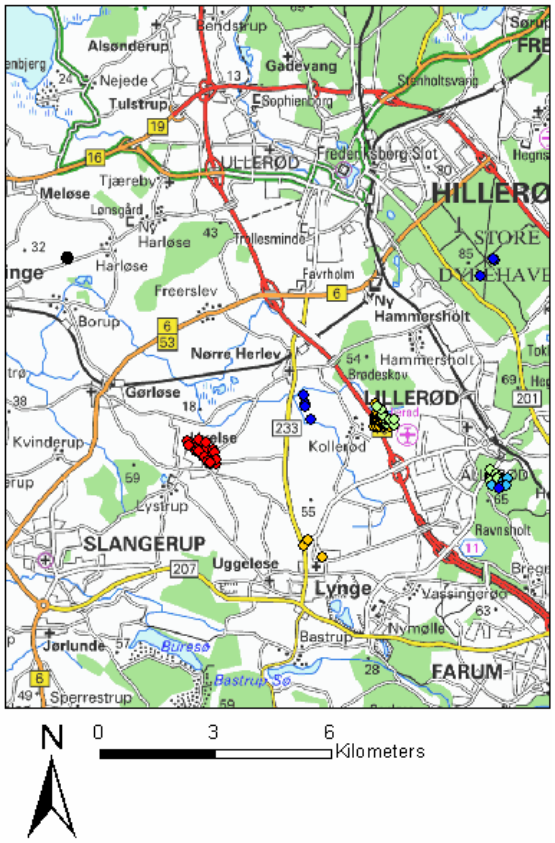

Travel time particles

- 90 - 130
- 130 - 220
- 220 - 300
- 300 - 480
- 480 - 940

- Well location

Figure 4.9C Infiltration zone to the Slangerup well and the mean travel time (years) of the particles to the well.

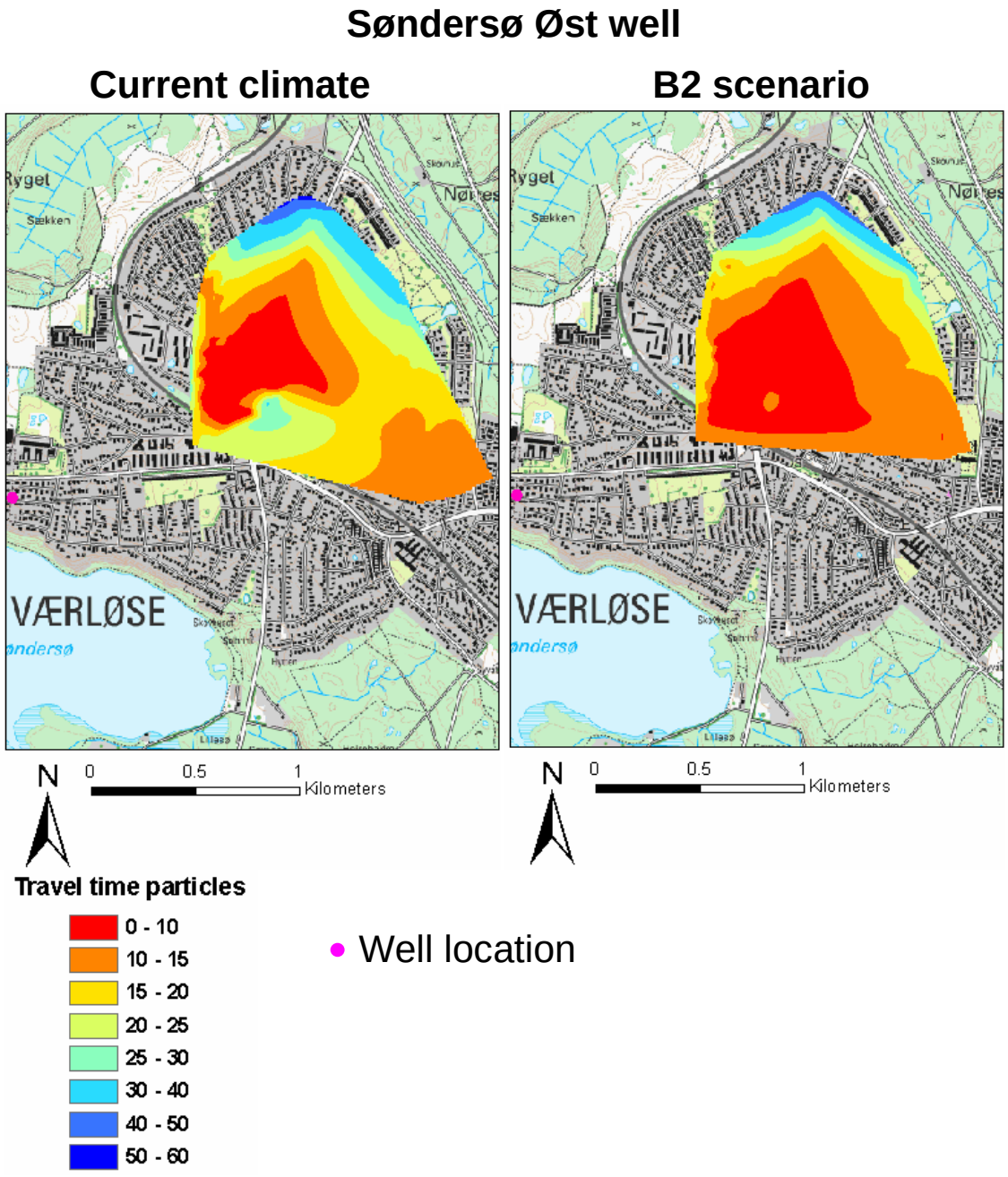

Figure 4.9D Infiltration zone to the Søndersø Øst well and the mean travel time (years) of the particles to the well.

5. Summary and conclusions

This report presents the results of a study on the possible direct and indirect impacts of climate change on the hydrological cycle in Western Jutland, Denmark. The direct impacts of climate change were simulated by introducing climate-forcing data sets for two climate scenarios, A2 and B2, and by raising the sea level to +1 masl. The anomalies used to construct the climate-forcing data sets were calculated using RCM output for the current climate (1961–1990) and for the scenarios (2071–2100). The indirect effects included the changes in irrigation and the effects of land-use changes. Results, such as the water balance, groundwater heads, stream discharges, irrigation volumes, and actual evapotranspiration, were compared for a 15-year period of the hydrological simulations (1990–2004).

The analysis of the results of the direct effects of climate change on the water resources in the area leads to the following conclusions:

- Both scenarios showed significant increases in mean annual recharge. The B2 scenario showed the largest increase, 20%, whereas the A2 scenario resulted in an increase of 12%. The seasonal dynamics in recharge were amplified, with more recharge occurring in the period from December to March and decreasing recharge during the late summer period from July to September. In December/January the recharge increased with 45 mm, whereas September showed decreases equal to 31 mm.
- The mean groundwater heads increased in the upper, unconfined aquifer, and the deeper, main aquifer. The largest absolute increase of 0.45 m occurred in the deeper aquifer, for the B2 scenario and the simulation not including abstractions and irrigation. This simulation showed an increase in groundwater head greater than 0.25 m in 58% of the catchment area. The smallest increase of 0.17 m occurred in the upper aquifer, for the A2 scenario and the simulation including abstractions and irrigation.
- The stream discharges increased due to more base flow and drain flow. The A2 scenario resulted in a relative increase around 13%, and the B2 scenario resulted in an increase around 21%. The seasonal dynamics of stream discharges increased, with larger flow during the winter months, but also significant decreases during the late summer months. The largest increases were simulated for the B2 scenario, while the A2 scenario showed the largest decreases during the summer months.
- The 1 m sea level rise influenced the groundwater heads up to 10 km inland along the coast. The higher sea level mostly resulted in an increase up to 0.5 m in the coastal region, though some areas showed an increase up to 1m. The effect of sea level rise is mainly significant for low-lying areas, where the combined effects of sea level rise and climate change can result in groundwater tables close to or above the ground surface.

The following conclusions can be drawn from the simulations of the effects of climate change on irrigation, the effects of land-use changes in combination with climate change, and the effects of climate change on abstraction wells:

- The absolute differences in annual values for recharge, mean groundwater levels and discharges were not very large, when comparing the simulations including and not including abstractions and irrigation because the abstractions only constitute a small

part of the annual mean water balance. However, the abstractions for irrigation had a pronounced effect on the groundwater heads and baseflow to streams during summer because irrigation water was primarily extracted from June to September, when recharge was close to zero or negative.

- From March to August the soil moisture deficit increased considerably for both scenarios, with especially August showing much more drying as compared to the current scenario. This larger deficit caused increases in annual irrigation of 91% and 50% for the A2 and B2 scenario, respectively. The increase in irrigation volume was likely underestimated because only the irrigation for grass was taken into account and not for any other crops, nor were changes in cropping pattern and the length of the growing season included.
- Especially in August and September irrigation increased the most, with the peak irrigation month shifting from July for the current climate to August for the climate scenarios.
- The mean monthly discharges during the summer months were a few percent lower for the simulations including abstractions and irrigation than when abstractions and irrigation were not included and the low flows were reduced even more in the scenario runs due to the increased abstractions for irrigation.
- Changing the land use from grass to forest or from grain to forest in the subcatchment resulted in a decrease in recharge to the SZ for the current climate of 5% and 4%, respectively. This was due to the higher actual evapotranspiration from forested areas. Changing the land use to forest counteracts the effects of climate change. For example, for the A2 scenario the recharge in the subcatchment increased with 13% when land-use change was not included, but only increased with 8% when the land use was changed from grass to forest.
- The B2 scenario results in a reduction of the mean relative age of particles to an abstraction well, due to the higher recharge for the B2 scenario compared to the current climate. Only slight changes occur in the location of the infiltration zones to the wells.

This study has shown that not only the direct effects of climate change have a significant effect on the hydrological cycle, but that indirect effects should also be taken into account. Indirect effects can both enhance and reduce the direct effects of climate change. Here a very coarse approach was used to study the effects on irrigation and for land-use changes. Future work should include modeling of the vegetation's adaptation to climate change and changes in cropping pattern and growing season. Also, future scenarios for abstractions for households and industry are important to include, as it can be expected that changes will occur in the population of the area and that different economic scenarios will result in changing water demands for industry.

To accurately simulate the combined effects of climate change and land-use change a direct coupling between the hydrological model and the climate model is necessary. In this way feed-back processes such as latent heat flux from soil moisture and vegetation to the atmosphere are included. A direct coupling would also make it possible to study the impact of the changes in hydrological extremes, which is not included in this study because the transfer method for the climate data sets is based on the variability of the current climate. Last but not least, this would also facilitate the use of multiple GCMs and climate scenarios, which is necessary to cover the scope of uncertainties related to climate model output.

Acknowledgments

The authors would like to thank the Danish Water and Waste Water Association (DANVA) and Copenhagen Energy for their financial support to this study.

References

Allerup, P., H. Madsen, and F. Vejen (1998) Standard values (1961–90) for precipitation correction. Tech. Rep. 98-10, Danish Meteorological Inst., Copenhagen, 64 pp (In Danish).

Andréasson, J., S. Bergström, B. Carlsson, L.P. Graham, and G. Lindström (2004) Hydrological change – climate change impact simulations for Sweden. Ambio, 33, 228–234.

Arnell, N.W. (1999) The effect of climate change on hydrological regimes in Europe: a continental perspective. Glob. Environ. Change, 9, 5–23.

Caballero, Y., S. Voirin-Morel, F. Habets, J. Noilhan, P. LeMoigne, A. Lehenaff, and A. Boone (2007) Hydrological sensitivity of the Adour-Garonne river basin to climate change. Water Resour. Res., 43, W07448, doi:10.1029/2005WR004192.

Christensen, J.H., O.B. Christensen, P. Lopez, E. van Meijgaard, and M. Botzet (1996) The HIRHAM4 regional atmospheric climate model. Sci. Rep. 96-104, Danish Meteorological Inst., Copenhagen, 51 pp.

Christensen, O.B., J.H. Christensen, B. Machenhauer, and M. Botzet (1998) Very high-resolution regional climate simulations over Scandinavia - Present climate. J. Clim., 11(12), 3204–3229.

DHI Software (2007) MIKE SHE User Manual Volume 2: Reference Guide. DHI Water and Environment, Hørsholm, Denmark.

Graham, D.N., and M.B. Butts (2006) Flexible, integrated watershed modelling with MIKE SHE. *In* Watershed Models, edited by V.P. Singh and D.K. Frevert, CRC Press, 245-272, ISBN: 0849336090.

Graham, L.P., S. Hagemann, S. Jaun, and M. Beniston (2007) On interpreting hydrological change from regional climate models. Clim. Change, 81(supplement 1), 97–122.

Hay, L.E., R.L. Wilby, G.H. Leavesley (2000) A comparison of delta change and downscaled GCM scenarios for three mountainous basins in the United States. J. Am. Water Res. Ass., 36, 387–398.

Henriksen, H.J., and A.B. Sonnenborg (2003) The freshwater cycle. NOVA Theme rep., Geol. Surv. of Denmark and Greenland, Copenhagen, 266 pp (In Danish).

Henriksen, H.J., L. Troldborg, P. Nyegaard, T.O. Sonnenborg, J.C. Refsgaard, B. Madsen (2003) Methodology for construction, calibration and validation of a national hydrological model for Denmark. J. Hydrol., 280(1-4), 52-71.

IPCC (2000) Special report on emissions scenarios (SRES): a special report of working group III of the intergovernmental panel on climate change. Cambridge Univ. Press, Cambridge, 570 pp.

IPCC (2007) Summary for Policymakers, *In* Climate Change 2007: The Physical Science Basis. Contribution of Working Group I to the Fourth Assessment Report of the Intergovernmental Panel on Climate Change, edited by Solomon, S., D. Qin, M. Manning, Z. Chen, M. Marquis, K.B. Averyt, M. Tignor, and H.L. Miller, Cambridge University Press, New York, NY.

Kleinn, J., C. Frei, J. Gurtz, D. Luthi, P.L. Vidale, and C. Schar (2005) Hydrologic simulations in the Rhine basin driven by a regional climate model. J. of Geophysical Res.-Atmospheres, 110(D4).

Makkink, G.F. (1957) Examination of the Penman formula. Neth. J. Agric. Sci., 5, 290–305 (In Spanish).

Meehl, G.A. et al. (2007) Global Climate Projections, *In* Climate Change 2007: The Physical Science Basis. Contribution of Working Group I to the Fourth Assessment Report of the Intergovernmental Panel on Climate Change, edited by Solomon, S., D. Qin, M. Manning, Z. Chen, M. Marquis, K.B. Averyt, M. Tignor, and H.L. Miller, Cambridge University Press, New York, NY.

Mertz, E.L. (1924) Overview of the late- and postglacial changes in elevation in Denmark. Geol. Surv. of Denmark and Greenland, Copenhagen, II. Raekke, Nr. 41 (In Danish).

Mossin, L., and U.L. Ladekarl (2004) Simple water balance modeling with few data – calibration and evaluation: investigations from a Danish Sitka spruce stand with a high interception loss. Nordic Hydrol., 35(2), 139–151.

Refsgaard, J.C., and B. Storm (1995) MIKE SHE. *In* Computer Models of Watershed Hydrology, edited by V.P. Singh, Water Res. Publications, Highlands Ranch, CO, pp. 809–846.

Roosmalen, L.v., B.S.B. Christensen, and T.O. Sonnenborg (2007) Regional differences in climate change impacts on groundwater and stream discharge in Denmark. Vadose Zone J., 6, 554-571, doi:10.2136/vzj2006.0093.

Scharling, M. (1999) Climate grid – Denmark. Precipitation, temperature and potential evapotranspiration 20*20 & 40*40 km. Tech. Rep. 99-12, Danish Meteorological Inst., Copenhagen, 48 pp (In Danish).

Sonnenborg, T.O., B.S.B. Christensen, P. Nygaard, H.J. Henriksen, and J.C. Refsgaard (2003) Transient modeling of regional groundwater flow using parameter estimates from steady-state automatic calibration. J. Hydrol., 273, 188-204.

Thodsen, H. (2007) The influence of climate change on stream flow in Danish rivers. J. of Hydrol., 333(2-4), 226-238.

van der Salm, C., L. Rosenqvist, L. Vesterdal, K. Hansen, H. Denier van der Gon, A. Bleeker, R. Wieggers, and A. van den Toorn (2006) Chapter 3, Interception and water recharge following afforestation: Experiences from oak and Norway spruces chronosequences in Denmark, Sweden and the Netherlands. *In* Environmental effects of afforestation in north-western Europe, edited by G.W. Heil et al., Springer, 53-77.

Yan, J. and Smith, K.R. (1994) Simulation of integrated surface water and ground water systems – model formulation. Water Resources Bulletin 30(5), 879–890.

Annex 1

Omme Å

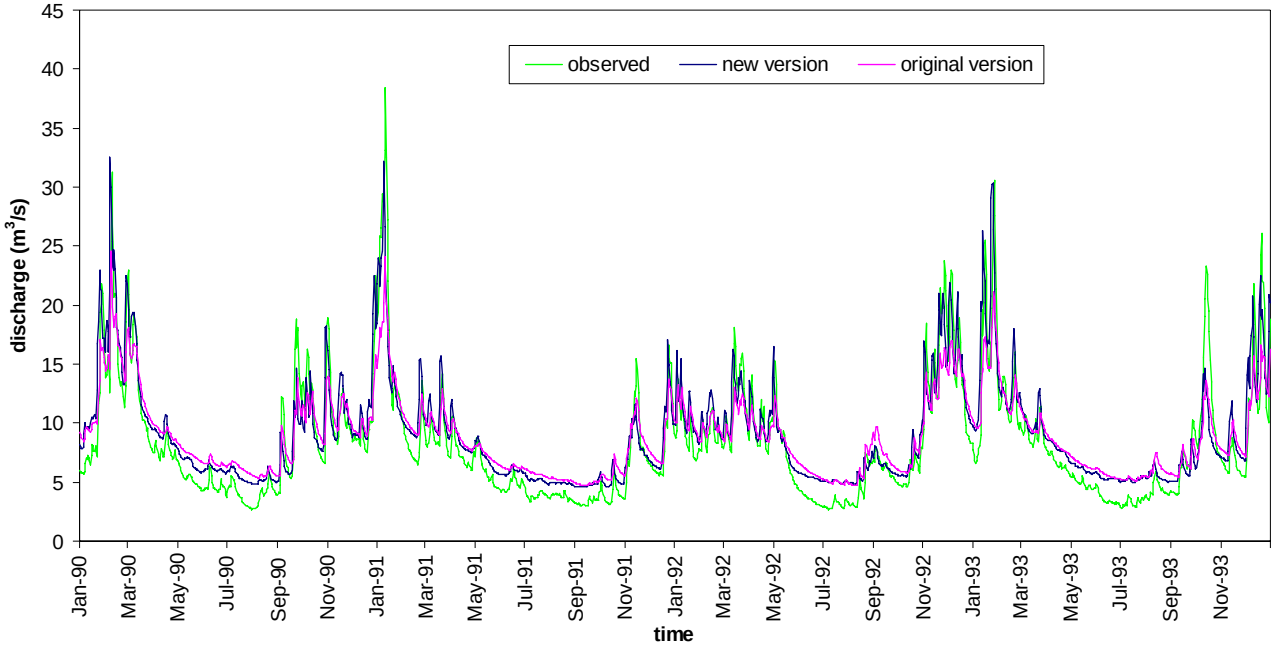

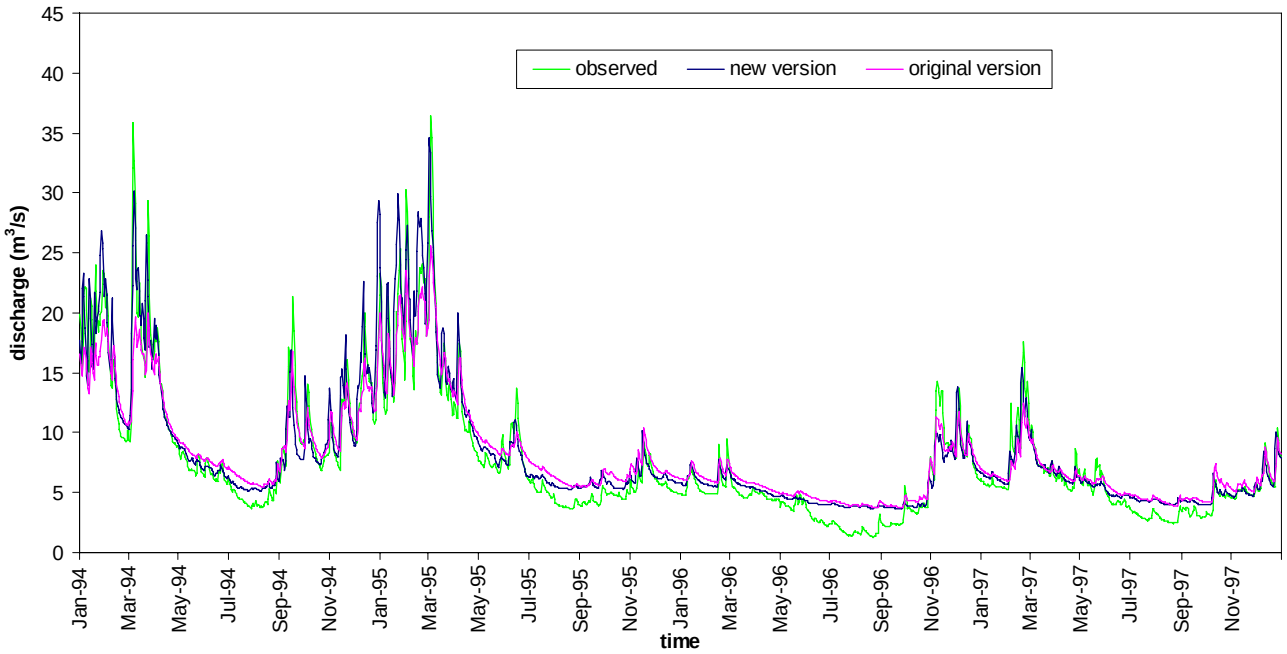

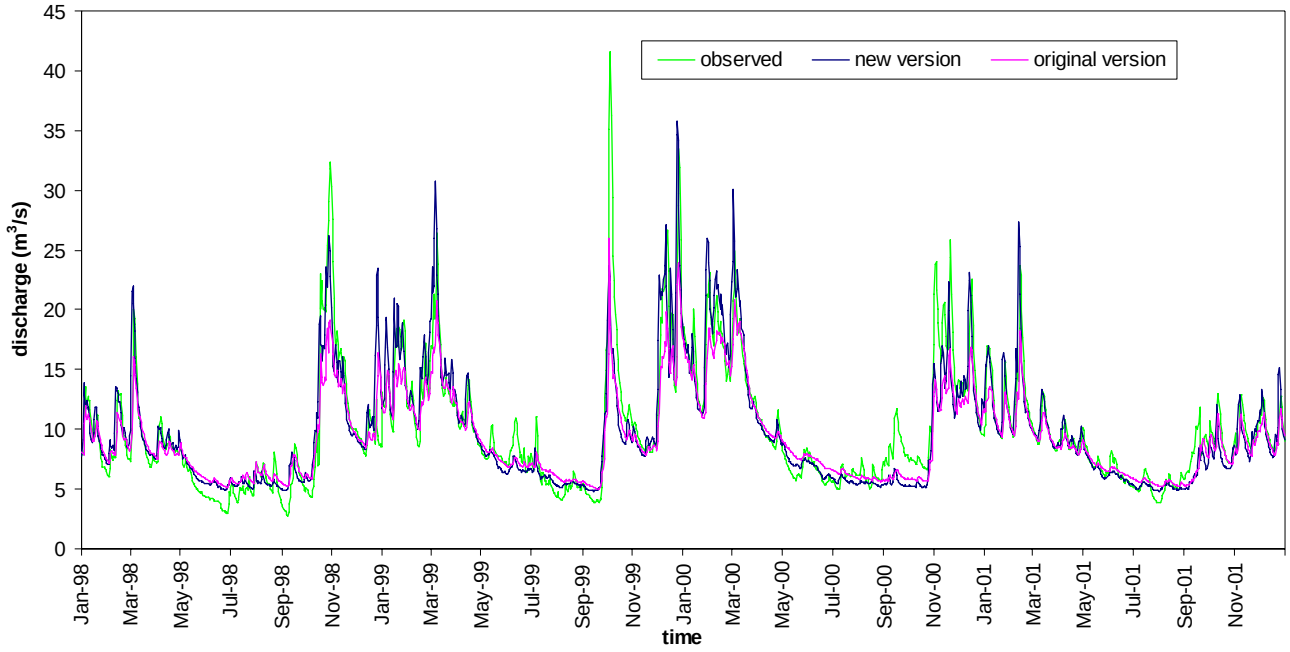
observed
new version
original version
discharge (m3/s)
time
0
5
10
15
20
25
30
35
40
45
Jan-98
Mar-98
May-98
Jul-98
Sep-98
Nov-98
Jan-99
Mar-99
May-99
Jul-99
Sep-99
Nov-99
Jan-00
Mar-00
May-00
Jul-00
Sep-00
Nov-00
Jan-01
Mar-01
May-01
Jul-01
Sep-01
Nov-01

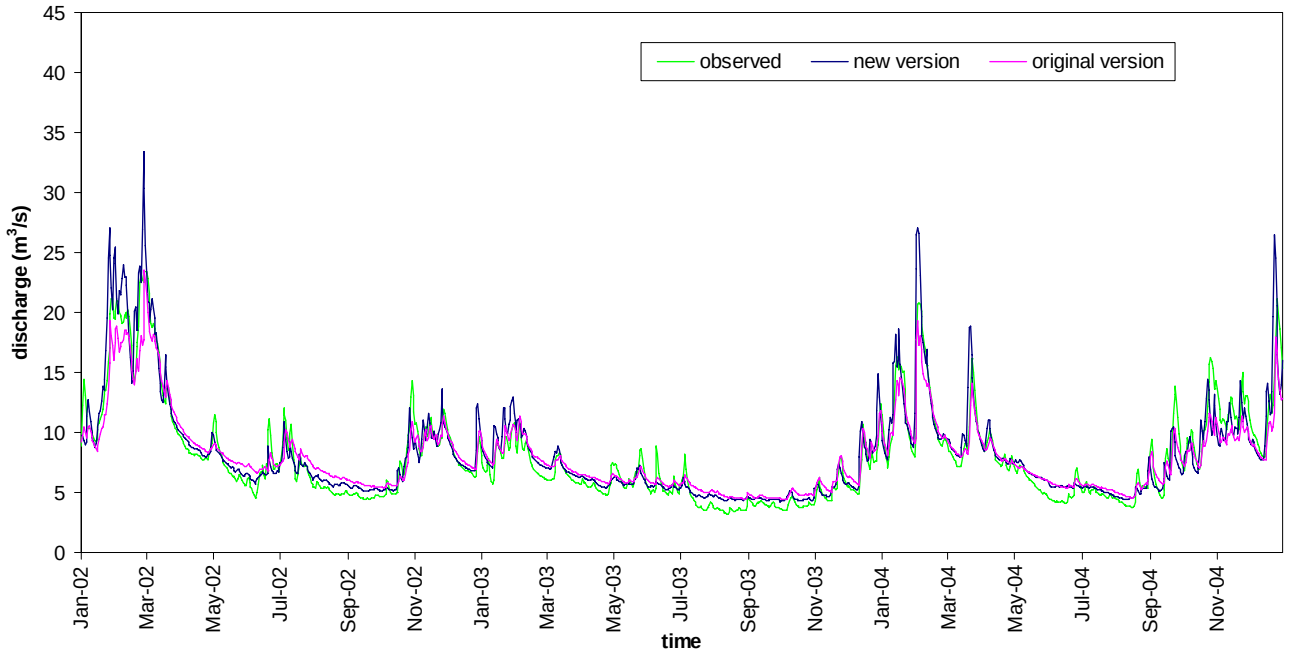
observed
new version
original version
discharge (m3/s)
time
0
5
10
15
20
25
30
35
40
45
Jan-02
Mar-02
May-02
Jul-02
Sep-02
Nov-02
Jan-03
Mar-03
May-03
Jul-03
Sep-03
Nov-03
Jan-04
Mar-04
May-04
Jul-04
Sep-04
Nov-04

Varde Å (nr. 31.13)

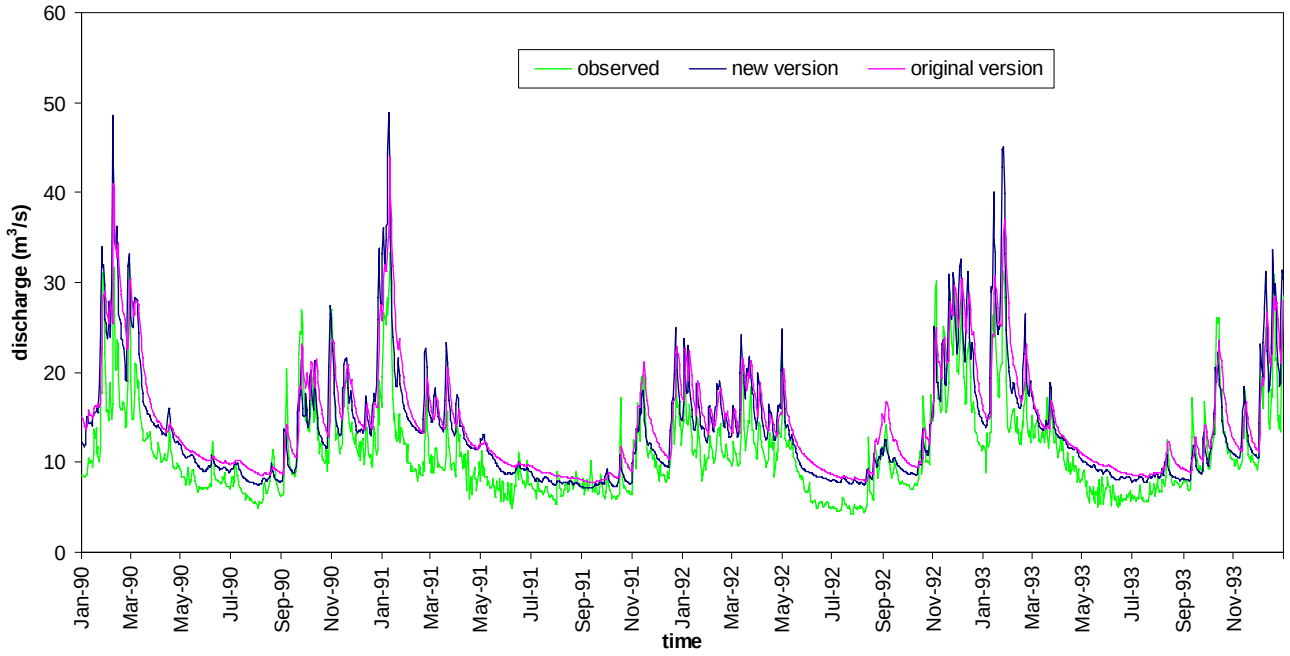

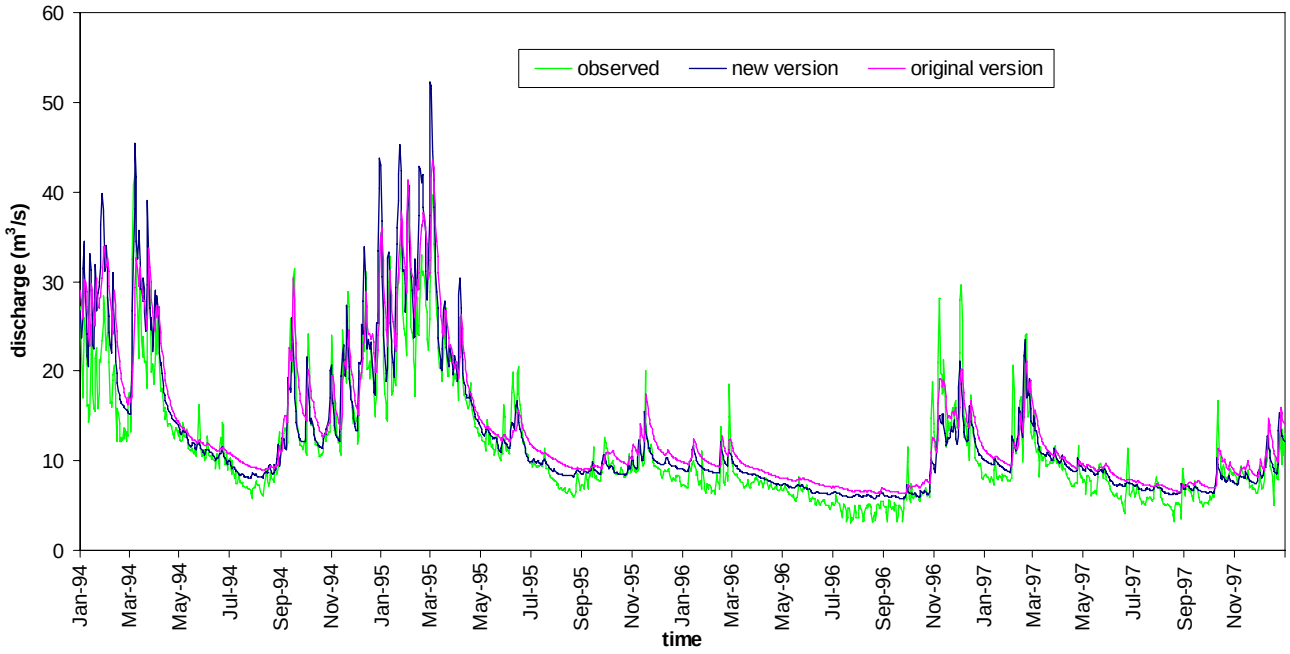

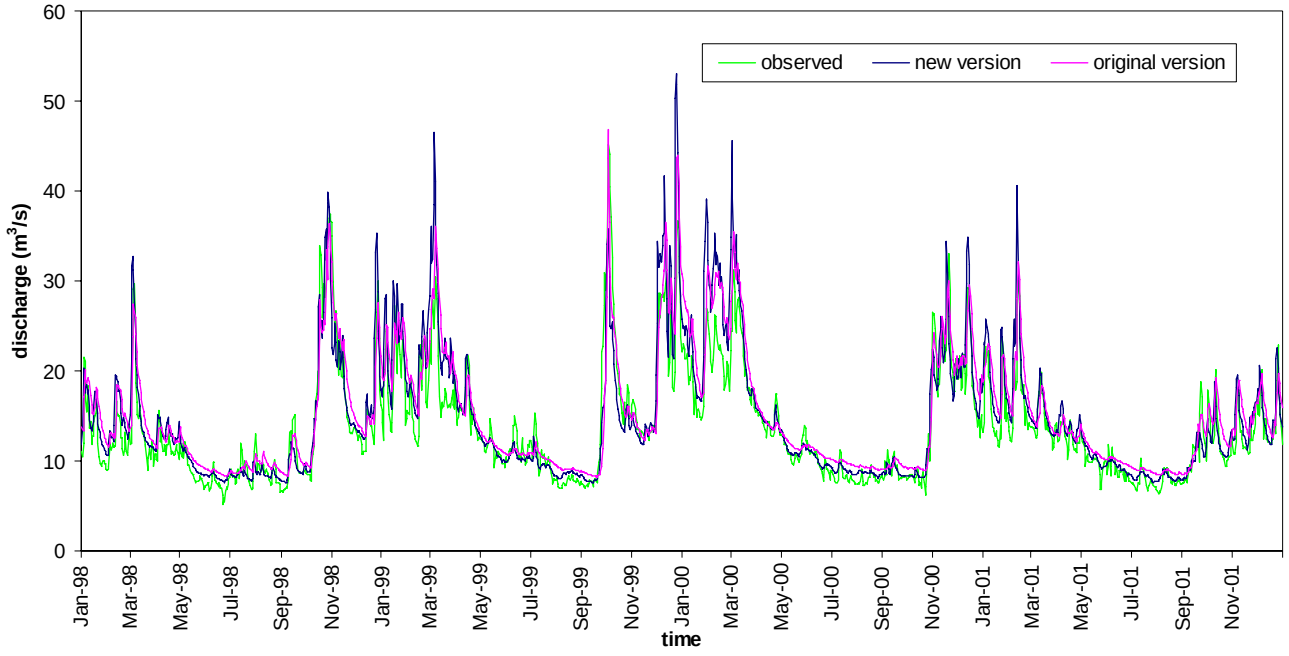
observed
new version
original version
discharge (m3/s)
time
0
10
20
30
40
50
60
Jan-98
Mar-98
May-98
Jul-98
Sep-98
Nov-98
Jan-99
Mar-99
May-99
Jul-99
Sep-99
Nov-99
Jan-00
Mar-00
May-00
Jul-00
Sep-00
Nov-00
Jan-01
Mar-01
May-01
Jul-01
Sep-01
Nov-01

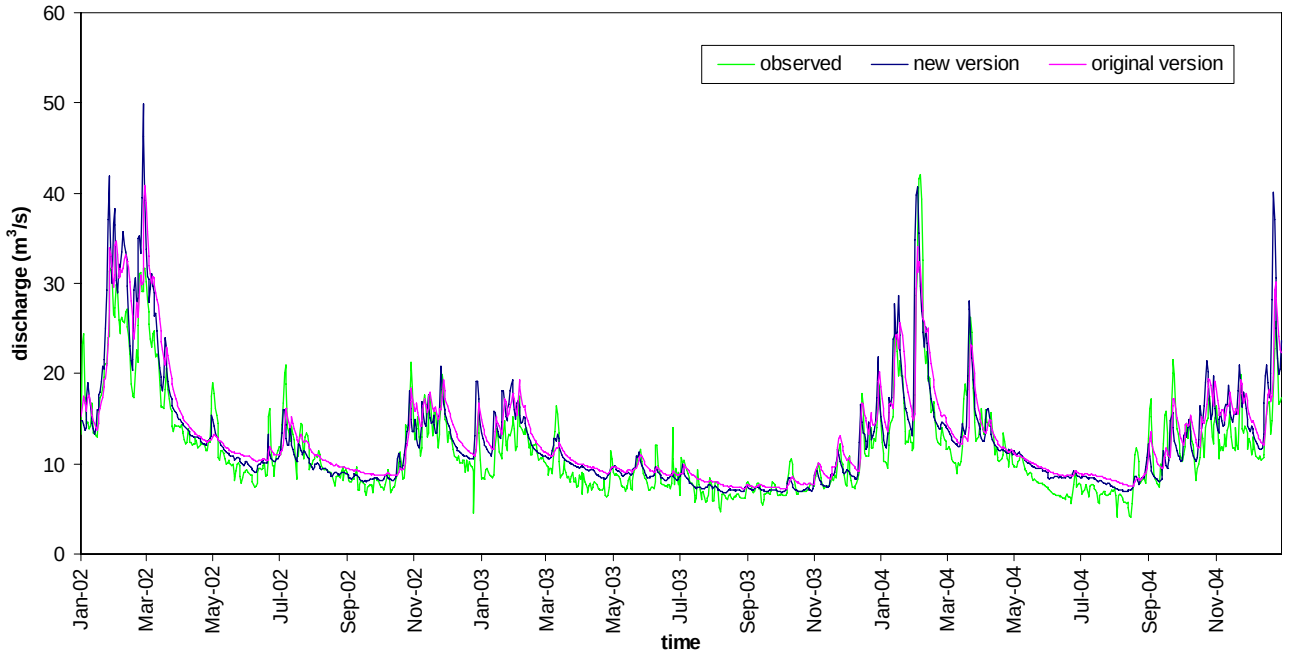
observed
new version
original version
discharge (m3/s)
time
0
10
20
30
40
50
60
Jan-02
Mar-02
May-02
Jul-02
Sep-02
Nov-02
Jan-03
Mar-03
May-03
Jul-03
Sep-03
Nov-03
Jan-04
Mar-04
May-04
Jul-04
Sep-04
Nov-04

Sneum Å (nr. 35.03)

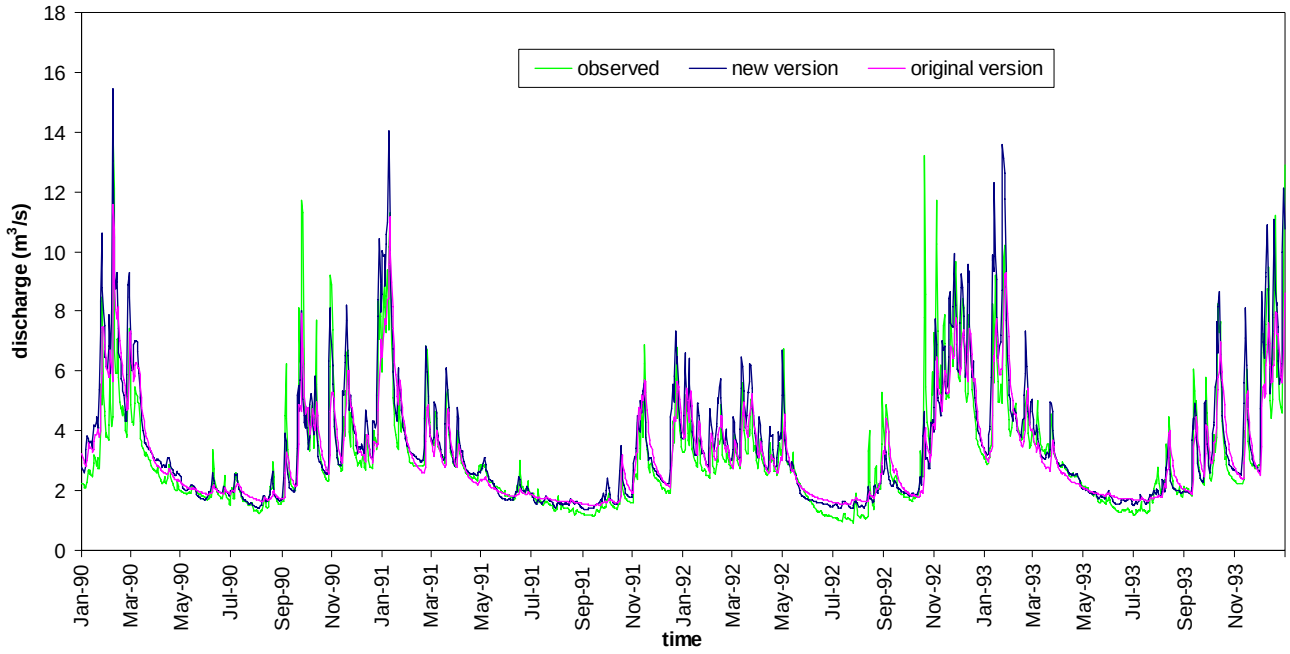

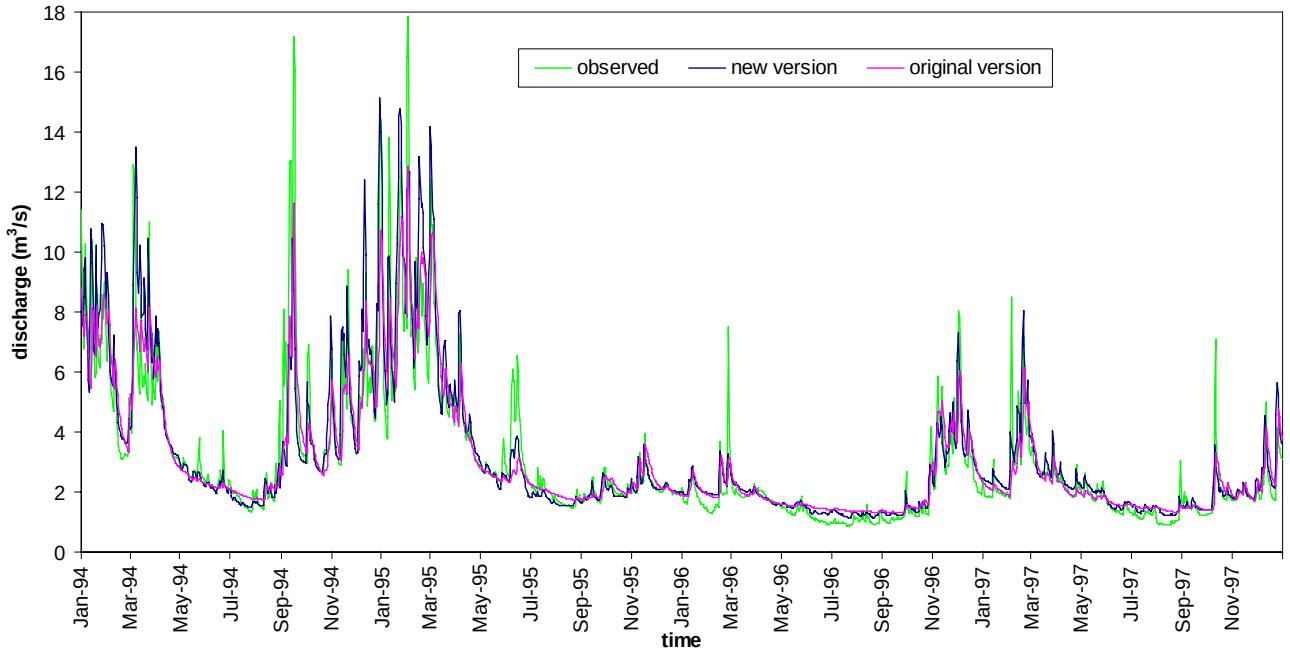

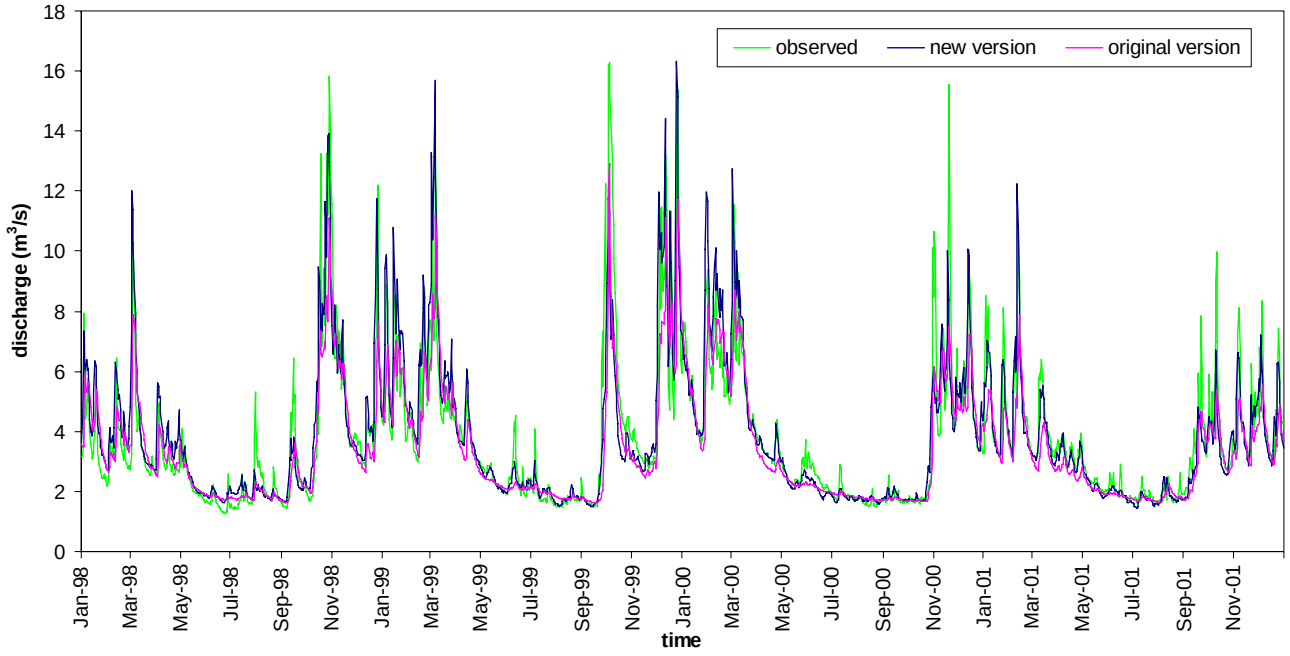
observed
new version
original version
discharge (m3/s)
time
0
2
4
6
8
10
12
14
16
18
Jan-98
Mar-98
May-98
Jul-98
Sep-98
Nov-98
Jan-99
Mar-99
May-99
Jul-99
Sep-99
Nov-99
Jan-00
Mar-00
May-00
Jul-00
Sep-00
Nov-00
Jan-01
Mar-01
May-01
Jul-01
Sep-01
Nov-01

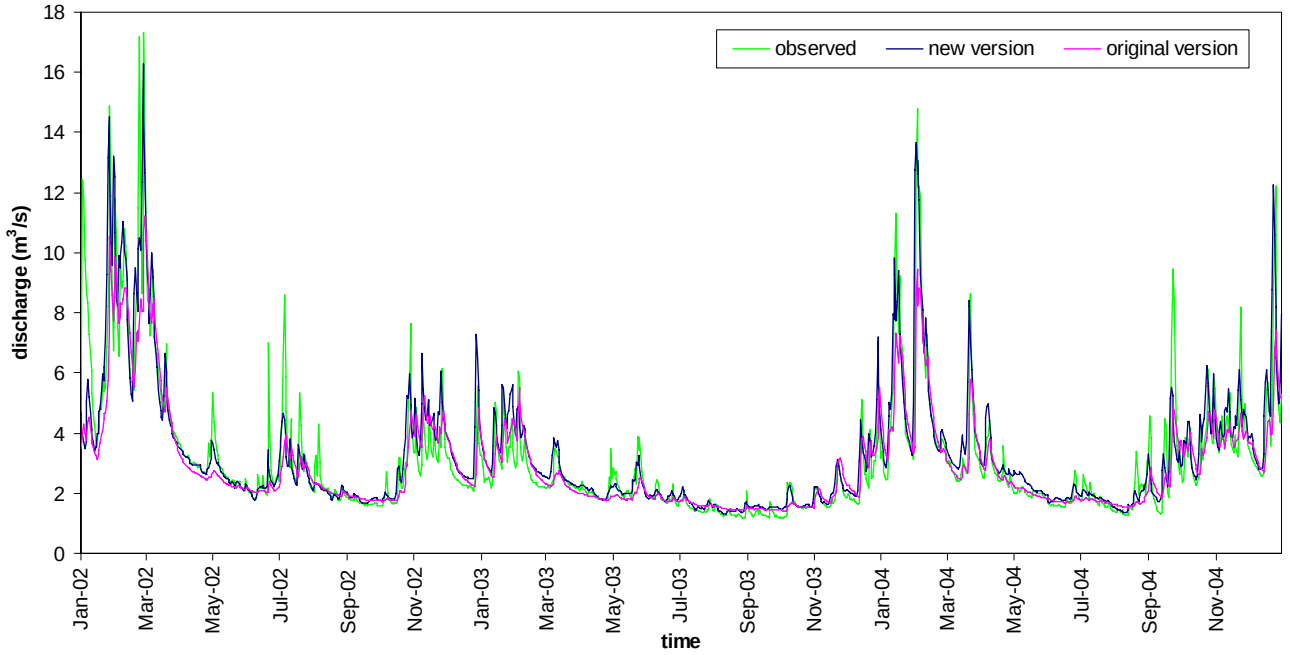
observed
new version
original version
discharge (m3/s)
time
0
2
4
6
8
10
12
14
16
18
Jan-02
Mar-02
May-02
Jul-02
Sep-02
Nov-02
Jan-03
Mar-03
May-03
Jul-03
Sep-03
Nov-03
Jan-04
Mar-04
May-04
Jul-04
Sep-04
Nov-04

Skjern Å (nr. 25.14)

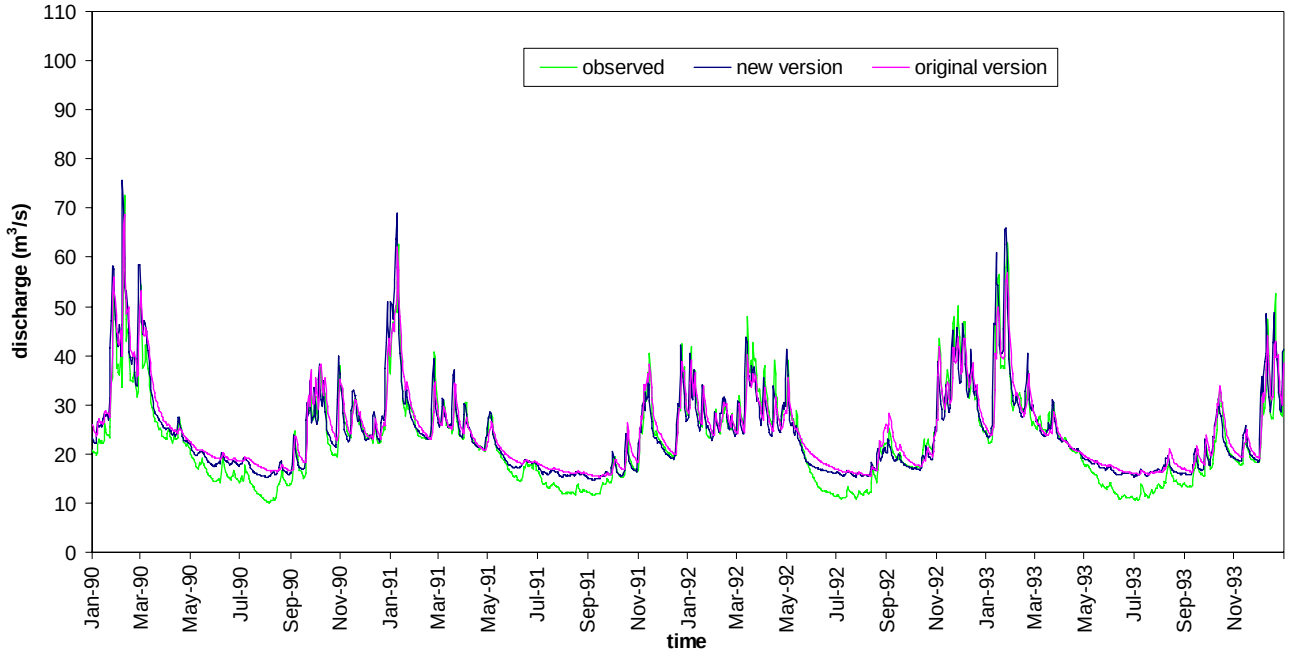

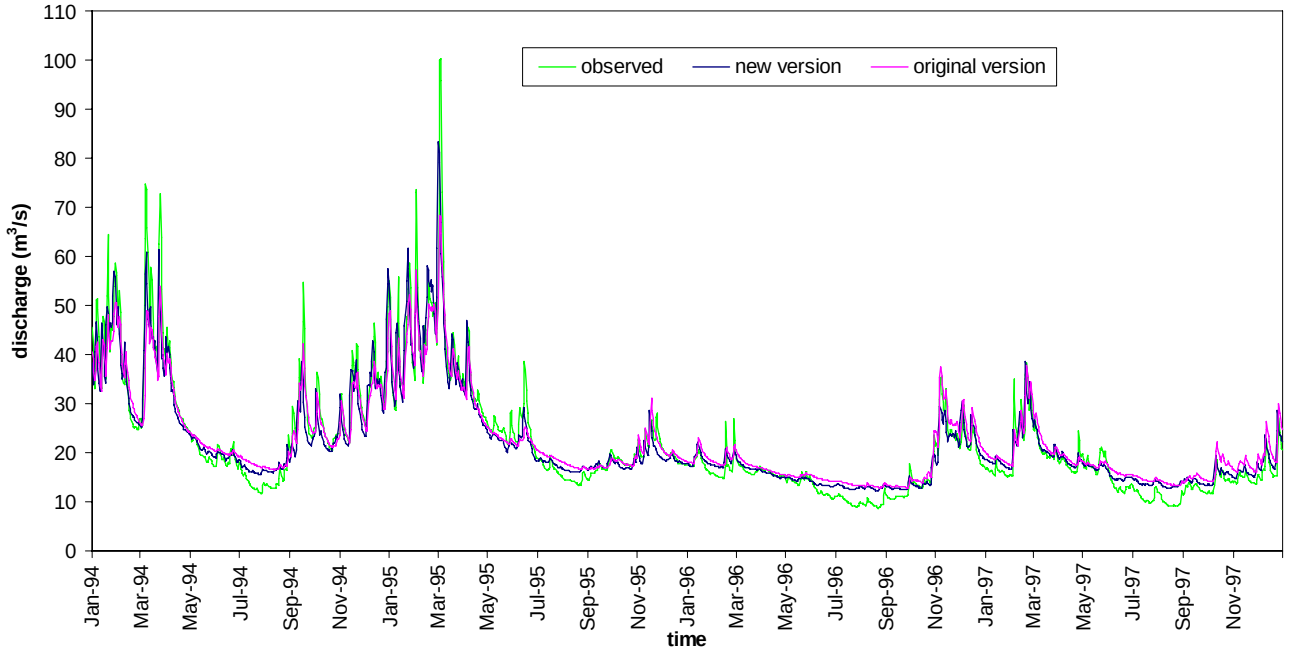

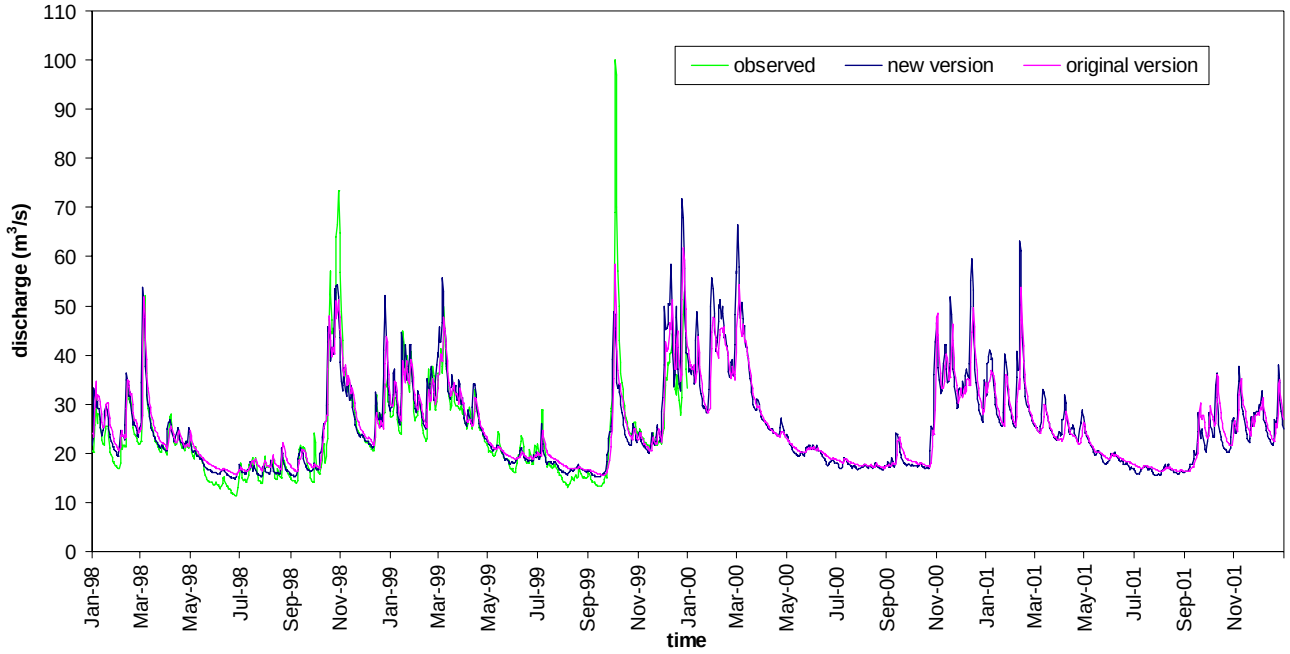
observed
new version
original version
discharge (m3/s)
time
0
10
20
30
40
50
60
70
80
90
100
110
Jan-98
Mar-98
May-98
Jul-98
Sep-98
Nov-98
Jan-99
Mar-99
May-99
Jul-99
Sep-99
Nov-99
Jan-00
Mar-00
May-00
Jul-00
Sep-00
Nov-00
Jan-01
Mar-01
May-01
Jul-01
Sep-01
Nov-01

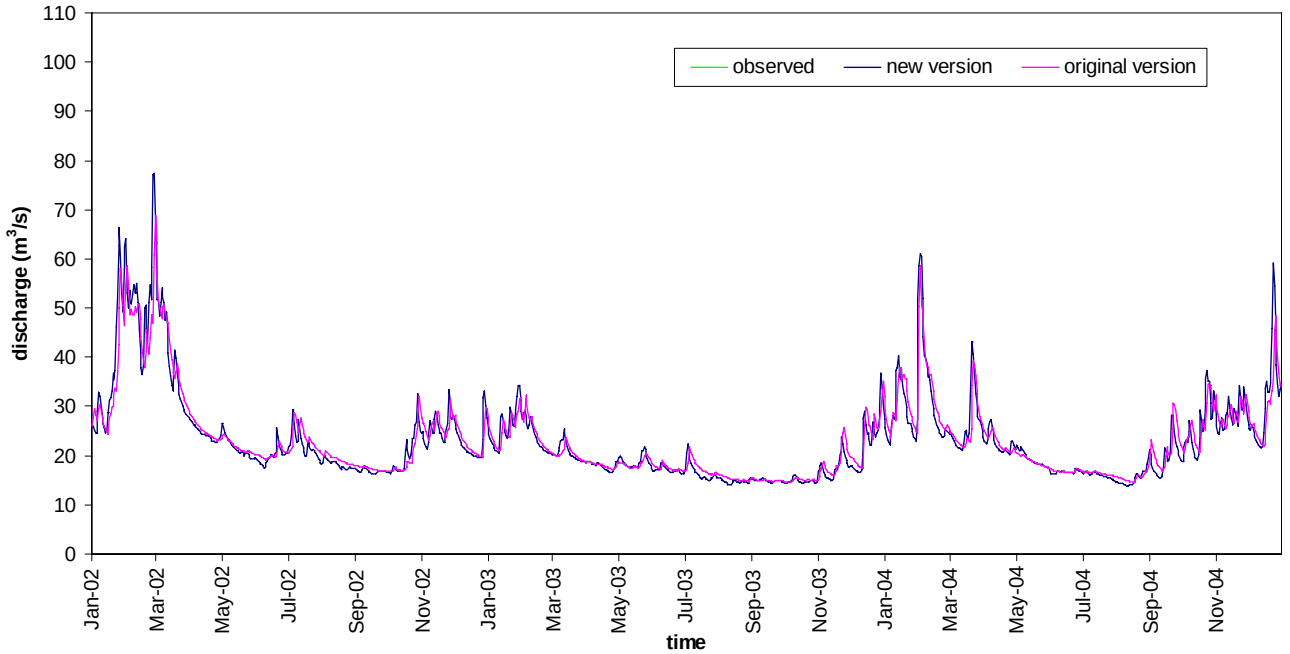
observed
new version
original version
discharge (m3/s)
time
0
10
20
30
40
50
60
70
80
90
100
110
Jan-02
Mar-02
May-02
Jul-02
Sep-02
Nov-02
Jan-03
Mar-03
May-03
Jul-03
Sep-03
Nov-03
Jan-04
Mar-04
May-04
Jul-04
Sep-04
Nov-04

Hoven Å (nr. 25.37)

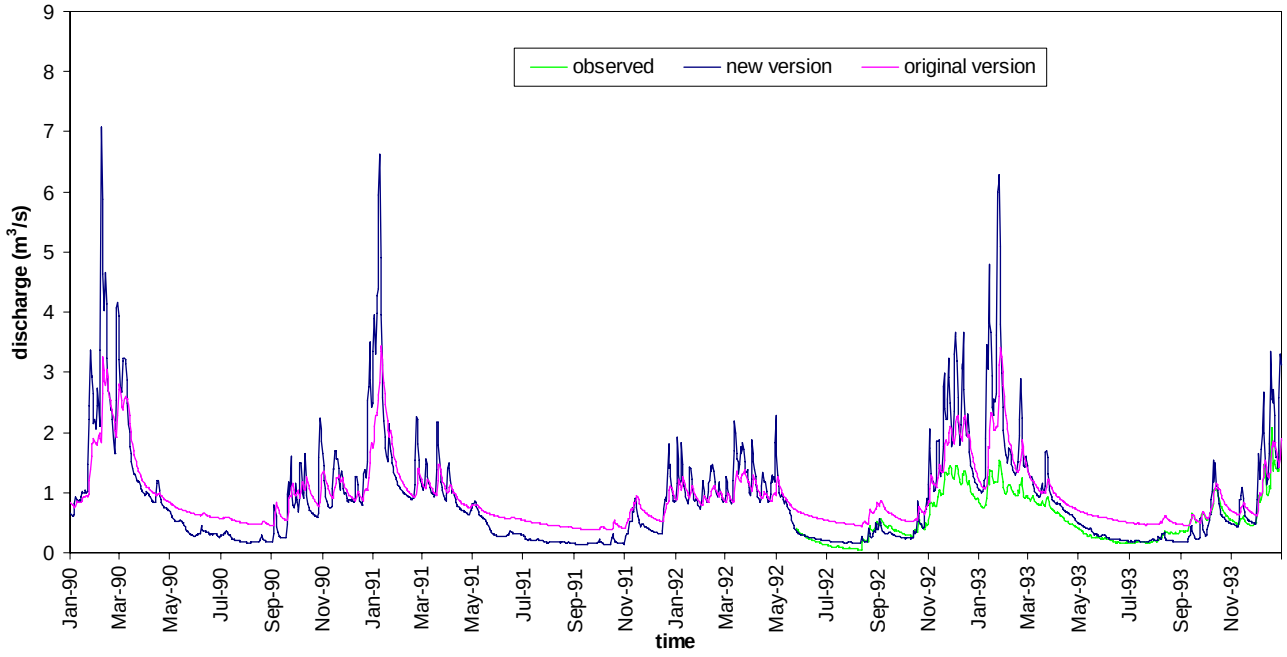

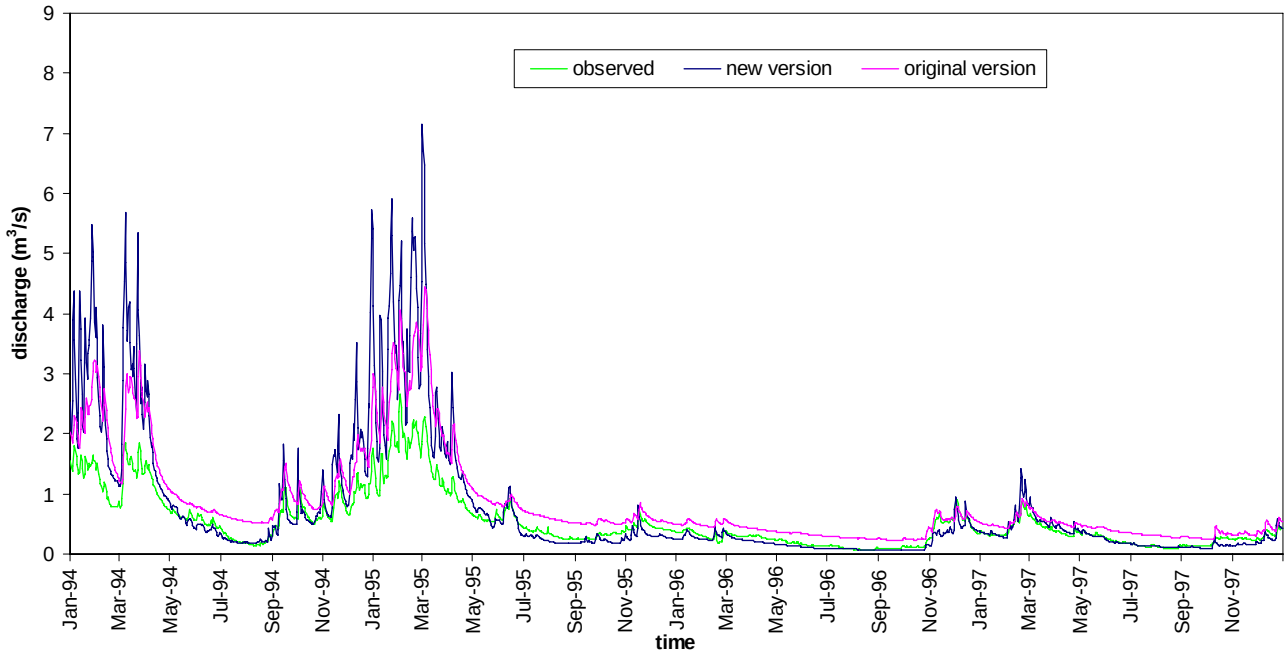

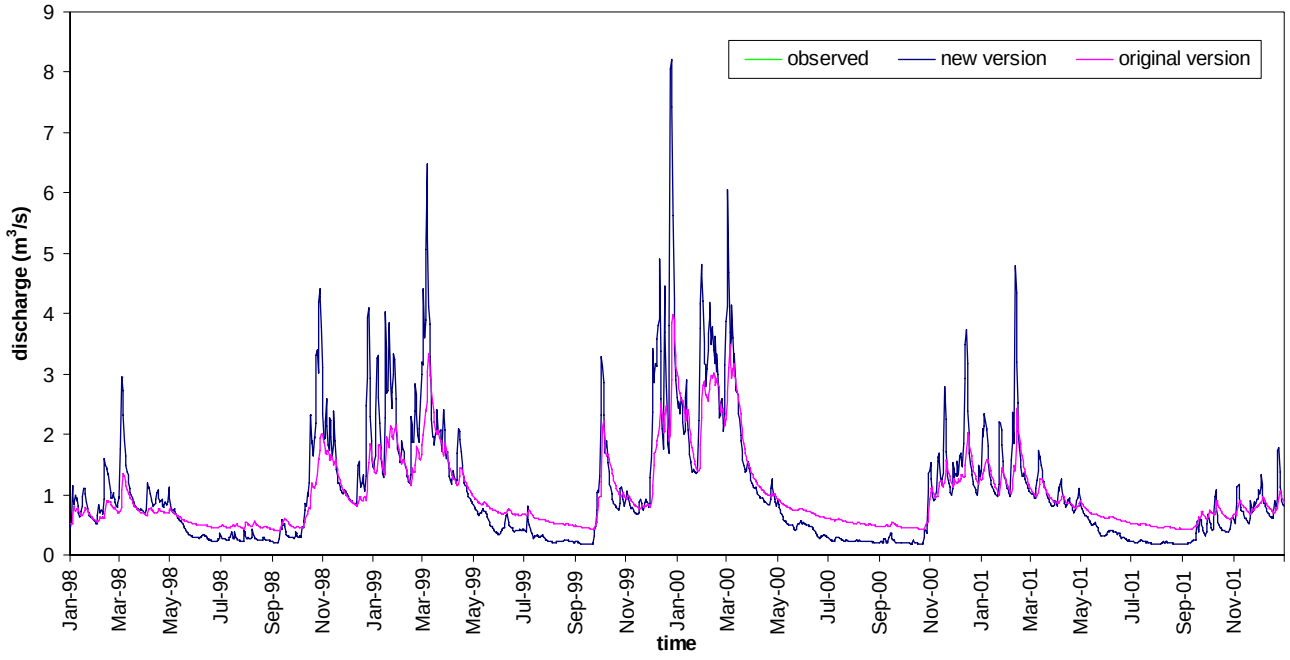
observed
new version
original version
discharge (m3/s)
time
0
1
2
3
4
5
6
7
8
9
Jan-98
Mar-98
May-98
Jul-98
Sep-98
Nov-98
Jan-99
Mar-99
May-99
Jul-99
Sep-99
Nov-99
Jan-00
Mar-00
May-00
Jul-00
Sep-00
Nov-00
Jan-01
Mar-01
May-01
Jul-01
Sep-01
Nov-01

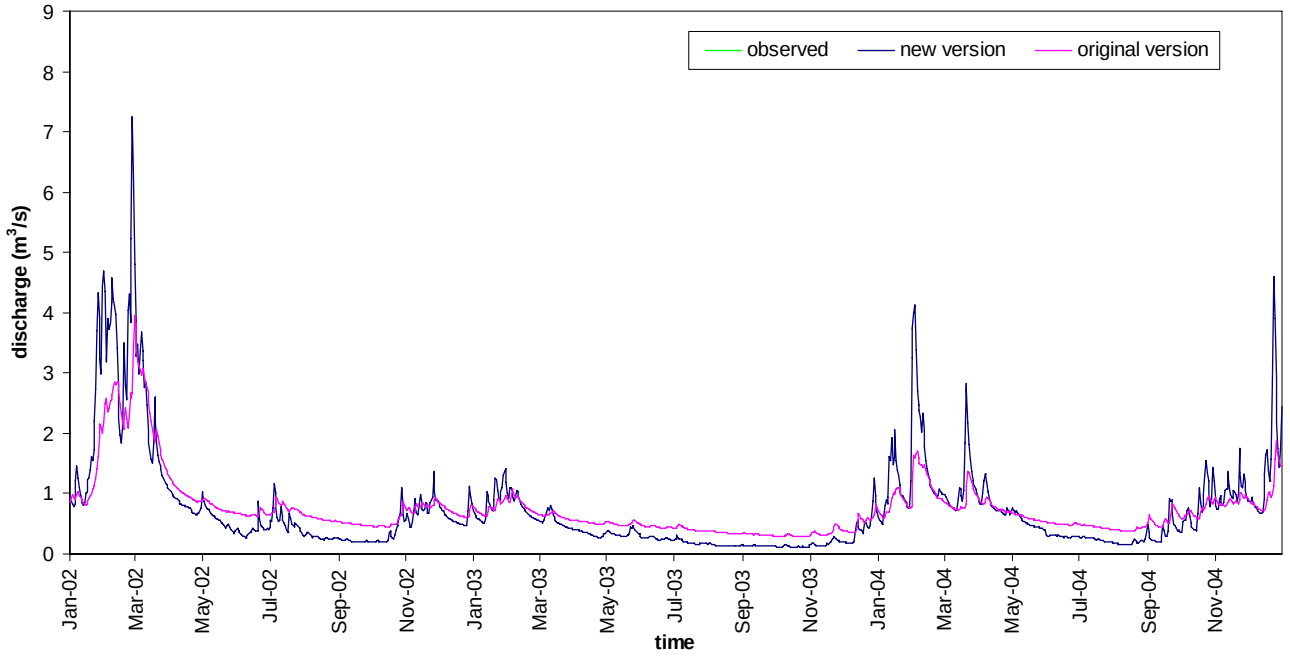
observed
new version
original version
discharge (m3/s)
time
0
1
2
3
4
5
6
7
8
9
Jan-02
Mar-02
May-02
Jul-02
Sep-02
Nov-02
Jan-03
Mar-03
May-03
Jul-03
Sep-03
Nov-03
Jan-04
Mar-04
May-04
Jul-04
Sep-04
Nov-04

Skjern Å (nr. 25.08)

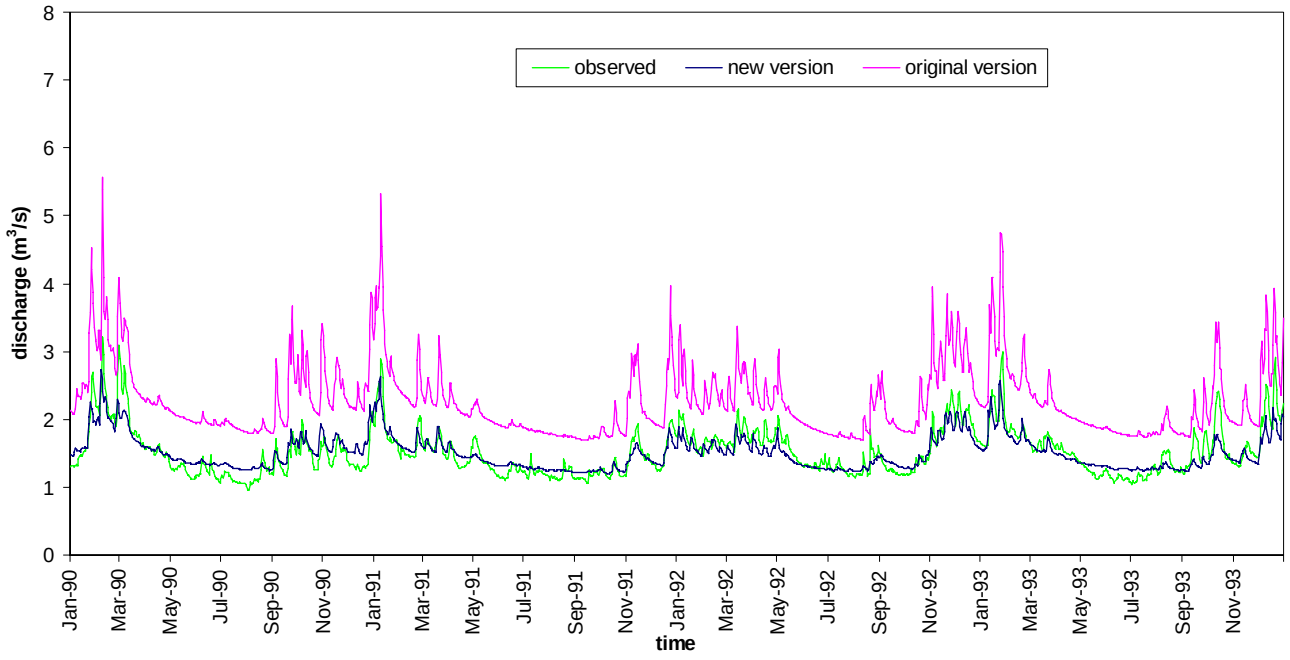

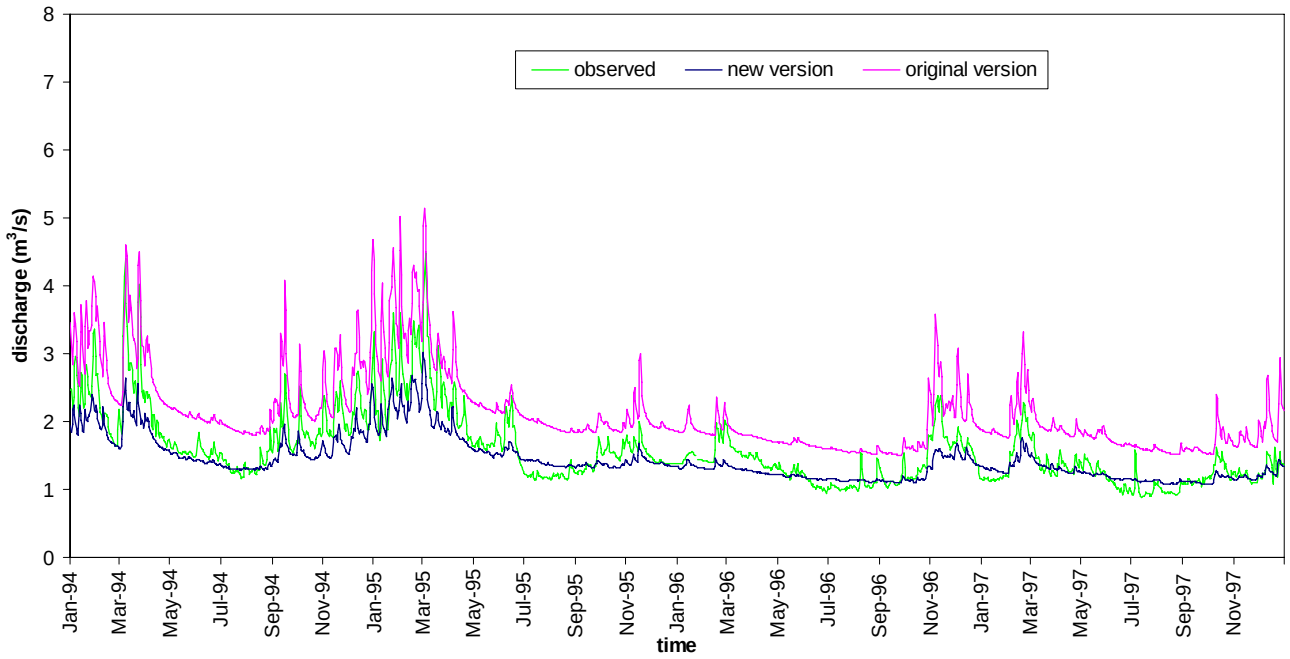

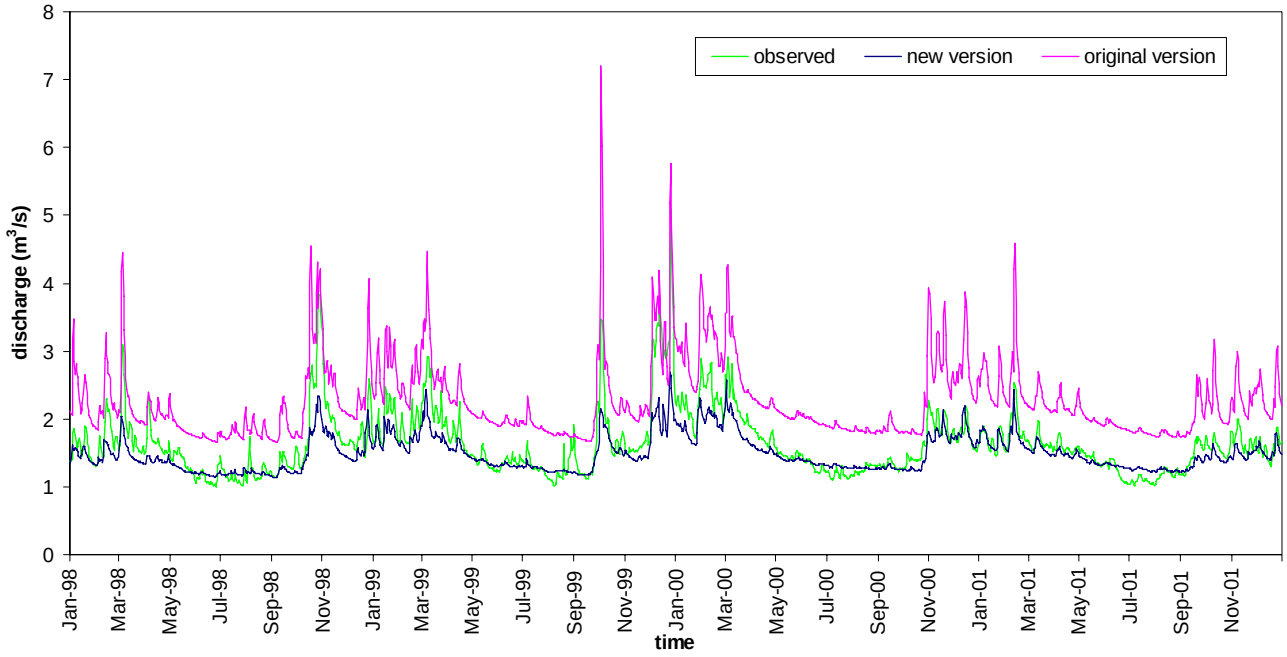
observed
new version
original version
discharge (m3/s)
0
1
2
3
4
5
6
7
8
Jan-98
Mar-98
May-98
Jul-98
Sep-98
Nov-98
Jan-99
Mar-99
May-99
Jul-99
Sep-99
Nov-99
Jan-00
Mar-00
May-00
Jul-00
Sep-00
Nov-00
Jan-01
Mar-01
May-01
Jul-01
Sep-01
Nov-01
time

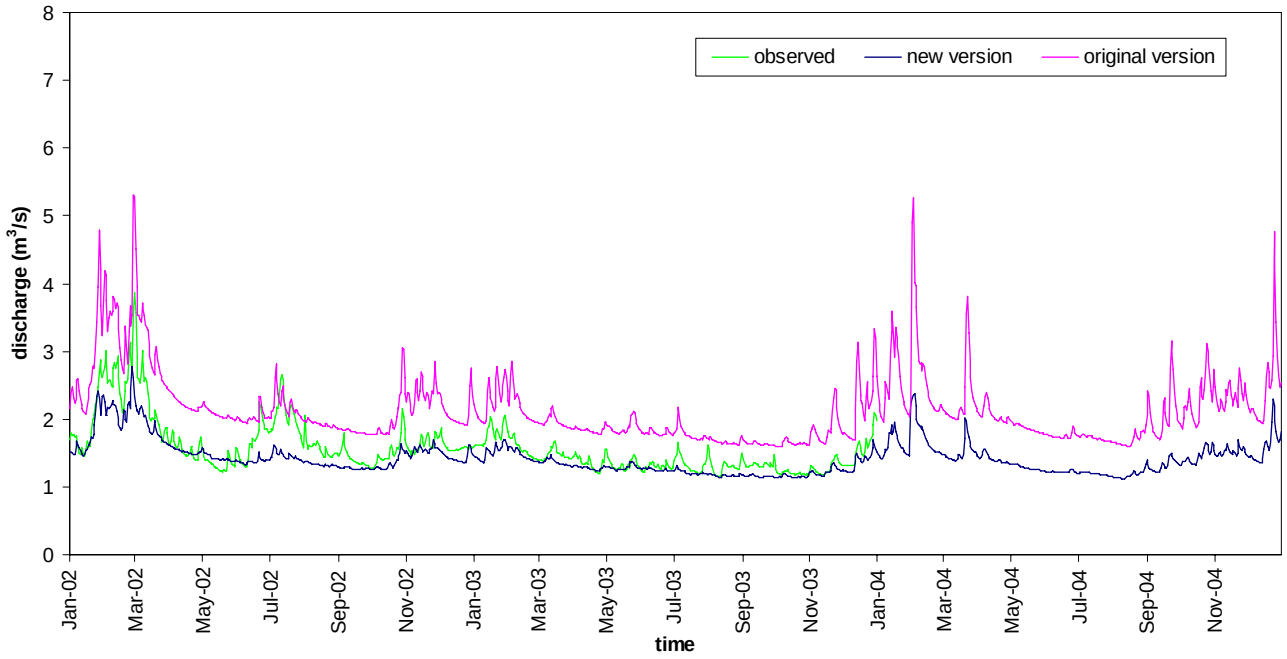
observed
new version
original version
discharge (m3/s)
0
1
2
3
4
5
6
7
8
Jan-02
Mar-02
May-02
Jul-02
Sep-02
Nov-02
Jan-03
Mar-03
May-03
Jul-03
Sep-03
Nov-03
Jan-04
Mar-04
May-04
Jul-04
Sep-04
Nov-04
time